SOURCING TREE WATER IN THE SACRAMENTO MOUNTAINS OF NEW MEXICO: A STABLE ISOTOPE STUDY

By

Casey Gierke

Submitted in Partial Fulfillment

of the Requirements for the Degree of

Master of Science in Hydrology

New Mexico Institute of Mining and Technology

Socorro, New Mexico

August 2012

ABSTRACT

The Sacramento Mountains of southeast New Mexico serve as the primary recharge area to adjacent regional aquifers, including the Roswell Artesian Basin, the Tularosa Basin and the Salt Basin. Under pressures of population growth and climate change, land and water managers are interested in identifying land management and forest restoration methods that may increase local and regional groundwater recharge in the high mountains. This study was designed to determine the role that trees play in the hydrologic cycle by using the stable isotopes of oxygen and hydrogen to identify tree water sources. It is part of the Sacramento Mountain Watershed Study which is designed to assess the effects of tree thinning in mountain watersheds as an effective method of increasing groundwater recharge.

The study is being conducted in a 1st order watershed with no perennial outflow stream where vegetation is dominated by Douglas Fir (*Pseudotsuga Menziesii*). Ridges are capped with San Andres Limestone while lower slopes and the valley bottom are underlain by the Yeso Formation which is composed of sandstones, mudstones and interbedded carbonate layers. The area has thin soils covering shallow fractured bedrock or epikarst features. Some of the fractures within the epikarst zone provide direct

conduits to the larger groundwater system while others are isolated rendering the reservoir inactive.

From March 2011 to February 2012, we collected soil and twig samples from which water was extracted by cryogenic vacuum distillation. Soil water was also sampled with passive capillary samplers (PCAPS). The isotopic composition of bulk soil water appears to be controlled by evaporation of snowmelt stored within the soil matrix. The isotopic composition of soil water sampled by wick samplers reflects mixing of non-evaporated rainfall with evaporated bulk soil water. As the monsoon season progressed and cumulative rainfall increased, the isotopic composition of mobile soil water evolved towards that of local precipitation. The isotopic composition of tree water samples resembled that of bulk soil water from March and July 2011. In August, September and into November, twig water isotope values appeared to have both bulk soil water and mobile soil water contributions.

The conceptual model that we have developed to explain this phenomenon relies on different infiltration mechanisms for snowmelt and monsoon precipitation which determine where water is stored. Snowmelt infiltrates soil and is stored in shallow soils where trees can easily access it. Short duration, high intensity monsoon rains in the late summer exceed infiltration capacity, exploit preferential flow paths and quickly flush through profiles to recharge groundwater and shallow epikarst reservoirs in the underlying bedrock. As epikarst storage increases, a secondary root system is able to begin exploiting the newly available source in the epikarst feature. The contribution of

this secondary source manifests in tree water as an integrated mixture of bulk soil water and mobile soil water. Continued use into November of these two water sources by certain trees while others returned to bulk soil water usage suggests spatial variation in epikarst storage and drainage.

Keywords: Stable isotopes; soil hydrology; trees; watershed hydrology; ecohydrology;

To my parents who gave me the gifts to get to where I am. To my brother for giving me the strength, courage, motivation and support to be where I am and to my friends and family for giving me reason to keep climbing higher.

ACKNOWLEDGEMENTS

I would like to take a moment to thank all the people that have helped me on this project and through this journey. Among them, I would like to specifically thank Talon Newton, Fred Phillips, Andrew Campbell, Nathan Canaris, Trevor Kludt, Brigitte Felix-Kludt, Bruce Harrison, Norton Euart and Bonnie Frey. I won't take the time to name everyone who has helped me in some way during this time but I can't leave out mention of my friends and family who have supported me and kept me moving forward. I also would like to extend thanks to the Otero Soil & Water Conservation District, New Mexico Geologic Society, Graduate Student Association and the Geologic Society of America who have helped fund this study.

TABLE OF CONTENTS

LIST OF FIGURES

LIST OF TABLES

1 INTRODUCTION

This study aims to assess tree water sources in a small watershed in the Southern Sacramento Mountains. This aim will be achieved by characterizing the end member reservoirs, and examining their spatial and temporal variability. This research will be used to better understand controls on recharge and the role trees play in the hydrologic system. Knowing how trees interact with the larger hydrologic system, this information will be used in an encompassing study to assess tree thinning as an effective mechanism to increase groundwater recharge in the system.

This study was designed to test the hypothesis that ridge-top trees will only use soil bound water due to inaccessibility of groundwater sources and valley-bottom trees will use shallow groundwater sources. It will also test the hypothesis that trees will use groundwater during times of water stress. Additionally, this study hypothesizes that trees will increase sap flow following monsoonal rains and exhibit an isotopic signature reflecting monsoonal precipitation due to a switch back to soil-water usage. These aims will be tested by sampling trees at ridge-top and valley-bottom locations, during times of water stress and during the monsoon season.

This study is supplemental to a study which intends to test the hypothesis that removing trees from a hydrologic system will decrease evapotranspiration and ultimately, increase aquifer recharge. Were the watershed overgrown, this could raise groundwater levels and induce discharge from springs that have not flowed in recent history. Previous studies have examined tree thinning as an effective tool for increasing groundwater recharge and raising aquifer levels in various hydrogeologic settings [*Rusanen et al.*, 2004; *Simonin et al.*, 2007] and anecdotal evidence of inactive springs resuming discharge in the Northern Sacramento Mountains has been reported. The current study aims to quantify some of the effects of tree thinning on the hydrologic system.

The stable isotopes of hydrogen and oxygen in water provide a powerful, nondestructive tool for determining tree uptake sources [*Brooks et al.*, 2009; *Brunel et al.*, 1997, 1991; *Dawson and Ehleringer*, 1991; *Ehleringer and Dawson*, 1992; *Goldsmith et al.*, 2011; *Tang and Feng*, 2001]. Additionally, isotopic analysis provides information about temporal changes in water sources as opposed to excavation, which gives only a single, temporally discrete indication of tree water sources. Excavation also overlooks the possibility of temporarily inactive or preferential roots.

Processes such as evaporation, which cause isotopic fractionation within the vadose zone, make different water sources distinguishable through stable isotope analysis. Several processes within the vadose zone dictate the isotopic composition of soil-bound water while groundwater is generally thought to be a reflection of precipitation [*Lee et al.*, 1999; *Winograd et al.*, 1998]. The Sacramento Mountain Hydrogeology Study laid much

of the groundwork for this study by characterizing precipitation, establishing the local meteoric water line (LMWL), the groundwater evaporation line and delineating recharge zones [*Newton et al.*, 2012].

Water resources are essential for the functioning of society and sustaining population and industry and their importance is even greater in arid environments. The Southern Sacramento Mountains of Southeast New Mexico serve as a recharge area for aquifers in the surrounding area including the Pecos Slope, the Artesian Basin, the Salt Basin and the Tularosa Basin [Newton et al., 2012]. As such, the area is of extreme importance to the region's water resources. As demands for water increase due to population and industrial growth, solid understanding and efficient management of water resources becomes increasingly important.

The benefits of tree thinning are multifaceted. The Little Bear Fire in the Lincoln National forest near Ruidoso, NM burned nearly 40,000 acres in the summer of 2012. Part of the reason the fire burned so extensively is the proliferation of forests in the area [*Simonin et al.*, 2007]. At the turn of the 19th century, tree densities were approximately 100 trees/acre while today there are areas that have nearly 3000 trees/acre. The fire did not advance into areas where tree thinning had taken place because the fuel supply had been reduced.

Numerous previous studies have employed stable isotopes to trace sources of tree water [*Adar et al.*, 1995; *Brunel et al.*, 1997, 1991; *Dawson and Ehleringer*, 1991; *Ehleringer*

and Dawson, 1992; *Tang and Feng*, 2001; *White et al.*, 1985] but, to the best of the author's knowledge, few have examined seasonal variations of tree water sources and none have been done in the Sacramento Mountains. A single, discrete sample may tell a lot about a system that is not readily apparent at the surface but sampling over a longer period of time helps to build an understanding of the dynamics of a system and how that system responds to change. This study will present results of seasonal sampling over the larger portion of a year and discuss their implications to the dynamic role of trees in this system. The implications of these findings to the larger hydrologic system will be reported in the larger watershed study. This study will give a detailed description of

1) Soil water dynamics in this system
2) Tree uptake patterns and responses to soil water availability.

2 STUDY AREA

2.1 Regional Geology

The Sacramento Mountains are located in southeastern New Mexico. They form the eastern boundary of the Tularosa Basin and slope eastward to the Pecos Slope and Roswell Artesian Basin. They serve as a recharge area for aquifers that supply the surrounding areas including the heavily agricultural Roswell Artesian Aquifer, the Salt Basin to the south and the Tularosa Basin. In a comprehensive examination of the region, the Sacramento Mountain Hydrogeology Study [Newton et al., 2012] laid the geological and hydrological framework for the Sacramento Mountain Watershed Project under which this study is being conducted (Figure 1).

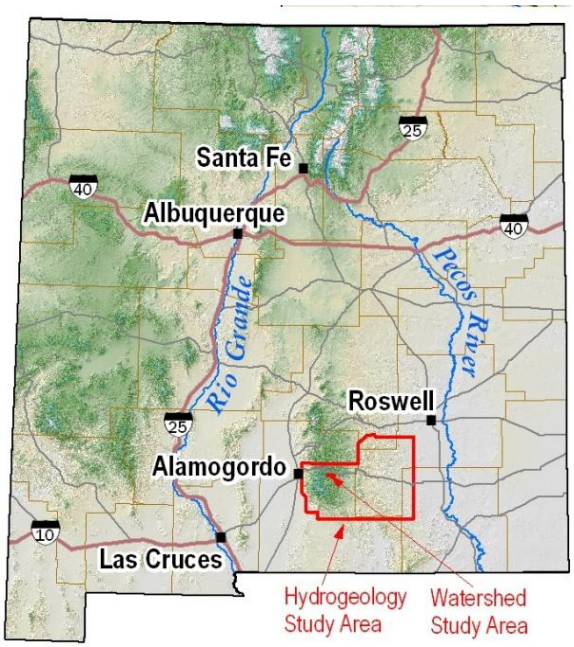

Figure 1: Location of Sacramento Mountains and the Hydrogeology Study conducted by Newton et al. [2009]

2.1.1 Geology

Rifting has resulted in a large escarpment that rises out of the Tularosa Basin to form its western boundary (Figure 2). The crest of the Sacramento Mountains is at the top of this steep escarpment. The Sacramento Mountain Highlands gently dip to the east toward the Pecos Slope and Roswell Artesian Basin. The highlands are characterized by ridges capped by San Andres limestone with valley bottoms cutting into the Yeso formation (Figure 3).

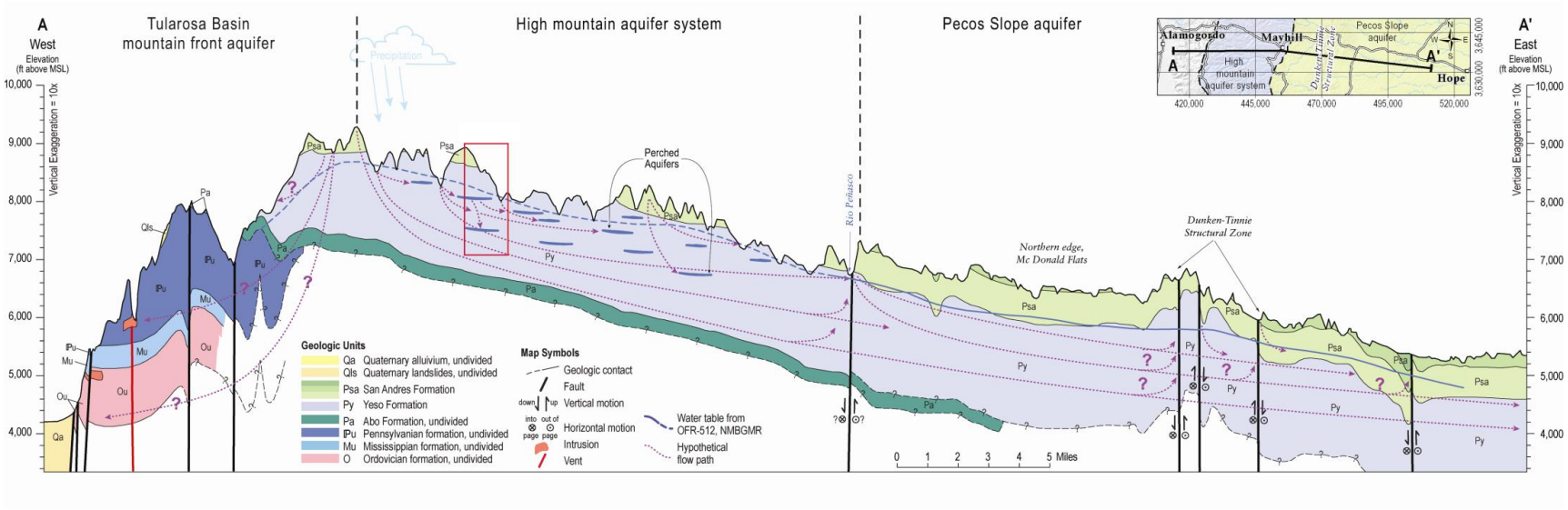

Figure 2: Cross section of the southern Sacramento Mountains. The San Andres and underlying Yeso Formations dip to the east from the crest. Regional groundwater flow paths generally flow eastward in the Yeso Formation from the crest and follow the shallow topographic gradient. The Pecos Slope Aquifer begins after the Mayhill Fault. Red box is location of schematic in Figure 5. Reproduced from Newton et al. [2009].

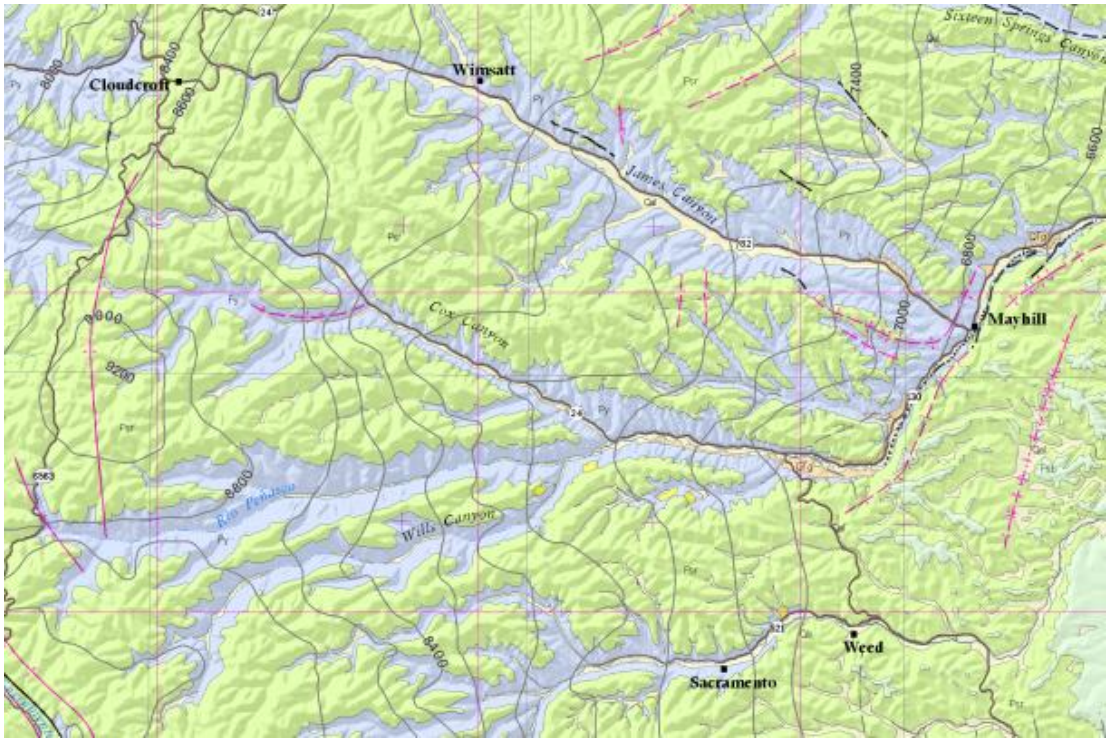

Figure 3: Geologic map of the southern Sacramento Mountains. Note the contact between the San Andres Limestone (green) and underlying Yeso Formation (blue). In the high mountain area, valley bottoms typically have Yeso exposure while ridge tops are capped with San Andres. Reproduced from Newton et al. [2012].

The Yeso Formation consists of yellow to tan siltstone and fine sandstone, red to pink muddy siltstone and fine sandstone [*Newton et al.*, 2012]. Gray to tan, often silty, carbonate rocks, both limestone and dolomite, make up 35-40% of the formation and will be referred to generally as carbonates. Outcrops of the Yeso Formation are rare because it is less resistant than the overlying San Andres limestone and it is usually covered with colluvium and valley bottom alluvium. Pray [1961] and Kelley [1971] estimated total thickness to be 400 to 425 m (1300 to 1400 ft).

Evaporite minerals such as gypsum, anhydrite, and halite have been dissolved from the upper portions of the Yeso Formation and are primarily found only deeper in the profile.

This dissolution results in chaotic bedding dips and individual beds are often not laterally traceable for more than a few tens of meters [*Newton et al.*, 2012]. On a regional scale, the gypsum content in the Yeso Formation tends to increase to the north and carbonate content tends to increase to the south [*Kelley*, 1971; *Pray*, 1961].

The San Andres Formation is composed of light to dark gray and bluish-gray carbonate [*Newton et al.*, 2012]. Freshly broken surfaces are darker gray than weathered surfaces and often fetid. Based on interpretation of aerial photographs by Kelley [1971], the San Andres has been subdivided into the lower dominantly thick-bedded Rio Bonito Member and overlying dominantly medium- to thin-bedded Bonney Canyon member. Thicknesses are 175 and 120 m (580 and 400 ft) respectively. Thickness variations on the order of 30 m (100 ft) are likely in both members across the study area.

The Yeso and San Andres formations both dip shallowly eastward at an angle of approximately 2˚ and are complicated by faulting and folding. The strata dip gently to the east from an anticline situated at the range crest. The elevation of the contact between these two units is nearly 2,750 m (9000 ft) near the range crest and less than 1,800 m (6000 ft) at the end of the Pecos Slope.

2.1.2 Structural Controls on Stream Orientation

Structural features that control surface water include faults, folds, joints, and the uplifted mountain block itself [Newton et al., 2012]. Uplift has created a drainage divide between

shallow sloping streams draining eastward toward the Pecos Slope and steep canyons draining westward into the Tularosa Basin. An exception to this pattern is the Sacramento River, which drains southeast along a half-graben into the Salt Basin. Major drainages are often located along slight v-shaped contours, which indicates that broad folds likely influenced their formation and likely continue to influence the direction of groundwater flow. Faults influence stream flow in several areas. Stream flow has been shown to increase by nearly 60% along a section of the Rio Penasco near the Mayhill fault [Newton et al., 2012]. This increase is likely due to upwelling along the fault.

Carbonate rocks throughout the study area are deformed by joints that have been characterized into two predominant types; northeast-southwest and northwest-southeast, oriented consistently throughout the study area. Stream orientations often follow such joints, which is likely due to preferential erosion of fractured rock. Many fractures have been enhanced by dissolution due to flowing groundwater, indicating that joints beneath stream valleys provide access for surface water to recharge groundwater and for groundwater to discharge back to streams. As joints are prominent throughout the Sacramento Mountains, this type of recycling is likely quite common.

2.1.3 Hydrostratigraphic Units

Most wells in the Sacramento Mountains west of Mayhill derive their water from the Yeso Formation [*Newton et al.*, 2012]. Well logs indicate that aquifers are situated primarily in vertically and horizontally distributed, fractured limestone, collapsed

breccias formed by dissolution of gypsum and/or limestone, and less frequently, sandstone. These aquifers are comprised of numerous individual but variably interconnected water-bearing zones. The spatially variable permeability associated with heterogeneous lithology and the secondary permeability associated with fractures and conduits, leads to a complex hydrologic system.

East of Mayhill the San Andres becomes more important as an aquifer unit. In this region, water storage occurs in the matrix of the formation instead of local fracture and conduit features. The lower part of the formation hosts saturated zones and is often characterized by karstic features and sinkholes.

2.1.4 Soils

In general, soils tend to be quite dry at the surface and moisture content increases with depth. Ridge tops have little to no soil cover with low relief bedrock outcrops and are often sandy to loamy in character. In contrast to the low storage capacity of ridge top soils, valley bottom soils are often deeper and better developed providing for much more storage. Valley bottom soils are deeper due to erosion from the uplands and subsequent deposition in the valleys. They are better developed due to increased infiltration from runoff as well as having less resistant parent material in which to develop. It is common to find clay-rich soils overlying several meters of colluvial and alluvial carbonate parent material in the valley bottoms.

2.2 Regional Hydrology

2.2.1 Precipitation

To understand the hydrology of a system the inputs and outputs must be identified. Precipitation is the primary input in the Sacramento Mountains. Evapotranspiration and groundwater flow are the primary outputs. To understand how water moves through the system and to accurately estimate the precipitation input, it is necessary to understand how precipitation in the area varies with space and time. The high mountain region receives an average of 65 cm (26 in) annually and the lowlands to the east average 35 cm (14 in). Figure 4 shows stable isotope data from precipitation collected in the region. This precipitation data was used to establish the local meteoric water line (LMWL), a trend line upon which precipitation samples tend to plot [Newton et al., 2012].

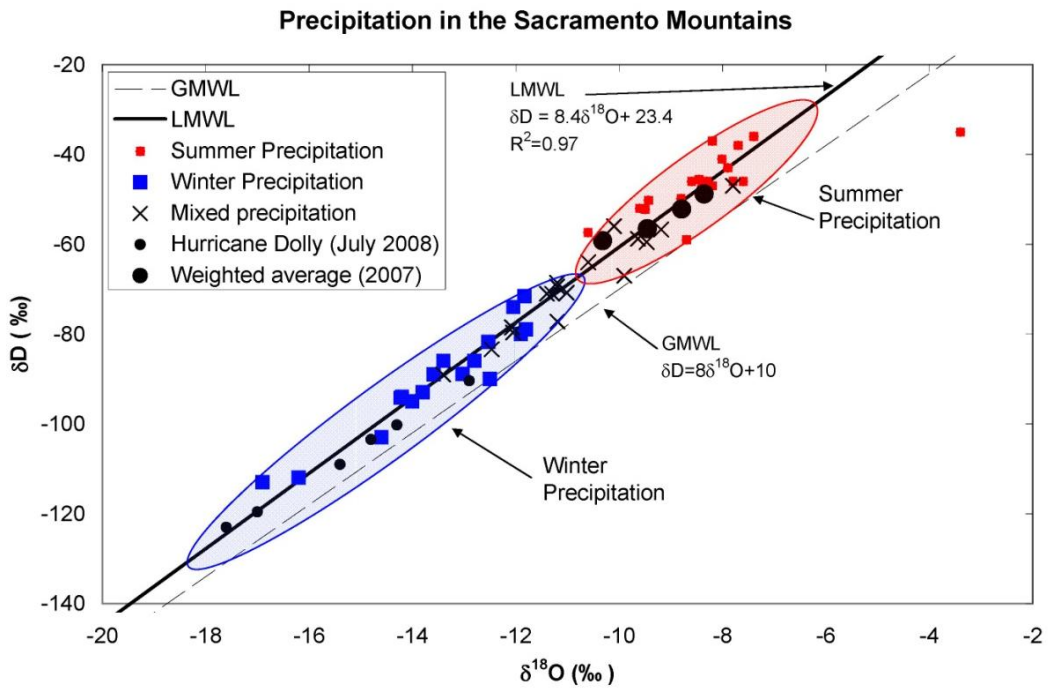

Figure 4: Precipitation samples collected in the Sacramento Mountains, the global meteoric water line (GMWL) and the local meteoric water line (LMWL) defined by the precipitation data. The equation of the line is $\delta D = 8.4*\delta^{18}O + 23.4$. Lighter winter precipitation and heavier summer precipitation have been separated based on their different compositions. The different weighted average samples are grouped by elevation with lower elevations being the most enriched. Reproduced from Newton et al. [2009].

Regional precipitation displays seasonal and elevation trends and the LMWL exhibits a deuterium excess with respect to the global meteoric water line (GMWL). This excess is indicative of the monsoonal type precipitation inputs typical of the region [*Tian et al.*, 2001].

Seasonal variations in the stable isotopic composition of precipitation are due to three factors: 1) seasonally changing temperature; 2) seasonally modulated evapotranspiration flux; and 3) seasonally changing source areas of vapor and/or different storm trajectories

[*Rozanski et al.*, 1993]. All three of these factors play a role in the observed seasonal variability of stable isotopic composition in Sacramento Mountains precipitation.

Stable isotope composition of precipitation varies with condensation temperature [*Dansgaard*, 1964] and seasonal temperature fluctuations in the Sacramento Mountains average approximately 15 ˚C between summer and winter. Due in part to this seasonal temperature fluctuation, there is a seasonal isotopic signature in precipitation. Newton et al. [2009] characterized this seasonal variability by categorizing precipitation samples as winter or summer precipitation (Figure 4).

The Sacramento Mountains are heavily vegetated compared to the surrounding region. During the summer, this results in a significant amount of water vapor being returned to the atmosphere via evapotranspiration. This addition of water vapor to the atmosphere effectively reduces the extent of isotopic enrichment of precipitation during the summer [*Rozanski et al.*, 1993].

Finally, the source area of winter frontal storms is different from that for storms associated with the North American Monsoon which produce summer precipitation. Winter precipitation originates as frontal storms in the eastern Pacific before moving inland. Summer precipitation, the largest contributor to annual precipitation, is a result of thunderstorms created from tropical moisture brought into the state by monsoonal air flows from the Gulfs of Mexico and California. Additionally, tropical storms are sometimes swept into the greater Southwest, providing additional summer rains. The

different sources as well as the different storm generation processes lead to isotopically distinguishable precipitation categories.

Elevation effects have also been characterized in the Sacramento Mountains. Different collection sites produced different annual weighted-average isotopic compositions due to their relative elevations [Newton et al., 2012]. This is due to two related factors: the elevation effect and the temperature effect associated with different elevations. The elevation effect is created by condensation of atmospheric vapor as an air mass is driven up mountain slopes. This results in cooling due to adiabatic expansion, which in turn affects the isotopic composition of precipitation due to lower condensation temperatures and thus greater fractionation [*Gonfiantini et al.*, 2001].

2.2.2 Streams

East of the crest of the Sacramento Mountains, valley bottoms and streams generally drain eastward with an approximate overall dip similar to that of the geologic contact between the San Andres and Yeso Formations (2-3°). There are few perennial streams in the Sacramento Mountains. Perennial reaches tend to persist over relatively short distances before infiltrating to recharge the shallow ground water system. These short surface exposures contribute to the evaporative enrichment observed down gradient.

Minor spring-fed wetlands are common in flat sections and are characterized by saturated soil with single or multiple coalescing channels draining them. Wetlands tend to

evaporate more water than steeper, flowing stream channels due to their larger surface area and more stagnant nature. Because they are permanently saturated, wetlands are likely groundwater recharge sites, but their contribution likely bears an evaporative signature.

2.2.3 Springs

Springs are the source of most perennial streams in the Sacramento Mountains. They are common throughout the southern Sacramento Mountains and tend to discharge primarily from the Yeso Formation. They often issue from fractured limestone beds underlain by less permeable clay or siltstone layers and discharge from several depths relative to the San Andres-Yeso contact plane, with a median of 46 m (150 ft) below the contact [Newton et al., 2012]. This indicates that the groundwater flows at several levels within the Yeso Formation (Figure 5).

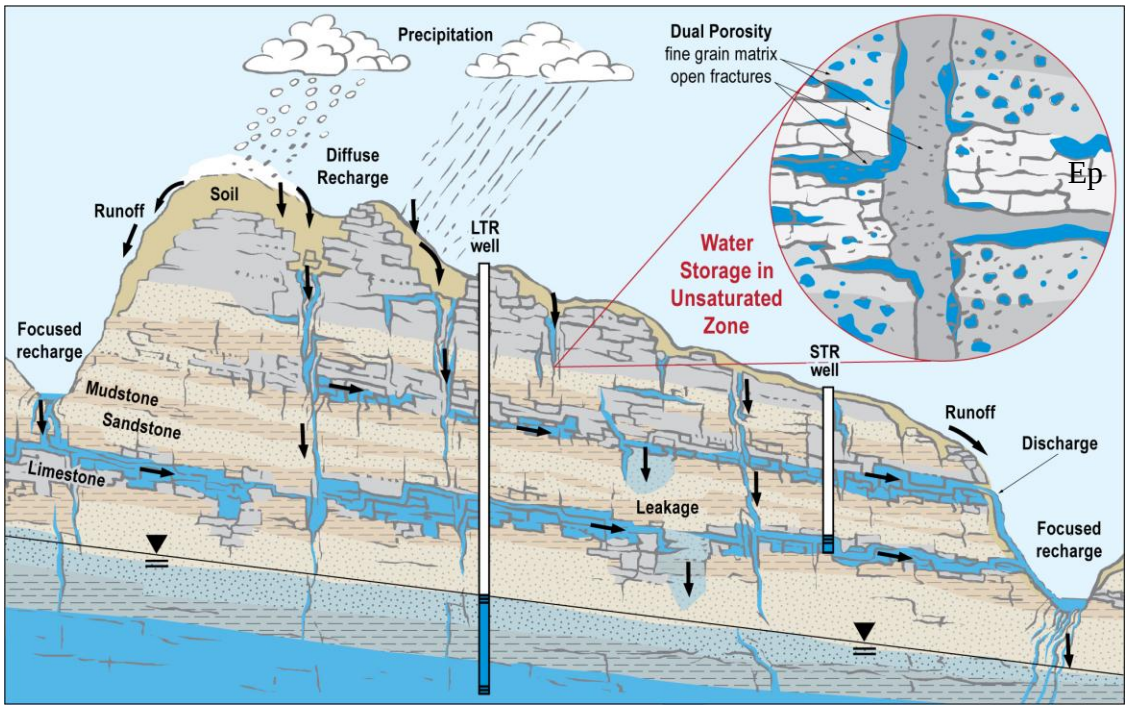

Figure 5: Schematic of local hydrogeology. Recharge through soils infiltrates aquifers of varying degrees of connectivity. These carbonate aquifers may transport water to the greater groundwater system or discharge as local springs. Springs often mix in streams while exposed at the surface before re-infiltrating. Groundwater is generally stored in fractured bedrock and moves through fractures and karst type conduits. Epikarst water is depicted in the inset as water bound in fractured bedrock that is either poorly connected or entirely disconnected from the greater hydrologic system. Reproduced from [Newton et al., 2012]

Isotopically, spring discharge reflects groundwater compositions and exhibits increasing enrichment as elevation decreases. This trend is attributed to the fact that most stream reaches, both perennial and ephemeral, infiltrate back to shallow groundwater. While exposed at the surface, water is evaporatively enriched, thus spring water discharged at lower elevations has been exposed to more evaporation than that discharging at higher elevation. This trend implies a circular "recycling" relationship reflecting the interconnection between surface water, springs, and shallow ground water.

Tritium analysis has shown that the residence times of spring waters in the Sacramento Mountains generally increase from the west to the east, or down gradient [Newton et al., 2012]. This spatial trend provides further support to there being a regional connection between springs. However, there are also cases where apparent tritium ages of spring discharge vary significantly over small spatial scales, suggesting leaky perched groundwater systems that have varying characteristic residence times. Once into the Pecos Slope aquifer, apparent tritium ages become more consistent and exhibit a trend of increasing age along the flow path [*Morse*, 2010].

2.2.4 Groundwater

Regional groundwater in the high Sacramento Mountains appears to underlie a system of local and intermediate perched aquifers (Figure 5). Isotopic values of groundwater samples from the high mountain aquifer tend to plot along a single evaporative trend line suggesting a well-mixed system [Newton et al., 2012]. A well-mixed system is geologically plausible due to the heterogeneity with respect to hydraulic conductivity, and the presence of large fracture systems and karst features such as conduits. Additionally, the presence of groundwater flow paths with a large range of flow velocities can result in mixing of waters of different ages.

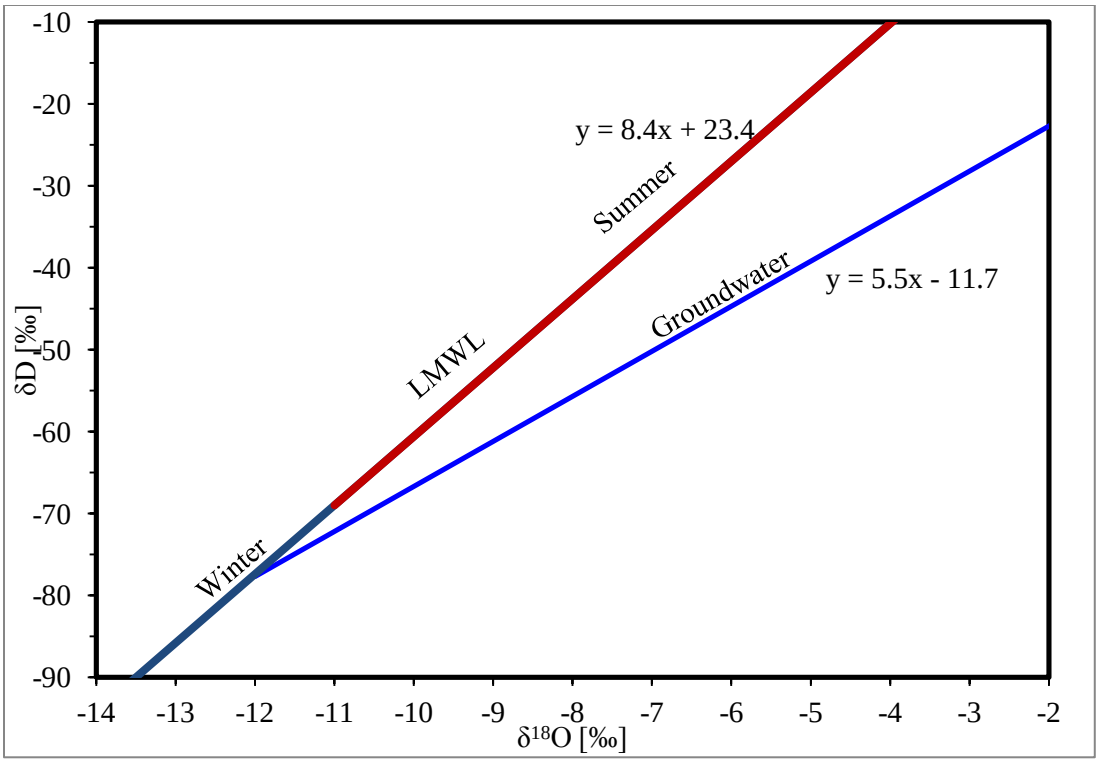

Figure 6: Local meteoric water line (LMWL) and groundwater evaporative trend line developed from well water and spring samples collected across the region [Newton et al., 2012].

The shallow slope of the groundwater trend line in Figure 6 suggests an evaporative signature [*Newton et al.*, 2012]. This signature is a result of the regional pattern of spring discharge feeding losing streams that infiltrate after short perennial reaches. During surface exposure, water is exposed to evaporation and the isotopic composition is enriched. Upon infiltration and reintegration with groundwater, this signature is transferred leading to the observed evaporative trend in bulk groundwater.

There are four regional aquifers whose boundaries are largely based on topography (surface water drainage basins) as well as regional water table surfaces [Newton et al., 2012]. Water-level elevation contours in the high mountains generally follow topography

though, on local scales, trends are much more complex due to fracture controlled heterogeneity. This correspondence indicates that there are shallow perched aquifers throughout the high mountains at several elevations. Water-elevation contours suggest that some groundwater flows from the high mountains into the northern Salt Basin and to the Tularosa Basin mountain front aquifer (Figure 7).

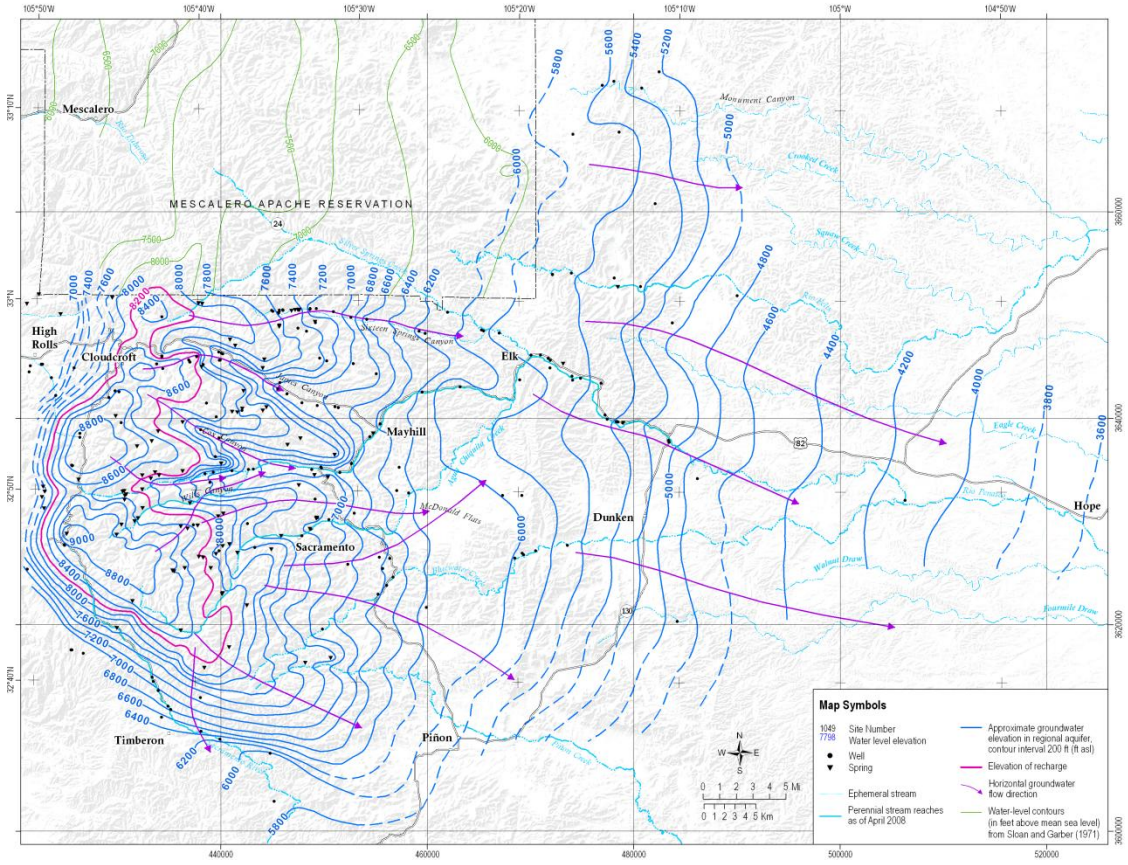

Figure 7: Groundwater surface contour map. A regional west-to-east gradient can be seen as well as some possible north-to-south flow into the northern Salt Basin and minor east to west flow from the crest into the Tularosa Basin [*Newton et al.*, 2012].

The division between the high mountain and the Pecos Slope aquifers lies where the Yeso Formation dips underground. This division is supported by water chemistry data as well as flow characteristics. The average gradient of the Pecos Slope aquifer surface is

shallow, approximately 100 feet per mile, or 1 degree with groundwater flowing to the east, parallel to bedding planes and permeable rock layers. Water chemistry and stable isotope data suggest that the Pecos Slope aquifer behaves similar to a single continuous aquifer within the San Andres and Yeso Formations. Additionally, $\delta^{18}O$ values decrease and level off between -9 and -9.5 ‰ near Mayhill, which has been designated the division between the high mountain aquifer and the Pecos Slope Aquifer. This stabilization of isotopic values at Mayhill suggests that allotropic recharge or seepage from streams, is not significant east of that point and that recharge to the Pecos Slope aquifer comes from groundwater flow leaving the high mountain aquifer system.

2.2.5 Epikarst water

Newton et al. [2009] observed significant changes in the isotopic composition of spring discharge during the course of their hydrogeology study. These fluctuations were associated with two discrete recharge events: 1) The 2006 monsoon season and 2) Hurricane Dolly in 2008, both of which produced large amounts of precipitation. The fluctuations were attributed to a contribution of relatively immobile water from the epikarst reservoir.

Spring samples collected following these large recharge events displayed an isotopic shift away from the groundwater trend line towards the LMWL and expected summer precipitation values. For the 2006 monsoon season, this seemed to suggest that recent precipitation was quickly flushing through the system. However, precipitation delivered

via Hurricane Dolly was isotopically light and bore resemblance to expected winter precipitation values, yet the shift produced by this event was towards summer precipitation values (Figure 8). Based on these events, Newton et al. [2009] inferred that young meteoric water associated with large recharge events displaces water from a relatively immobile reservoir and forces it into the more mobile hydrologic system. This recently mobilized water then discharges, at springs causing the observed isotopic shifts.

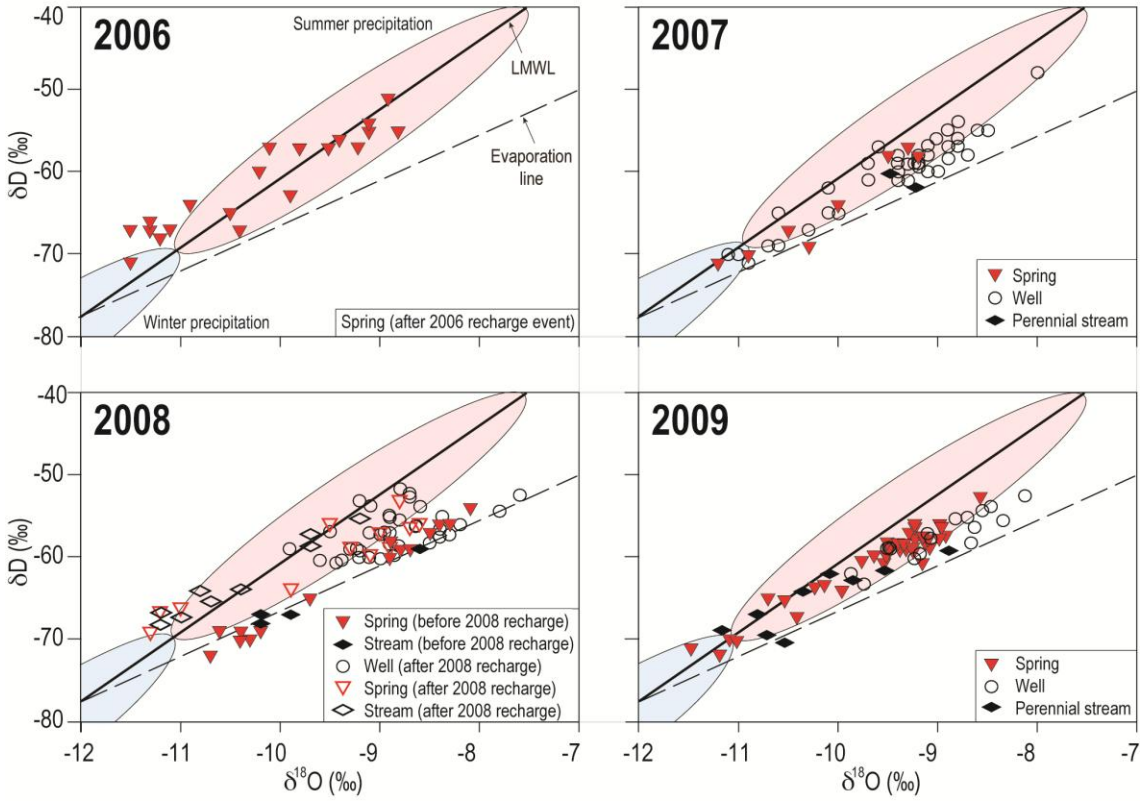

Figure 8: The evolution of spring samples between 2006 and 2009. After the 2006 recharge event, springs did not exhibit an evaporative trend but rather resembled meteoric water. Spring samples regained an evaporative signature by 2007. In 2008, springs were observed to change from bearing an evaporative signature in March to exhibiting a shift toward the LMWL in September. This shift is likely due to the large precipitation input from Hurricane Dolly. In 2009 springs had once again regained their evaporative signature. Reproduced from Newton et al. [2009]

Conceptually, epikarst water is an inactive reservoir bound in bedrock fractures having either apertures small enough to prevent gravity drainage or in dead end fractures (Figure 5). This reservoir is isolated under normal circumstances but large recharge events seem to be able to displace the bound water and reintroduce it to the larger hydrologic system.

2.2.6 Recharge

Newton et al. [2009] determined the recharge area to be above a threshold elevation of 2,500 m (8,200 ft) making the high mountain aquifer the primary recharge area. They state that the primary contributions to recharge in this area are snowmelt and infiltration of streams. These mechanisms contribute to a system of interconnected shallow perched aquifers that create a well-mixed system with an evaporative signature. Following the evaporative trend line established by well and spring samples from this area back to the meteoric water line yields an intersection in the heavy winter precipitation region (Figure 6). This suggests that snowmelt is a larger contributor to groundwater than heavier summer precipitation [*Campbell et al.*, 1996; *Earman et al.*, 2006].

Though seepage from streams and snow melt in the high mountains are important recharge mechanisms, it is apparent that extremely wet periods during summer months, such as those observed in 2006 and 2008, contribute significant recharge to the groundwater system. This secondary recharge mechanism is episodic and is characterized by pronounced increases in groundwater levels and rapid changes in groundwater stable isotope composition. This mechanism relies on flushing a less active

epikarst storage reservoir into the larger hydrologic system via a large precipitation input. Shifts in isotopic composition of spring and well water toward the LMWL produced by this recharge mechanism suggest that the water stored in such an epikarst reservoir experiences very little alteration from that of precipitation.

Whereas primary recharge from snowmelt and streambed infiltration are predominant in the high mountain aquifer region, epikarst flushing and secondary recharge appears to occur throughout the region (Figure 9). It is also apparent that the secondary recharge mechanism requires that some threshold precipitation input be surpassed whereas primary recharge seems to be at or near steady state.

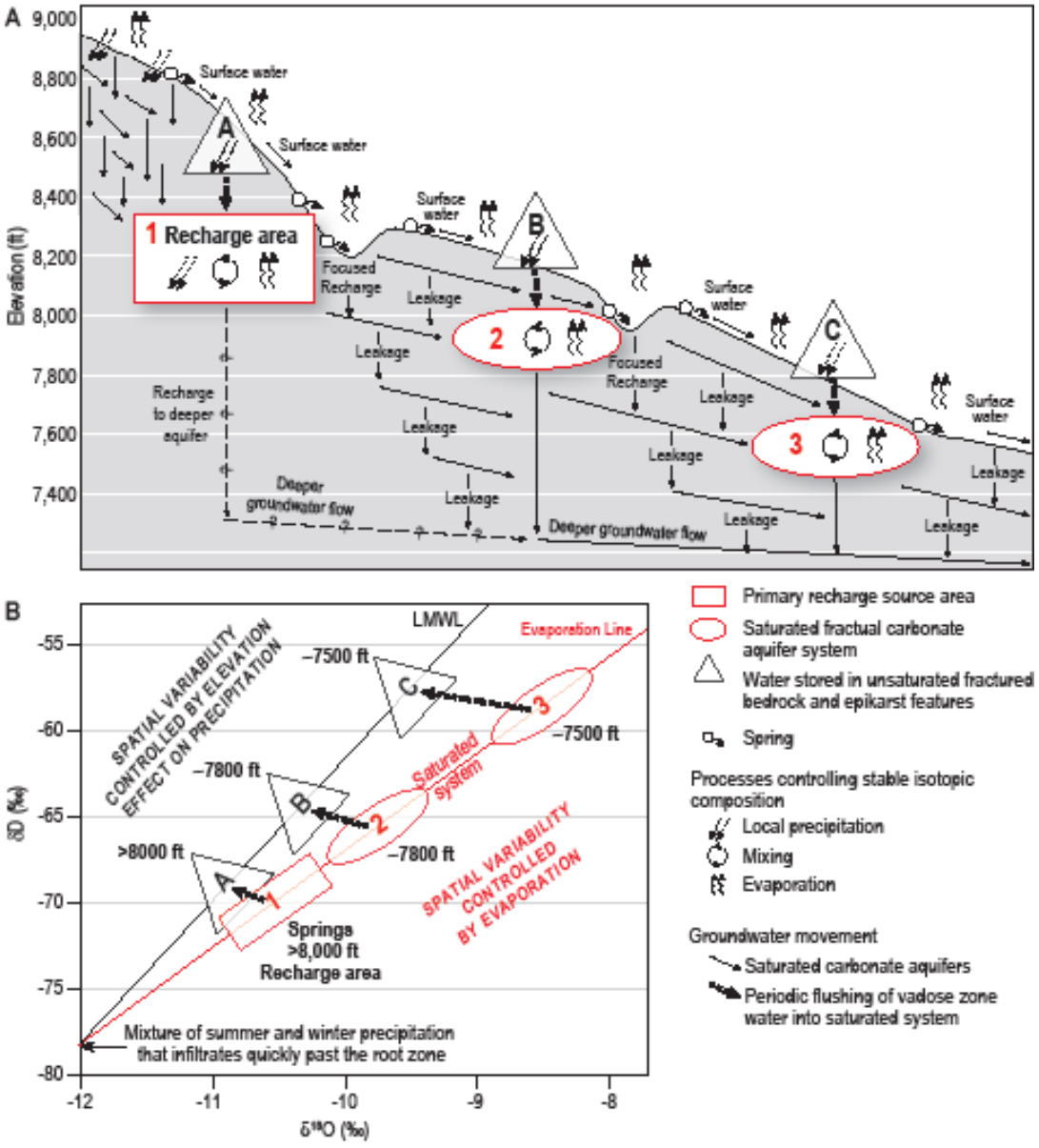

Figure 9: Schematic depicting secondary recharge or epikarst flushing. Triangles represent the local epikarst and unsaturated fractured bedrock reservoirs and bear isotopic signatures consistent with their respective elevations. Primary recharge occurs only at high elevations but secondary recharge occurs at all elevations once certain threshold precipitation input is surpassed (A). This input then shifts the isotopic composition of springs to reflect that of the local epikarst storage reservoir (B). Reproduced from Newton et al. [2012].

2.3 Field Site- Three L Canyon

The Sacramento Mountain Watershed Project is being conducted in a small watershed within the bounds of the larger Sacramento Mountains Hydrogeology Study. The watershed is Three L Canyon on private land located off US Highway 82 between Mayhill and Cloudcroft, NM. The watershed is about 840 acres located in the Sacramento Mountains highlands and ranges in elevation from 2,300 to 2,550 m (7,600 to 8,400 ft) (Figure 10).

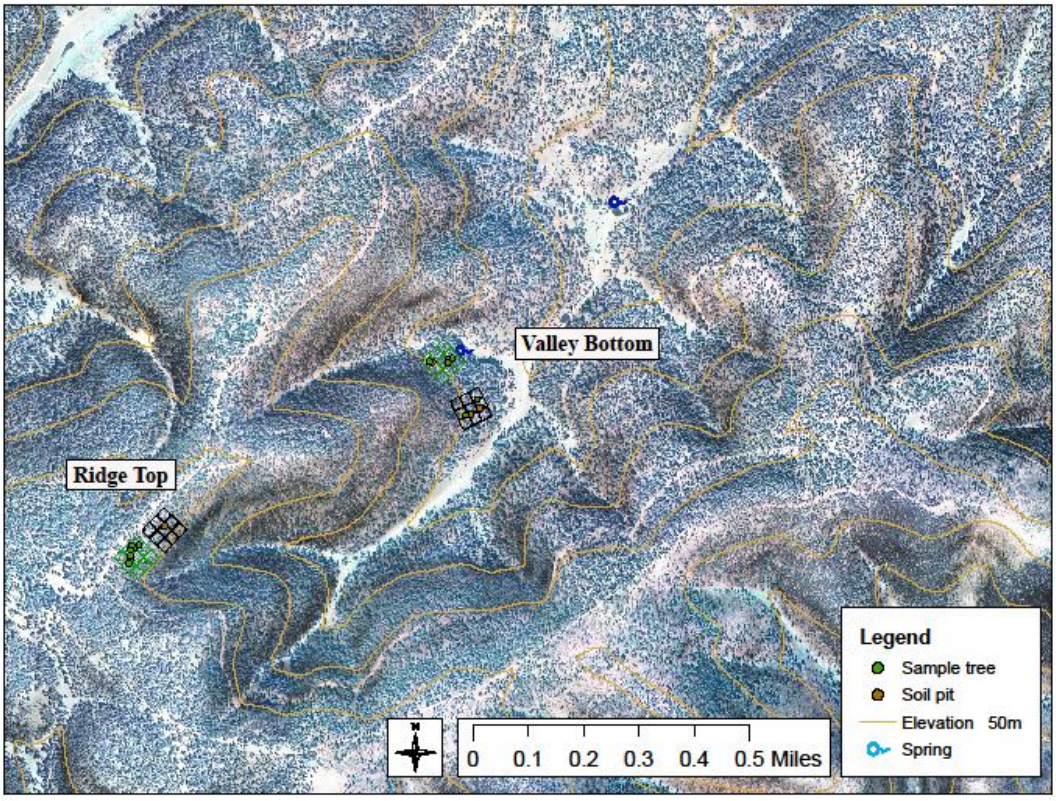

Figure 10: Topographic map of Three L Canyon where the Sacramento Mountain Watershed Project is being conducted. The watershed is about 840 acres and ranges in elevation from 7,600 to 8,400 ft. Reproduced from Newton et al. [2009].

2.3.1 Geology

Like the greater region, ridge tops are capped by the San Andres Formation, a highly fractured unit. The material is generally white exhibits an interconnected fracture system with early stages of karst conduit formation. Soil profiles overlying the San Andres Carbonate on the ridges are generally thin (0-40 cm) and poorly developed consisting largely of sand and organic material.

The valley bottom is underlain by the Yeso Formation, which is composed largely of mud and siltstones. Due to erosional processes, fan and colluvial material is interspersed in the profiles. Soil profiles on the Yeso are generally clay rich and deeper than those overlying the San Andres Formation with observed thicknesses of up to 5 m. Geophysical electromagnetic inductance (EMI) surveys, which measure the apparent electrical conductivity of soil showed lower values for soils on the San Andres Formation and higher values for soils on the Yeso Formation.

2.3.2 Soils

Soils in the study area are quite variable and highly dependent on slope and catena position. Frechette [2008] described three soil stratigraphic units: San Andres and upper Yeso soils, Yeso soils and Basin soils. Ridge-top soils have been described as detachment limited while valley bottom soils are transport limited [*Frechette*, 2008]. The Basin soils will not be discussed as this study did not examine them at any point.

The San Andres and Upper Yeso soil stratigraphic unit is characterized by soils which have formed in resistant carbonates of the San Andres limestone and upper Yeso Formation. Bedrock weathers largely by physical processes that result in subangular to angular blocks that are scattered about the surface and form the parent material for the unit. Soils tend to be thin on the ridge crests where erosion dominates and increase in thickness at foot slope positions where there is cumulic deposition of upslope material [*Frechette*, 2008].

A horizons, observed to be spatially variable with respect to hydrophobicity, overlie interlocking saprolite carbonate blocks that transition to fractured bedrock with depth [*Frechette*, 2008]. Despite the carbonate parent material, there was little to no carbonate accumulation in these soils suggesting they were not weathered in situ from the parent material and that the fine mineral content must originate from another source. Eolian dust is consistent with the lack of carbonate as well as the observed high silt content [*Frechette*, 2008].

The loose-to-weakly-coherent and loamy texture of this soil unit is likely to encourage infiltration. Tortuous flow paths typical of the rocky and debris littered surface are also likely to enhance infiltration rates. The surface and shallow subsurface fractured bedrock likely allow for rapid integration of precipitation to the groundwater system.

The Yeso soil stratigraphic unit is less widespread than the San Andres and much more developed [*Frechette,* 2008]. B horizons are common and few clasts or outcrops appear at the surface. In situ weathering of this unit is much more likely than for the San Andres due to the relative weakness of parent material. Clay is more common in this unit than in the San Andres. Brown silt loams are observed in both the San Andres and Yeso units suggesting eolian deposition.

Infiltration rates in the Yeso soil stratigraphic unit are also likely to be high due to weakly coherent structure and loamy texture of A horizons. However, soil water residence time is likely much greater due to thicker profiles and lack of fracture controlled preferential flow paths. This increased residence time will also lead to higher potential evapotranspiration rates compared to San Andres soils.

A soil depth survey in the watershed revealed trends consistent with Dietrich et al.'s [1995] soil depth distribution model that predicts the thinnest soils on ridges and the thickest in drainage bottoms (Figure 11). It is also consistent with Frechette [2008] who attributes the deeper soils of the upper Yeso to be a combination of soils developing in situ and material transported from higher on the slope.

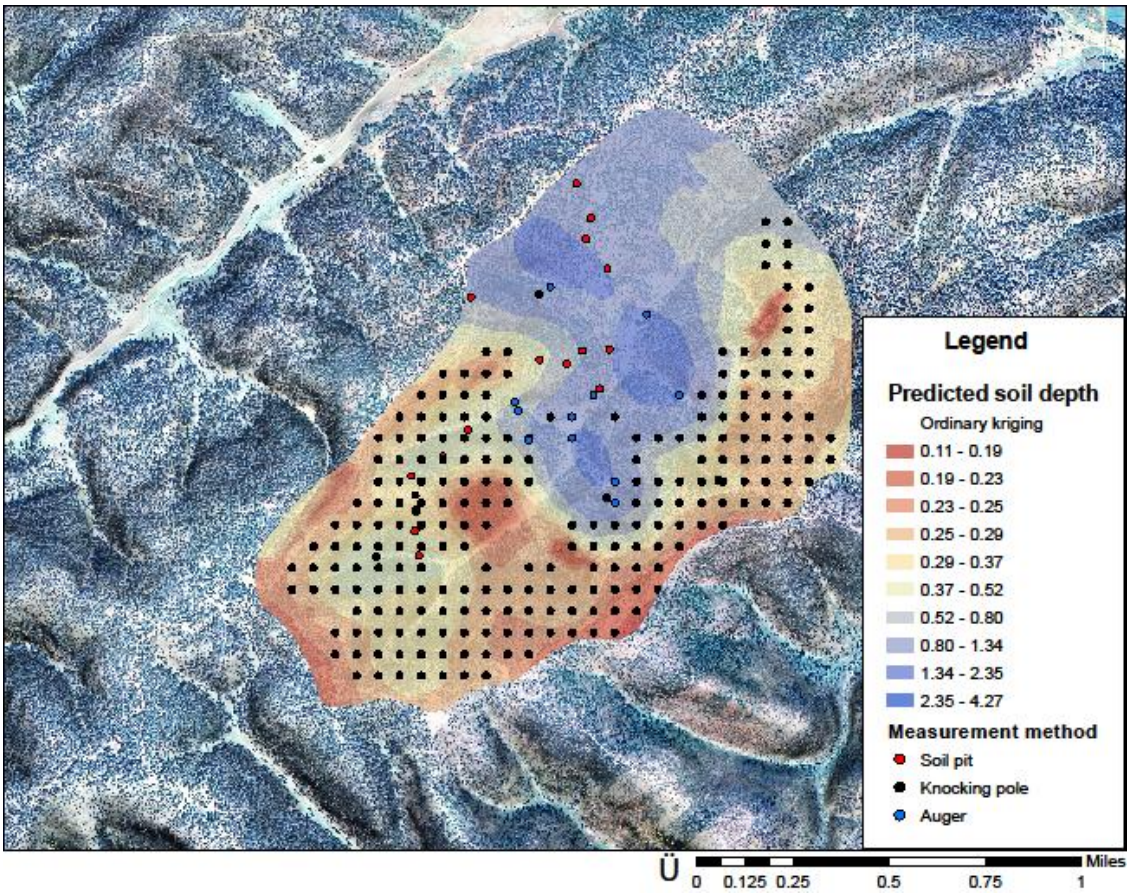

Figure 11: Three L Canyon soil depth map. Depths range from shallow (10 cm) colored red to deep (5 m or more) colored blue. 228 knocking pole locations, 12 hand auger locations and 17 soil pits were used to develop this map. Knocking pole location depths were determined by pounding a steel rod until it encountered bedrock or saprolite. Used with permission from N Canaris, NMBGMR unpublished map.

2.3.3 Hydrogeology

The watershed has two main springs, though no perennial outflow stream. Both springs have exhibited delayed responses to seasonal inputs, suggesting that they are not locally derived [Newton et al., 2012]. The upper spring flows into a series of collection ponds where much of the water infiltrates into the vadose zone and will eventually reenter the

shallow groundwater system. While it is exposed at the surface, water is subjected to evaporation and undergoes isotopic enrichment.

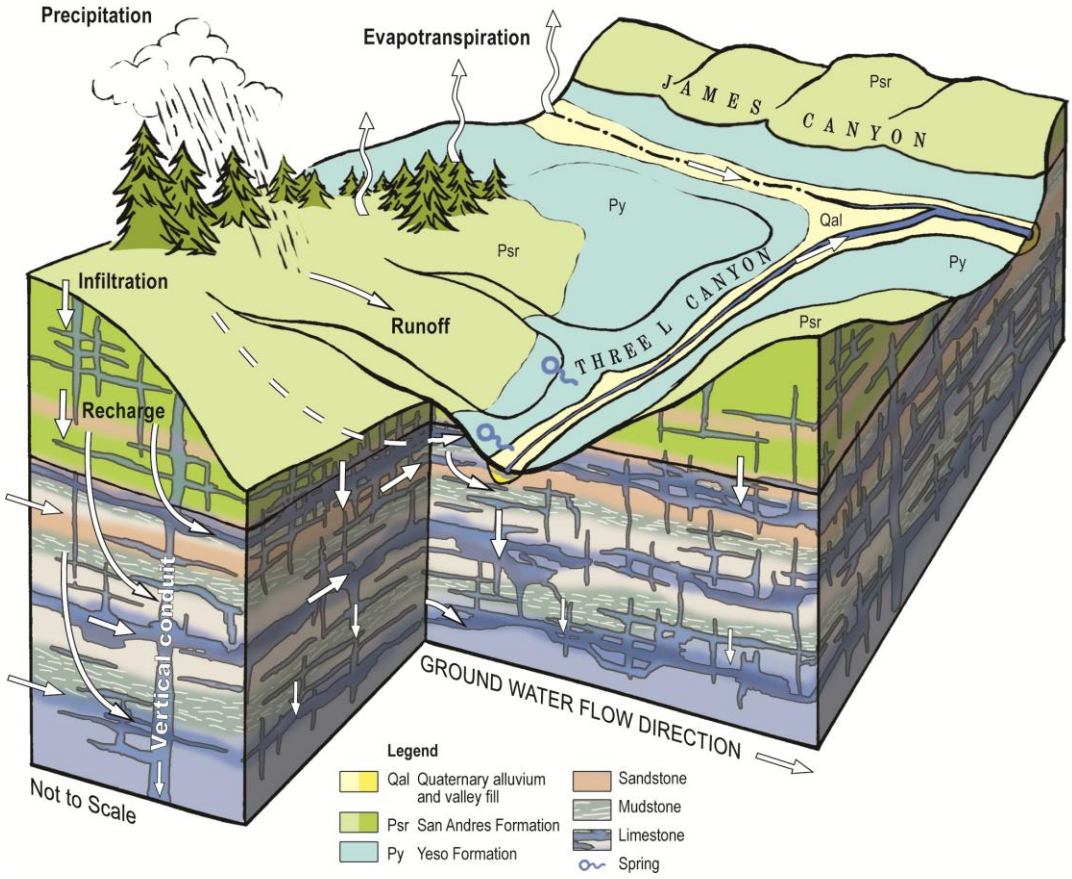

Figure 12: Schematic of the local hydrology in Three L canyon. Inputs depicted are precipitation and groundwater inflow while outputs are evapotranspiration, surface water runoff and groundwater outflow. Reproduced from Newton et al. [2009].

In this watershed, inputs include local precipitation and groundwater flowing in from outside the watershed bounds. Outputs include evapotranspiration, surface water runoff and groundwater leaving the watershed. A schematic of the local hydrology is depicted in Figure 12. Important features in the schematic are the geologic contact between the Yeso and the San Andres Formations, the karstic subsurface, the regional and local flow paths and the spring discharges.

2.3.4 Vegetation

Douglas Fir (*Pseudotsuga Menziesii*) is the dominant tree species in Three L Canyon though Ponderosa Pine (*Pinus ponderosa*) and Southwestern White Pine (*Pinus strobiformis*) are co-dominant to dominant in some stands. The prevalence of one species or another appears to be correlated to aspect and/or tree density [*Frechette,* 2008]. Alligator Juniper (*Juniperus deppeana*) and Piñon Pine (*Pinus edulis*) are found in drier areas, often on southern facing aspects and various oak species (*Quercus* species) make up much of the understory in the lower reaches of the watershed. Tree densities in the watershed can be seen in .

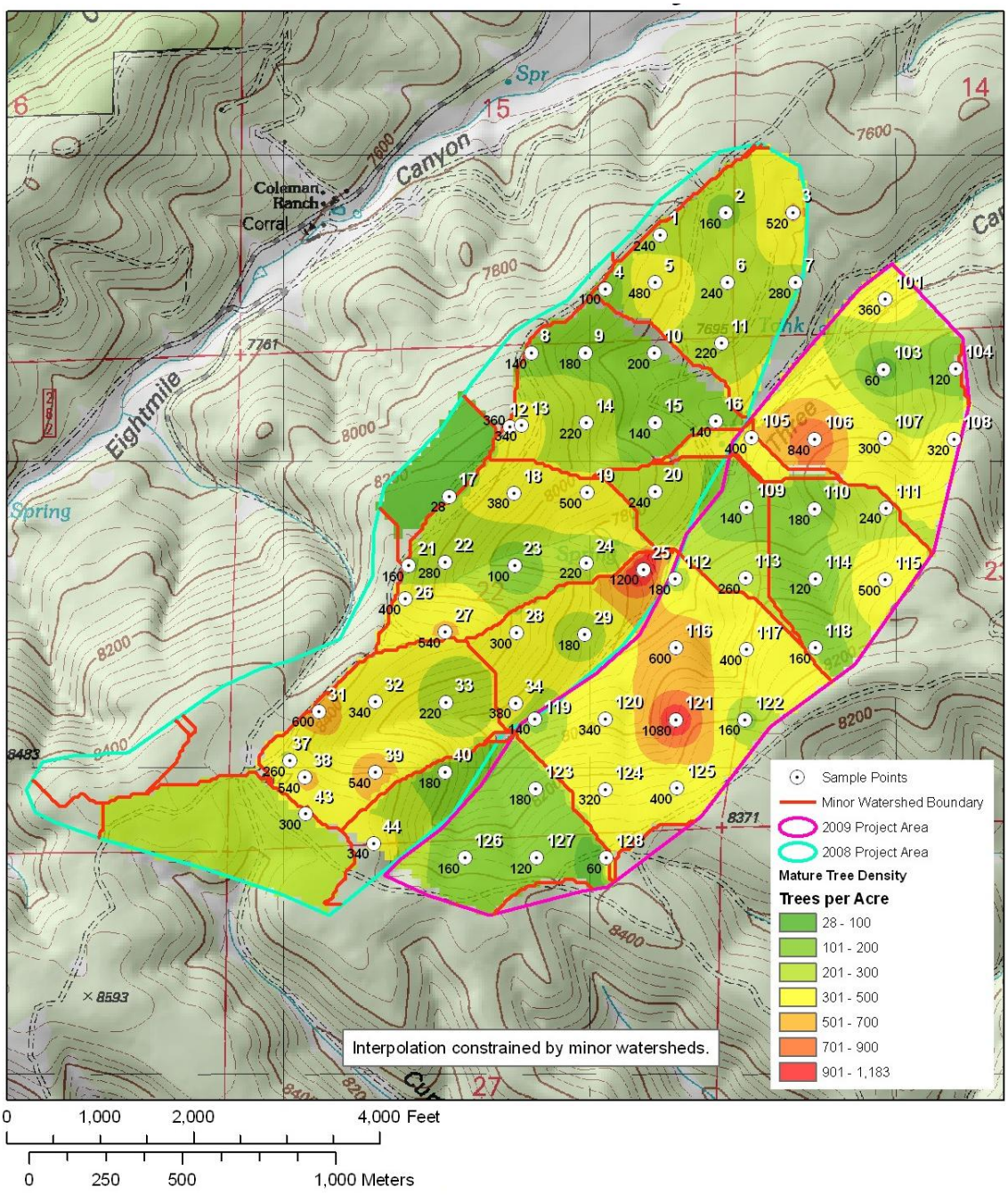

Figure 13: Tree density map of Three L Canyon.

2.3.5 Simultaneous Studies

Several studies are being conducted within the watershed. Primarily, there is the overarching Sacramento Mountains Watershed Study of which this study is supplemental. The Watershed Study aims to understand the effects of tree thinning on a watershed scale. To achieve this end the study monitors spring discharge, well levels, solar fluxes and characterizes and quantifies precipitation including throughfall, or the amount of precipitation that makes its way through the canopy and reaches the ground. To understand the effects of tree thinning specifically, eight 90x90 m plots were established. Of these eight plots, four had trees thinned and the other four were left untouched as control. On these plots, in situ soil moisture and soil matrix potential are being monitored for comparison between the thinned and control environments.

2.3.6 Tree Thinning

At the turn of the 20th century, tree densities in mountainous watersheds of the American southwest generally ranged from 30 to 100 trees/acre [*Simonin et al.*, 2007]. The watershed now has areas with density of approximately 1000 trees/acre. The State Forestry Division's Forest and Watershed Health Office (FWHO) provided technical assistance to the Natural Resources Conservation Service and Otero Soil and Water Conservation District to develop a site-specific tree thinning prescription. The tree thinning prescription is intended to restore a portion of Three L Canyon to historical tree densities. A pre-treatment tree density and ground cover density was established by the New Mexico Forest and Watershed Restoration Institute at Highlands University. Initial thinning was done privately with a large backhoe attachment. Chainsaw lop and scatter

thinning on the northern slopes of the canyon took place in the summer of 2011. Data is being collected on these slopes and on the ridge between Three L and Eight Mile Canyons.

Possible Effects of Tree Thinning on Outputs

Water storage occurs primarily in soil, the shallow groundwater system associated with springs and the regional mountain aquifer system. Surface water only leaves the watershed during flash floods. Much of the water that does run off hill slopes during intense precipitation events probably flows onto the valley bottom where it infiltrates into the groundwater system.

Tree thinning could affect watershed outputs by altering the amount of water leaving the system through transpiration or water used by trees. Decreased transpirative losses from soil and shallow saturated groundwater could lead to higher recharge and result in increased groundwater outflow leaving the watershed and possibly increased spring discharge.

3 LITERATURE REVIEW

3.1 Cryogenic Vacuum Distillation

Ecohydrology studies often need information about vegetative source water. Understanding where plants derive their water helps us to understand their role in the hydrologic system. This information is useful when determining water balances, estimating recharge, understanding storage in the vadose zone or any number of applications. This is particularly relevant for this study to understand how tree thinning will affect the hydrologic system.

When deciding to determine vegetation source water, one must choose a method. The most obvious may be digging up and following out roots. This method is destructive and will offer only a single discreet-in-time observation about water sources. It also does not account for permanently or seasonally inactive roots and simply assumes that where roots are present is where water is derived.

Stable isotope analysis of vegetation water is much less destructive. A single plant can be sampled several times, offering a dynamic view of biological processes through seasons and water availabilities. Matching stable isotope values of vegetative water with that of soil and groundwater can be used to determine where vegetation derives water [*Adar et al.*, 1995; *Brunel et al.*, 1997, 1991; *Dawson and Ehleringer*, 1991; *Ehleringer and Dawson*, 1992; *Goldsmith et al.*, 2011; *White et al.*, 1985].

There are several impediments to using stable isotope compositions of vegetative water to determine sources. Among them are the complexity of possible water sources, acquisition of such waters and how to interpret findings. This review will examine previous research about the complexities of source water, extraction techniques and the findings of similar studies.

Several researchers have worked to develop methods to extract vegetative water without altering the isotopic composition. Cryogenic vacuum distillation is one of these methods that is commonly employed.

Here we will review the available cryogenic vacuum distillation literature because this study will employ this method for extraction of tree water. This review will examine some of the main issues for obtaining accurate results: debarking, time requirements and sample preparation.

3.1.1 Debarking

Xylem transports relatively unaltered water from the roots to the leaves. Evaporative, photosynthetic and metabolic processes occurring at the leaves alter the isotopic composition of water within the plant [*Augusti et al.*, 2006; *Farquhar and Gan*, 2003; *Gat and Bowser*, 1991; *Libby and Pandolfi*, 1974; *McCarroll and Loader*, 2004; *Yakir and Deniro*, 1990; *Yakir*, 1992]. This water is then transported in the phloem, which is found in the bark, to the rest of the plant. Because we are interested in water sources, unaltered xylem water is of interest to this study. Inclusion of phloem in distillation samples produces samples that include water altered through such physiological processes and ultimately, gives erroneous values. Bark, and its associated phloem, should therefore be removed from samples before distillation.

In their study examining the extraction times for plant and soil materials, *West et al.* [2006] did not mention bark removal in their sample preparation or methods section which may indicate that it was not considered though this is not known. In their study using stable isotopes to identify transpiration sources in an Israeli sand dune terrain, *Adar et al.* [1995] states that, "Mixing of xylem and phloem revealed inaccurate results as the up-flowing sap via the stem toward the canopy is found only in the xylem." [*Adar et al.*, 1995]. Though Adar was not using cryogenic distillation but azeotropic distillation, his observation about the different compositions of xylem and phloem is quite relevant in this discussion.

In a study using stable isotopes to trace plant water uptake in Australia, *Brunel et al.* noted removing bark in their methods, although they did not explicitly mention a reason. In another study examining tree source water, *Brunel et al.* [1997] explained their decision to remove bark as, "in case it was in isotopic equilibrium with very isotopically depleted atmospheric water vapour." Similarly, in a study about how soil hydrology affects isotopic composition of plant source water, Tang and Feng [2001] justified their decision to remove bark saying that, "The bark was removed since it could exchange oxygen or hydrogen with the water vapor in the surrounding atmosphere." [*Tang and Feng*, 2001]. They were not interested in the lab atmosphere but the source water and because this contribution could give an undesirable bias to their results, they chose to remove the bark.

In their study attempting to reduce the time required for water extraction, Vendramini and Sternberg [2007] mentioned bark removal in their methods. *Unkovich et al.* [2001] focused on the effects of different distillation and sample storage times but also mentioned that bark was removed before distillation.

3.1.2 Time Requirements

The distillation process uses heat to drive water out of plant material via volatilization. This is a phase change which is known to alter isotopic compositions. The change of stable isotope abundances through phase changes follow Rayleigh processes. Figure 14 demonstrates the Rayleigh type behavior of the isotopic pools through such a process.

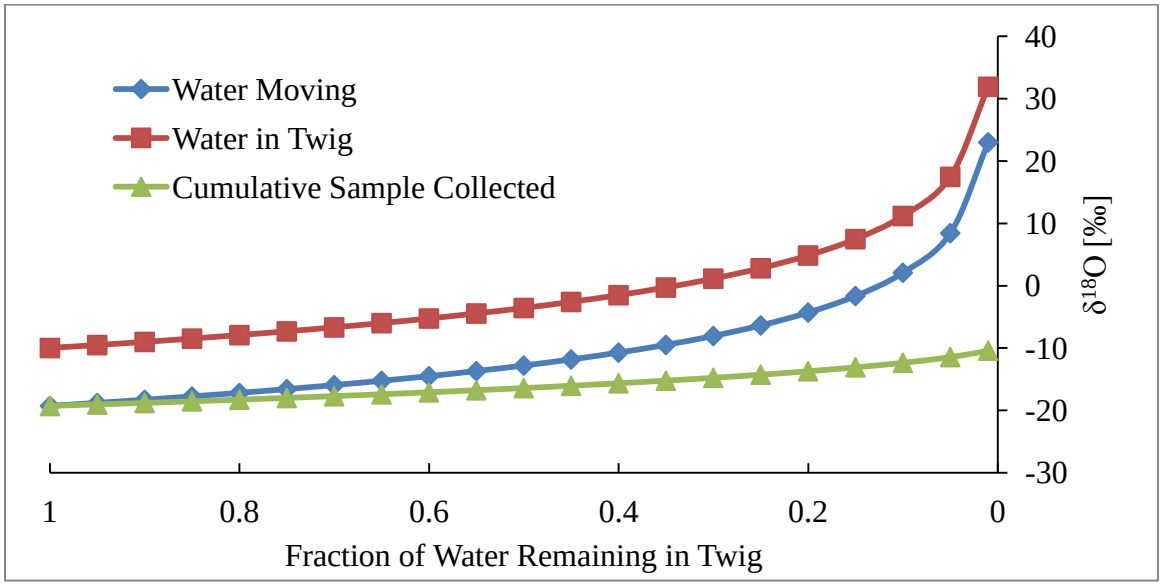

Figure 14: Compositions of the different components through the distillation process. The horizontal axis represents how much of the original water remains in the twig and the vertical axis isotopic abundance of oxygen isotopes. The original twig value is -10 ‰ as is the final composition of the cumulative sample collected. The water collected does not accurately reflect the original twig water value until the last of the twig water is collected and the remaining heavy isotopes are added to the sample. Stopping the process early would yeild an inaccurate result.

Figure 14 shows that the composition of the sample collected only reflects the original twig composition when the process is complete. Therefore, it is extremely important that the process be driven to completion and it is of great interest to understand the time requirements of the distillation process.

In a study designed to assess the time requirement for accurate distillations, *West et al.* [2006] reported 60 to 75 minutes for stems. *Vendramini et. al.* [2007] states, "Our results indicate that a distillation time of several hours might be needed … in contrast to the 60 to 75 min of distillation for the stems collected by *West et al.*" *Tang and Feng* [2001] and *Unkovich et al.* [2001] both reported distillation times of 2 hours. However, *West et*

al. [2006] claimed that distillations did not always have to be complete before distilled waters yielded the isotopically consistent results. They noted that full water recovery could sometimes take up to an addition three hours of distillation and that the removal of this period had no consequence on isotopic compositions.

3.1.3 Sample Preparation

Sample size and geometry can influence time requirements. Distillation methods apply heat to drive evaporation which occurs at liquid gas interfaces. Therefore, increasing surface area should decrease the time requirement for distillations. *Vendramini et. al.* [2007] used whole stem samples that were about 4cm long whereas *West et al.* [2006] cut their samples into 0.5 cm lengths. This could very well account for the discrepancy reported between their methods.

3.2 Soils

In a study such as this that aims to determine the source of tree water consumption, it is important to develop a strong understanding of how water is transported, transformed and stored in soils. Here we present a review of the available literature relevant to this study.

Soil water isotopic composition and chemistry are affected by many processes and are often found to be quite heterogeneous [*Brooks et al.,* 2009; *Landon et al.,* 1999; *Tang and Feng*, 2001]. Much of this heterogeneity can be attributed to spatial variations of soil type, vegetative cover, slope position and aspect. Additionally, soil water is generally composed of a mixture of meteoric waters from different events having different isotopic signatures [*Tang and Feng*, 2001]. Tang and Feng [2001] noted that variability between the isotopic composition of soil water and that of precipitation decreases with depth. They attributed the decreased variability with depth to be due to winter precipitation at the surface being replaced by summer precipitation but noted that a proportion of winter precipitation is retained below 20 cm. In a study comparing isotopic compositions of soil water collected with different methods, Landon et al. [1999] attributed this variability at shallow depth to be a result of different flow paths resulting in different residence times. In their study about lateral subsurface vadose zone flow, Newman et al. [1998] reported the variability of A-horizon lateral subsurface flow $\delta^{18}O$ values to be much less than that of precipitation. In some form, these researchers all note an attenuation of the isotopic signature of seasonal precipitation in soil waters.

Despite a fair amount of scatter in the data, the isotopic values of water samples distilled from bulk soil samples tend to plot systematically below the local meteoric water line (LMWL). From their study about water movement in clayey soils, Mathieu and Bariac [1996] note this to be due to, "a mixing between infiltrating rainwater and waters of the superficial part of the soil which were isotopically enriched." In their study examining separation of water between trees and streams, Brooks et al. [2009] noted that vertical variation in soil water isotopes at a single plot was much greater than spatial variation at any depth across the watershed.

3.2.1 Profile Development

The primary contributing factors to this depth variation are soil texture characteristics and the evaporative environment it hosts [*Barnes and Allison*, 1988]. Mathieu and Bariac, [1996] characterized 3 main soil zones in their study area. These were based principally on water content which they then correlated to the vertical variation of soil texture. They also noted that the upper meter showed variations induced by the annual alternation of infiltration and evaporation in the wet and dry seasons while the lower two zones displayed less variance.

Barnes and Allison [1988] did extensive work with soil water isotopic compositions and depth relationships. Their work showed that in addition to equilibrium fractionation and Rayleigh distillation that is commonly observed in evaporating water, kinetic fractionation due to the evaporative environment and, more specifically, turbulence in the

fluid-vapor interface, is important to the composition of the remaining soil water reservoir as it evaporates. They determined that the relationship between vapor and liquid diffusion varies with water content and observed an isotopic maximum that developed just below the surface whose position they attributed to the balance between vapor and liquid diffusion [*Barnes and Allison*, 1988]. A typical depth profile plotted from a simple model of theirs is shown in Figure 15.

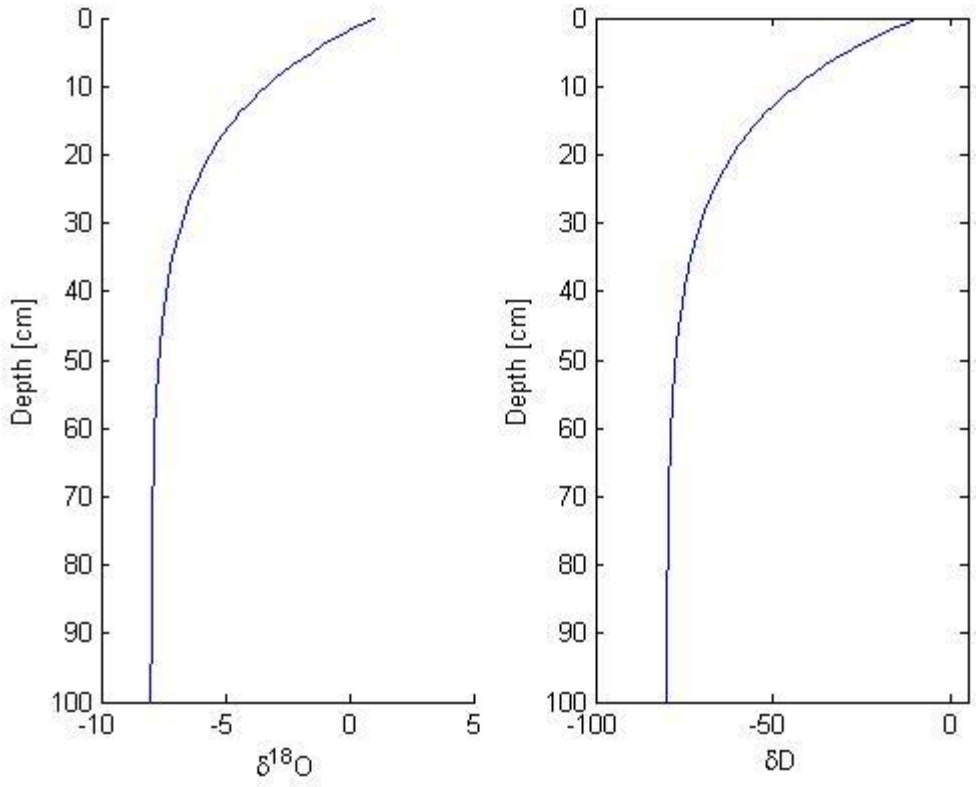

Figure 15: A characteristic isotopic depth profile as predicted by a simplified model from Barnes and Allison [1988]. The enrichment towards the surface is attributed to evaporative enrichment as well as vapor and liquid diffusion processes.

In a lab experiment to determine the effectiveness of a modified passive wick sampler, Frisbee et al. [2010] states, "Although soil water evaporated at a much lower rate (than

open water), kinetic fractionation was enhanced as a consequence of the deepening of the unsaturated zone." Barnes and Allison [1988] also point out that in moderately wet soils, the zone in which significant evaporation occurs is narrow and the soil profile can be divided into two parts: an upper on in which water movement is by vapor diffusion and lower one in which liquid transport is significant.

When characteristic depth profiles are developed in this manner, data points form a line on a $\delta^{18}O$ vs. δD plot which, when projected back to the meteoric water line, defines the isotopic composition of the un-evaporated, original precipitation. The slope of such an evaporation line is a function of both the relative humidity within the soil and the depth of the evaporation front [*Campbell et al.*, 1996]. These characteristic slopes range from 2 to 8 depending on evaporative conditions. Additionally, Barnes and Allison [1988] found that isotope moisture curves "collapse" onto one another with a Boltzman similarity transformation.

In their experiments, Barnes and Allison [1988] determined that coarse material resulted in slopes that were closer to those expected for evaporation through a fully turbulent boundary layer or rather, with no cover. This is significant for sandy to gravely soils that allow much vapor diffusion into the profile. They also found that grass cover leads to less soil evaporation and the development of deeper isotope profiles. Additionally, their work determined that temperature effects on soil-water profiles and fluxes can be significant but appear to have little effect on isotope profiles except that the evaporation

front for isothermal profiles was more than twice as deep as in non-isothermal conditions [*Barnes and Allison*, 1988].

One of their big contributions was to develop an understanding for the timescale upon which a characteristic typical isotopic depth profile would develop. They determined the major controlling factors to be evaporation rates and soil material and noted that for extremely low evaporation rates equilibrium may take millennia, while profiles developing under evaporation rates of 10 mm/d will be affected by only the previous 24 to 72 hours [*Barnes and Allison*, 1988]."

3.2.2 Mobile and Immobile Water Reservoirs

A common observation is the lack of both temporal and spatial variability in bulk soil samples. Tang and Feng [2001] attribute this stability to winter precipitation that is retained in the deep soil for a significant portion of the summer. Brooks et al., [2009] attribute the stability to water being held in small pore spaces and notes that, "this tightly bound water is not the same from year to year." This is similar to the "soil water reset" observed by Tang and Feng, [2001] who observed that large precipitation events would change the bulk soil water composition.

In their study, Mathieu and Bariac [1996] observed distillation waters that showed relatively heavy isotopic contents from the superficial part of the soil while water profiles extracted in situ (by ceramic cups) mirrored rainwater isotopic composition suggesting

the coexistence of two water reservoirs. Brooks et al. [2009] reported that bulk soil water was always more depleted in heavy isotopes than lysimeter water collected at the same depth and location. They attributed this difference to lysimeters collecting water that had not fully mixed with tightly bound bulk soil water. Newman et al. [1998] observed that the soil-core water analysis reflected soil-matrix pore-water chloride concentrations and that these were more concentrated than the lateral subsurface flow effluent for the three comparison dates when measurements were made. This difference, they argued, indicates that some of the flow bypasses the chloride-rich, B-horizon soil matrix and suggests that there is a more mobile soil water reservoir.

Based on these observations, Mathieu and Bariac [1996] distinguished three water categories: "(1) immobile water which was enriched by evaporation in the superficial part of the soil and which showed limited mixing with the other water categories, (2) a mobile water for which the transfer in the soil matrix was driven by capillary forces, with an intermediate isotopic content, and (3) a mobile water for which the fast transfer process was driven by gravity forces, with an isotopic content close to the rain composition." They associated the three water categories with microporosity, mesoporosity and macroporosity respectively and state that, "In the unsaturated zone macropores, the soil matrix, and immobile water zones coexist." [*Mathieu and Bariac*, 1996]

The presence of two distinct water reservoirs in soils is complicated by various degrees of mixing between the two. Brooks et al. [2009] attributes the difference to the bimodal distribution of pore sizes in which small pores fill first and drain last. In such a model it

follows that medium sized pores would fill and drain somewhere between first and last and would therefore have some intermediate form of water sequestered while having some degree of exchange with new water inputs.

Matrix soil waters are complicated by the various profile development processes, the range of times that waters reside in the matrix and the multiple input waters that may be present simultaneously. Mathieu and Bariac, [1996] explain the location of isotopic values from their soil waters below the local meteoric water line (LMWL) to be the result of a mixing between infiltrating rainwater and waters of the superficial part of the soil which were isotopically enriched." Landon et al. [1999] reported that their soil cores had isotopic values that reflected considerable mixing of infiltrating snow melt, having lower $\delta^{18}O$ values, with immobile (clayey loam) soil matrix water having relatively greater $\delta^{18}O$ values." They speculated that a large volume of immobile water attenuated the changes realized in the matrix water [*Landon et al.*, 1999].

Brooks et al. [2009] postulated that precipitation isotopes were relatively enriched when the shallower soil-water content increased and the smallest pore spaces were first occupied after the dry summer season. "Precipitation over the remainder of the year did not mix fully with water in those small pores." [*Brooks et al.*, 2009] Mathieu and Bariac [1996] reported that the enriched waters of the superficial zone of the soil were partly diluted by the relatively depleted infiltrating rainwater during rainy seasons. Additionally, Frisbee et al., [2008] noted that mixing can occur between newly infiltrating melt water and soil water that reflects previous infiltration. This mixing

creates conditions where subsequent melt water infiltration mixes with soil water that has already undergone various degrees of isotopic alteration with depth [*Merlivat,* 1978]."

Brooks et al., [2009] found that after the initial wetting of soils in the first rains following the dry season small pores spaces were saturated and that precipitation over the remainder of the year did not mix fully with water in those small pores. They attributed this to a two-domain system in which the macropore domain generates lateral subsurface flow and the matrix domain, water that manages to infiltrate, moves very slowly and is subject to transpiration, which causes chloride concentration to increase. This was supported by their observation that bulk soil water was always more depleted in heavy isotopes than lysimeter water collected at the same depth and location [*Brooks et al.*, 2009]. Landon et al. [1999] found that macropore development was common and that preferential flow is likely the dominant flow mechanism.

Once the smallest pore spaces are occupied, water flows vertically through larger pores, and seems not to mix with water in smaller pores during the rainy season [*Brooks et al.*, 2009]. This mixing happens to varying degrees depending on saturation conditions and the degree of macropore presence. Newman et al. [1998] reported that small amounts of dominantly old water flow result when lateral subsurface flow is generated under unsaturated conditions in the lower layer. They also noted declines in the chloride concentrations of effluent collected when flows increased that may have reflected increased preferential flow rates. Increased preferential flow rates reduces the time

available for diffusion of chloride from the soil matrix into the macropores resulting in the lower chloride concentrations observed [*Newman et al.*, 1998].

Brooks et al. [2009] compared chloride concentrations in matrix soil water with those in lateral subsurface flow to find that the two were not equilibrated. They interpreted this as lateral subsurface flow bypassing the salt-rich matrix and moving through macropores. Tang and Feng [2001] noted that if preferential flow was dominant, there would be a long residence time in the matrix. In a different setting, Newman et al. [1998] reported chloride accumulation during periods of no flow and flushing when flow began. They claimed that there must be significant matrix flow because, if macropores were the dominant pathway, then a less marked flushing effect would be expected. With a similar observation, Mathieu and Bariac, [1996] reported that a memory effect remained throughout the rainy season because the enriched waters present in the matrix at the end of the dry season were only partly leached by the depleted rains.

Mathieu and Bariac [1996] provided a fair amount of information about the specific range and geometry of macropores and preferential flow environments. They reported that a small proportion of macropores (0.1-5% of soil volume) can significantly increase infiltration rates. They reported macropores to be of various origin including subterranean fauna, roots channels, and shrinkage cracks in drying clayey soils. Shrinkage cracks were found to extend 0.4 to 0.8 m deep and root penetration was highly variable (0.2 – 1.8 m) and dependent on the vegetation type. They also reported that equivalent minimum diameters of macropores ranged from 0.01 to 1 mm.

3.2.3 Recharge

In any hydrologic study of soil water dynamics, deep percolation and groundwater recharge are topics of interest. In reference to depth profiles used to determine recharge to an arid climate aquifer, Campbell et al. [1996] stated that the isotopic composition of soil water at depth approximates a steady value and that is the composition of recharge water.

To understand recharge, one must understand how precipitation enters, is stored and travels through the vadose zone. In their work with soil hydrology, Barnes and Allison [1988] postulated that in semiarid regions, distributed recharge through the unsaturated zone is strongly biased towards the heavier rainfall events and little to no deep percolation occurs due to the numerous smaller events. Mathieu and Bariac [1996] state that the lightest rains, generally characterized by heavy δD values, are usually intercepted by the vegetation or are absorbed by the soil's top layer and are eventually lost by re-evaporation into the atmosphere.

Brooks et al. [2009] expanded on this idea further and claim that as precipitation becomes increasingly depleted through an event due to rainout effects, it reaches deeper and deeper soil [*Dansgaard*, 1964]. In this way, the upper soil layers will receive the first drops that have been evaporatively enriched as they fell. Once the upper layer is saturated and likewise the atmospheric vapor, more depleted rain will bypass the upper

layers to begin wetting deeper layers. Newman et al. [1998] brought up the notion of a threshold when they reported that the volume of precipitation and antecedent moisture conditions control the effect of various storms on the isotopic composition of lateral subsurface flow. This was supported by their observation that some isotopically distinct precipitation events produced large changes in B-horizon lateral subsurface flow while other isotopically distinct events produced little change at all.

Mathieu and Bariac [1996] found that in their study area, water content increased in the 1-2 m soil layer shortly after the first significant rain of the season while the upper soil layer remained unaffected. They also observed that soil layer between 2 and 3 m showed less frequent and limited variations, suggesting that direct infiltration rarely reached these depths. To further support their conclusion that direct infiltration is due to a conducting macropore system, they reported that the isotopic variations in these two layers were consistent with the isotopic evolution in rainwater, provided that the isotopic composition of rainwater was not modified by the infiltration process. As has been mentioned previously, slight modification to rainwater is consistent with macropore transport [*Mathieu and Bariac*, 1996].

In addition to the vertical variations noted by these researchers, spatially variable recharge patterns exist. Gee et al., [2009] found that lateral flow may dominate on sloping lands, causing down-slope areas to receive excess drainage water. They claim that in cases where there are fine soils that are highly aggregated or otherwise contain macropores, preferential flow conditions move ponded surface waters rapidly downward

through root channels, worm holes and other macropores, giving rise to highly variable drainage. Mathieu and Bariac [1996] identified a bimodal recharge mechanism in which there is both infiltration through soil and recharge that is transmitted by fissure "macroporosity" of fracture systems. Recharge by infiltration through soil, or autotropic recharge, leads to slow and damped variation of the groundwater isotopic composition. The second recharge mode was revealed by the isotopic reaction of groundwater to isolated and isotopically distinct rains and by the sudden rise of the water table in the heart of the rainy season.

Newman et al. [1998] made some instructive observations about the nature of throughflow generation. In their study, they observed that initial throughflow often had both chemical and isotopic compositions that resembled matrix bound water. This is consistent with existing literature that often attributed stream hydrograph rise in large storms to new water or recent precipitation while small event rises were attributed to old water [*Elsenbeer et al.*, 1995; *Návar et al.*, 1995]. Also instructive, and of particular interest to this study, Wilcox et al., [1997] noted that lateral subsurface flow was most active in the spring and moved mostly through dense clay.

3.2.4 Passive Wick Samplers

In order to develop an understanding of these different soil water reservoirs researchers must be able to sample the different reservoirs separately. Passive wick samplers consist of a wick with high capillarity placed in contact with the soil. When soil matrix potential

becomes less negative than that of the capillary wick (often <-60 cm matrix potential), a sample is collected from the soil profile. In a study comparing wick samplers, suction lysimeters and distilled bulk soil samples, Landon et al. [1999] determined that these methods collect different fractions of the total soil water reservoir. Their results showed that wick samplers collected the most mobile soil water, suction lysimeters collected the same mobile water with some less mobile soil water while bulk soil distillate collected all of the water present in the sample or a mixture of the mobile and immobile components.

Gee et al. [2009] noted that wick samplers work best with high drainage fluxes and that there is good agreement between wick samplers and lysimeters in coarse textured soils. Bengtsson and Saxena [1988] as well as Wenner et al. [1991] showed that the percentage of "immobile" water may be less in sandy soils than in more structured soils due to lower moisture contents and smaller, less negative, capillary tensions. Gee et al. [2009] also claimed that in fine soils that are highly aggregated, or otherwise contain macropores, passive wick samplers work much like they do in coarser soils, but for the purpose of measuring fluxes, they are subject to uncertainties associated with preferential flow conditions.

On a functional note, Frisbee et al. [2010] found that their wick samplers tracked soil water evaporation caused by a deepening of the unsaturated zone, not that of evaporation from the sampler, quite well. Landon et al. [1999] suggests that "during infiltration events, soil water collected by wick samplers is more representative of the composition of

mobile water, that is likely to recharge ground water during or soon after an infiltration event, than soil water collected from suction lysimeters or soil cores."

3.3 Tree Studies Employing Stable Isotope Methods

Many studies have employed the stable isotopes of oxygen and hydrogen to determine vegetative source water. Many factors influence how vegetation adapts to its environment and ultimately, how it derives its water. Among these factors are geologic setting, availability of water and type of vegetation. Here we will review previous work that is relevant to this particular study.

The most relevant themes to this study are as follow: available water sources, vegetation type and dimorphic rooting patterns. This study was designed to distinguish between soil water and groundwater usage, not specific soil depth of extraction. Vegetation type will dictate plant ability and preference to exploit different available water sources. The existence of a dimorphic rooting system is closely related to vegetation type and is also highly dependent on geologic and climatic setting. Studies that examined trees, particularly those with dimorphic root configurations, and studies in which soil and groundwater sources were sampled will be the focus of this review.

Several assumptions go into such a study. The main assumption is that there is no fractionation between uptake sources until enrichment in the leaves [*Brunel et al.*, 1997, 1991; *Dawson and Ehleringer*, 1991; *Zimmermann et al.*, 1967]. We also assume that there is no change to isotopic composition within the plant as water is transported to the leaves. We also must assume that soil is laterally homogeneous and that time delays due to transport from soil to plant are not significant. In order to assure that there are no

significant errors due to sampling, extraction or analysis, much care must be taken for these procedures.

When setting out to determine where vegetation derives its water, one must decide how specific to be. The primary concern of this study is distinguishing between soil and groundwater, so depth within soil profile may be more information than is needed. Several previous studies have used stable isotopes to distinguish between soil water and groundwater usage and obtained varying results [*Adar et al.*, 1995; *Brunel et al.*, 1991; *Ehleringer and Dawson*, 1992].

3.3.1 Previous Soil versus Groundwater studies

In a study conducted on a 7 m high eolian dune overlying an aquifer perched on a lacustrine clay layer, Brunel et al. [1991] found that vegetation (*Eucalyptus* spp.) used soil water. This was shown by matching isotopic signatures of vegetation to those of soil water. Additionally, soil matric-potential data was used to exclude soil regions that exceeded the extraction capabilities of roots. They also speculated that plants would not uptake the aquifer water due to its high salinity (TDS ≈ 40 g/L).

In a comprehensive study examining several different species from various geologic settings in Utah, Ehleringer and Dawson [1992] found relationships based on vegetation type. They were able to show that annual vegetation was dependent on summer rains and soil water while different categories of perennials had different levels of groundwater

dependence. Figure 16 shows the results of their findings. Their study showed use of both soil and groundwater as wells as mixtures most likely produced by dimorphic rooting systems.

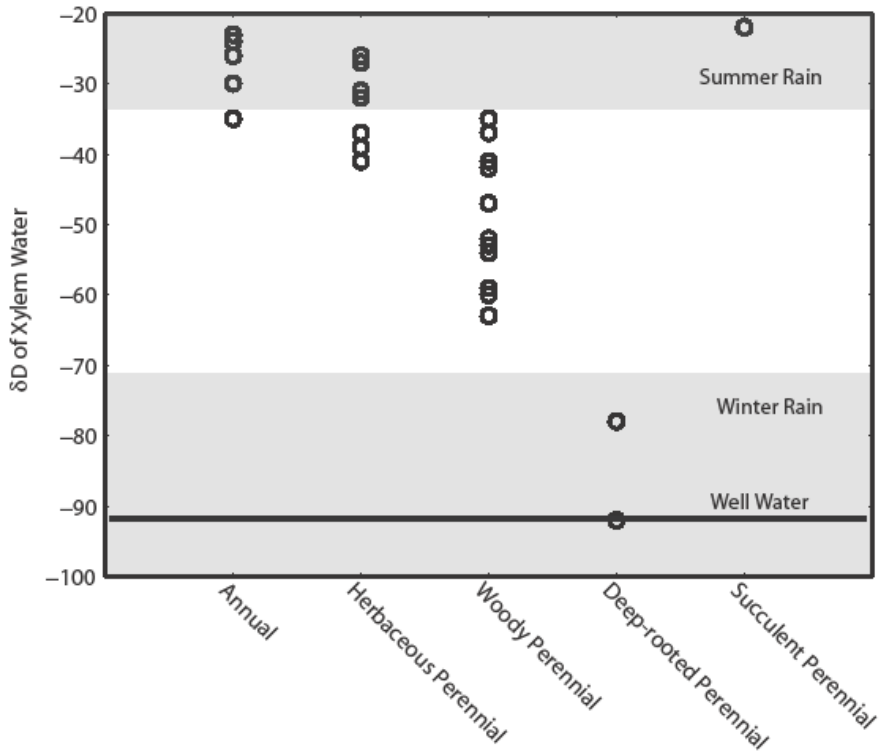

Figure 16: The hydrogen isotope ratio of xylem sap for different species (categorized by life form) at a desert site in southern Utah following summer rains. The gray areas represent the range of hydrogen isotope ratios for both summer and winter rain events. The solid line represents the hydrogen isotope ratio of groundwater at this site. Based on a figure and data in [*Dawson and Ehleringer,* 1991]. [*Ehleringer and Dawson,* 1992]

Adar et al. [1995] examined Tamarisk in the sand dune terrain located in the northwest Negev desert of Israel. They found that both soil water and groundwater contributed to transpiration. They noted a correlation between changes in upper root system soil moisture and changes to the groundwater contribution to total transpiration. These changes ranged from 41% to 59%. They attributed the consistent use of groundwater to difficulties in extracting soil water due to soil water salinity (osmotic potential) and soil

moisture content (matric potential). These factors resulted in an environment in which the hydraulic potential required to lift groundwater was less than that to extract soil water.

3.3.2 Integration of Multiple sources

Another issue in vegetative source-water studies employing stable isotopes has to do with multiple water sources mixing inside the tree. Ehleringer and Dawson [1992] noted that, "if the hydrogen or oxygen isotopic composition of water within xylem sap is analyzed before it has been exposed to evaporative processes, this isotopic composition is an integrated measure of overall water uptake, reflecting the various zone(s) and depth(s) from which the plant is currently extracting soil water" [*Ehleringer and Dawson*, 1992].

Adar et al. [1995] observed that water within deep tap roots had isotopic compositions similar to that of groundwater while water in the main upper root system was significantly enriched. This enrichment reflects a mixing of groundwater, from deeper tap roots with enriched soil water from closer to the surface. They reported this composition to be consistent throughout the rest of the tree.

Tang and Feng [2001], examining soil water dynamics with vegetative water stated that, "plant source water is thus a further integration (than that of soil) of water from multiple precipitation events and of variable degrees of evaporation." They were referring to

different precipitation events that become layered in a soil profile and are then integrated in the tree by the different levels of root uptake.

A problem that may arise due to this in tree mixing is that multiple sources may mix to give a composition that appears to be groundwater. Brunel et al. [1991] stated, "the isotopically depleted water from a previous rainfall event mixed with isotopically enriched soil water resulted in water of similar isotopic composition to groundwater. In the absence of soil isotope data, this may have been interpreted as the tree starting to use groundwater after the reserves of rainfall derived soil water had been depleted." Careful sampling must be conducted to avoid such confusion. Insufficient data could lead to incorrect interpretations.

3.3.3 Dimorphic Root Configurations

The other issue is that of dimorphic root configurations. This refers to root systems that have both an extensive near-surface component in combination with a deeper tap-root system. This rooting configuration allows vegetation to switch between, or simultaneously exploit, multiple water sources depending on source availability. Vegetation with the ability to choose between two water sources at different depths will have an obvious advantage over those with only shallow root systems.

White et al. [1985] found that eastern white pine (*pinus strobus*) switched its water extraction preference depending on recent precipitation events; surface layers were

exploited immediately following precipitation events and deeper layers were exploited as soils dried out. Dawson and Ehleringer [1991] found that many riparian trees did not use stream water but instead relied on groundwater. They attributed this to a "primary investment in the development of a single root system penetrating to deeper, more reliable, water sources" [*Dawson and Ehleringer*, 1991]. They also went on to discuss precipitation thresholds at which vegetation may develop dimorphic rooting systems in which there is an upper branch able to collect summer precipitation or soil water and a deeper zone for utilizing more reliable water sources such as groundwater. Figure 17 shows the relation between the predictability of summer rain and vegetative utilization.

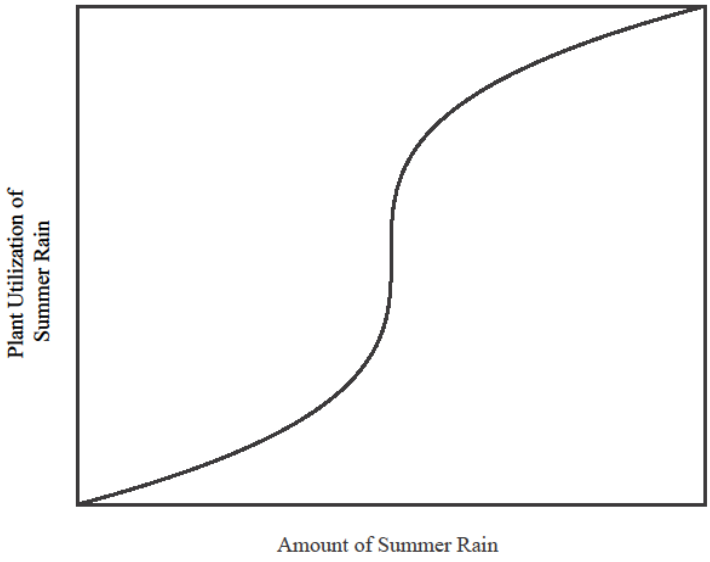

Figure 17: Conceptual model of the relationship between vegetative use of summer rain and amount or predictability of summer rain for plants in climates that receive winter, spring and summer precipitation. Reproduced from Ehleringer and Dawson, [1992].

4 METHODS

4.1 Soil water sampling

To completely understand the soil water end member and subsequently develop an understanding of fracture-bound water, soil water must be characterized. Different methods have been used to collect different types of soil water. For this study, in which the stable isotopes of oxygen and hydrogen were used, it is very important that care be taken to ensure no fractionation takes place while collecting, transporting and processing samples. Bulk soil samples were collected as grab samples with a hand auger and passive wick soil water was collected with passive capillary samplers (PCAPS) at several locations within the watershed. Passive wick soil water and bulk soil water differ in how they are stored, what role they play and how they move through watersheds.

4.1.1 Passive Capillary Samplers

PCAPS are designed to be passive and collect samples only when water in the soil matrix is abundant and likely to be mobile. PCAPS collect samples using a fiberglass wick. Water is collected from the soil matrix when the wick matric potential is greater than the soil matric potential. Soil matric potential varies inversely with saturation such that high saturation conditions have low matric potentials. Matric potential is measured from atmospheric pressure with more negative values being associated greater values. Water naturally flows from low to high matric potentials so that at low soil matric potentials, water moves from the soil to the wick resulting in removal of water from the soil matrix. Saturation conditions and thus, soil matric potentials fluctuate naturally with time so PCAPS collect samples only part of the time as soils dry out and soil matric potentials become greater than that of the wick.

Fiberglass wicks are used in PCAPS construction for their strong capillary properties. Because PCAPS function similar to a hanging water column [*Boll et al.*, 1992; *Frisbee et al.*, 2008], their wicking matric potential is a function of their length. Additionally, PCAPS are extremely convenient due to self sufficient nature. The level of maintenance required is very low, they do not need outside sources of suction and they are not dependent on positive pressure.

PCAPS will collect samples from all time periods when the necessary conditions are satisfied. This period will depend on collection frequency as well as weather patterns and

storm conditions. If PCAPS samples are collected between individual precipitation events, samples may be considered to be representative of those individual storms. If several events occur between sampling, the sample obtained should be considered as an integration of all events during which the PCAP was in place.

Construction

Following the methods of Frisbee et al. (2008), PCAPS were constructed using 9.5 cm (3/8 inch) diameter fiberglass wick. The wick was first soaked in deionized water for several days in order to remove any manufacturing residues that may have been present. This process was repeated 3 times to ensure the removal of all residues and wick was allowed to dry.

Approximately 17.8 cm (7 inches) of wick was coiled upon itself to form a disc like a fiddlehead fern with a surface 3-4 cm across. The fiddlehead was secured using a zip tie wrapped from the middle to one side of the surface. The tail of the wick was then inserted into a Tygon® tube (5/8 inch (1.59 cm) outer diameter, 3/8 inch (0.95 cm) inner diameter). Wick length averaged 60 cm (24 inches) but varied in order to adapt to field installation requirements. Wick length determines wick matric potential (ψ_{wick}) such that wick length equals matrix potential at soil fluxes equal to zero [*Frisbee et al.*, 2008; *Knutson and Selker*, 1994]. The design should aim to create a matric potential continuum between the wick and the soil matrix such that water movement is caused only by the capillary forces of the wick. The average wick length and corresponding matric potential

used in this study was 60 cm. This length was chosen over some of the shorter versions commonly employed (30 cm) because of its increased wicking potential. 30 cm gives about -2.94 kPa wicking potential while 60 gives -5.88 kPa. Matric potentials in Douglas Fir stands were measured by Brooks et al. [2009] to be -300 kPa at 1 m depth to -1,200 kPa at 20 cm.

The tubing was trimmed such that the wick was slightly longer than the tubing, allowing the wick hang out the end. The tubing and wick assembly was then inserted into a predrilled Nalgene® polyethylene lid and the junction was sealed with silicone in order to prevent leakage or flow along the outside of the tubing. To complete construction, 500 and 1000 mL Nalgene® polyethylene collection vessels were attached to the tube, wick and lid assembly.

Installation

Ten PCAPS were placed on thinned and control plots in both the valley bottom and on the ridge top. Locations were chosen based on proximity to trees to be sampled. Valley-bottom installations were dug first with a hand auger and then widened using a posthole digger. Pits were dug to bedrock, interlocking saprolite or about 1 m depth, whichever came first. Ridge-top installations were dug by removing large stones and as much more material after that as was possible.

Figure 18: Photograph of RT 2 PCAPS installation.

Figure 19: Close up photograph of RT 2 PCAPS installation.

Small holes were dug laterally approximately 13 cm (5 inches) into the upslope face of pits. PCAPS fiddleheads were then placed in these lateral holes and backfilled with material that had been removed. Mineral oil was poured into the Nalgene® polyethylene collection vessels to form a trap that isolated the water from evaporative and exchange processes. Vessels were secured in the pit whether by propping into position with a rock for shallow ridge-top locations or by supporting with an appropriately sized stick for the upper PCAPS in deep valley-bottom pits. Pits were then covered with plywood covers

dug slightly into the ground and covered with natural debris in order to mask their presence.

Collection

Samples were collected from PCAPS by digging up and removing plywood covers. Nalgene® polyethylene collection vessels were then removed from the wick, tubing and lid assembly and the sample was poured into an 8 oz. Ziplock® baggie. The sample was then allowed to settle to a corner of the baggie and then cut with a scissor to get the water sample from below the mineral oil.

4.1.2 Bulk soil water

Initial bulk soil samples were collected from excess material as PCAPS pits were being dug. Bulk soil samples are grab samples designed to include water bound in small pore spaces as well as any more mobile water that may be present in the sample. The location of these pits was already considered and designed to be close to sample trees. Further bulk soil samples were removed with a hand auger near trees being sampled.

Soil samples were placed and stored in quart-sized mason jars with screw band SNAP lids [*Newman et al.*, 1998]. Sample jars were further sealed with parafilm to prevent any evaporation or atmospheric exchange.

Distillations

Water was distilled from bulk soil samples by first placing 60-100 g of the sample material in a closed glassware system and placing the sample side of the system in a liquid nitrogen bath to immobilize the water present. More intact, clay-rich, samples were broken up to allow more evaporation and decrease distillation time requirements. The system was then put under vacuum (≈350 mbar) and resealed. Next, heat was applied with a southern-hemispherical-shaped hotplate to drive off soil bound water which was collected with another liquid nitrogen bath on the other side of the system. The original sample, the dried soil material and the distilled water were all weighed for calculation of moisture content and verification of water recovery. Sample distillate was stored in 30 mL glass vials fitted with polycone sealing caps.

4.2 Tree water sampling

Trees were selected based on location and likelihood of proximity to aquifers. Trees were selected in both ridge-top and valley-bottom locations (Figure 20). This sampling configuration was designed to test the hypothesis that valley-bottom trees would likely have access to and use shallow groundwater while ridge-top trees would have only soil water available. Trees located near spring discharges were chosen for their likelihood to use shallow groundwater.

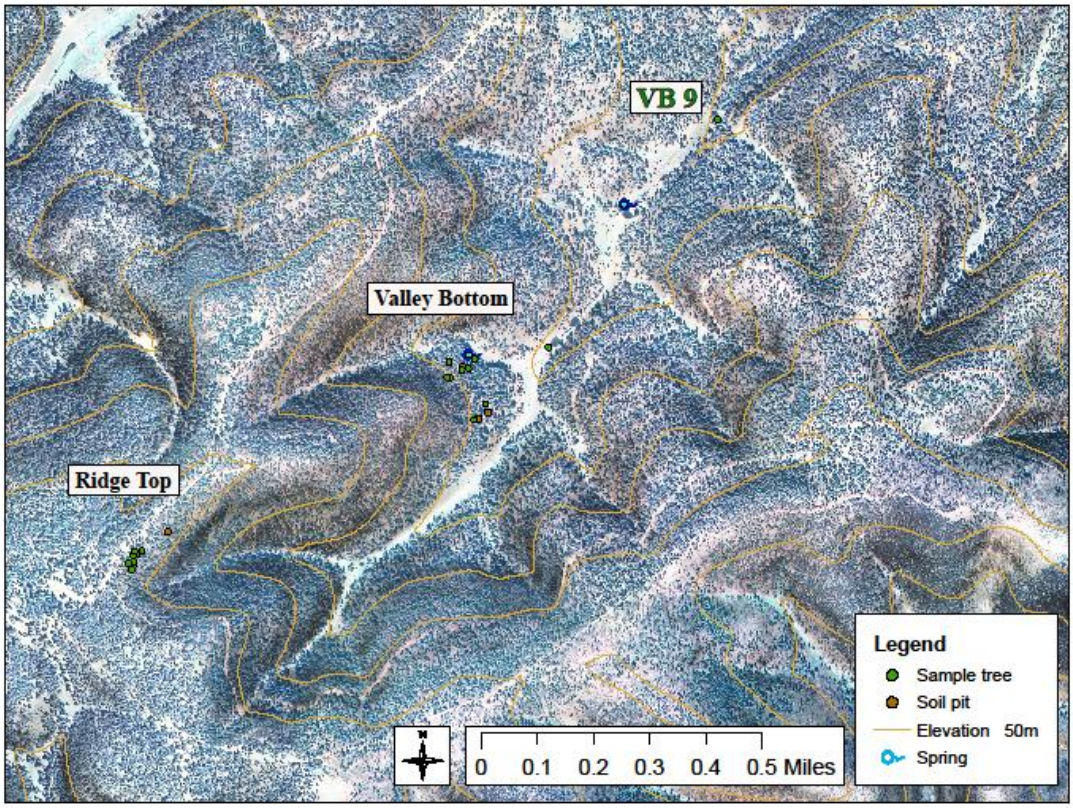

Figure 20: Map of watershed where study is being conducted. The ridge-top and valley-bottom locations were chosen to validate the hypothesis that trees would use shallow groundwater if available. Control and paired-plot locations were chosen for data sharing from a simultaneous soil moisture study. The VB 9 sampling location is shown because it is not in the range of the valley-bottom map.

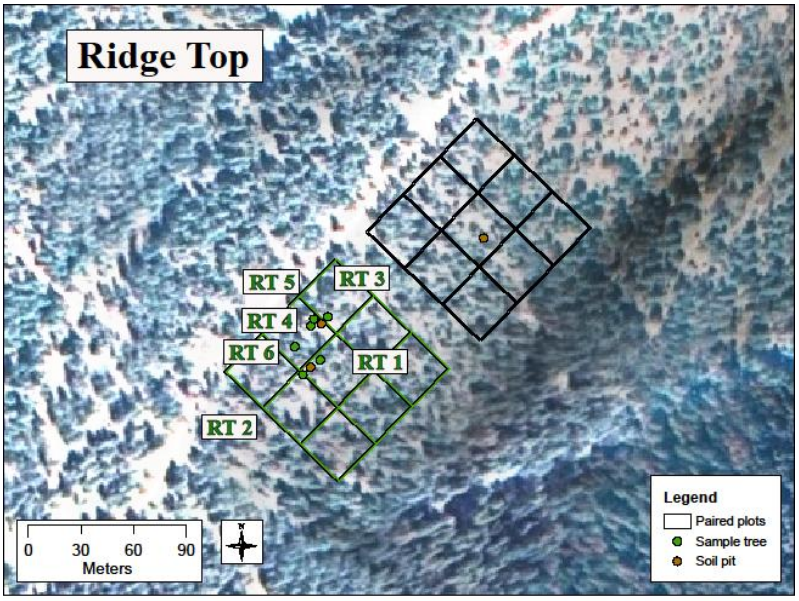

Figure 21: Map of ridge top sample sites. Satellite photo was taken before thinned plot trees were cut. The black boxes delineate the thinned plot and the green boxes delineate the control plot. Sample tree locations are green dots closest to respective label. Soil sampling locations are named based on the tree near them. Tree samples were taken only from the control plot due to the absence of trees on the thinned plot.

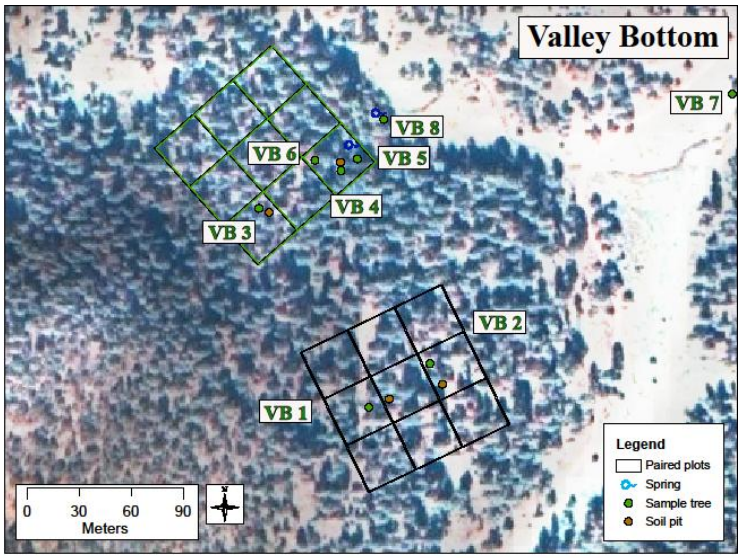

Figure 22: Map of valley-bottom sample sites. Satellite photo was taken before thinned plot trees were cut. The black boxes delineate the thinned plot and the green boxes delineate the control plot. Sample tree locations are green dots closest to respective label. Soil sampling locations are named based on the tree near them.

Trees were selected on thinned and control paired plots. These locations were chosen for three reasons. The first was for data coverage from a simultaneous study. The second was the guarantee of not being disturbed by thinning during the study. The third reason was for comparison of water usage patterns on the control and thinned plots.

Trees were selected based on availability of appropriately sized and accessible twigs. Availability of twigs for further samplings was considered when initially selecting individual trees. Twigs with a maximum diameter of about 2 cm were cut from the tree with pruning shears and limbs smaller than 0.5 cm diameter were trimmed off. The bark was left on to provide an extra layer of evaporative protection to the inner xylem. Samples were trimmed to fit into Ziploc® baggies (5-6 inch sections), wrapped in cellophane, placed in a Ziplock® baggie and stored on ice until returned to lab. In the lab, twig samples were stored in a freezer to immobilize water and minimize alteration of isotopic composition.

Distillations

Water was extracted from tree samples using cryogenic vacuum distillation similar to procedure described for bulk soil samples. However, heat for tree samples was supplied with a boiling water bath in order to cap maximum temperatures and prevent oxidation of the sample. Additionally, activated carbon was added to tree sample distillate to help reduce the milky appearance.

To quickly review the key points, sample twigs were removed from the freezer and debarked. Debarking was done using a Swiss Army pocketknife to shave off the heavy outer bark. The dull side of a plastic knife was then used to scrape off the softer inner bark and cambium. This is the fastest way the author found to remove bark. The time spent debarking should be minimized because the twig will quickly begin to thaw and dry out, which can cause fractionation.

Twig samples were cut into approximately 1 cm sections and placed in a 1000 mL distillation vessel until 15-20 g of material was present. The distillation vessel was sealed, frozen under a liquid nitrogen bath and vacuum evacuated. Once the system was evacuated to approximately 300 mbar, the distillation vessel was placed in a boiling water bath heated by a hotplate. The resulting distillate was captured in a liquid nitrogen trap. Distillate was then stored in 30 mL glass vials fitted with polycone sealing caps to prevent evaporation. Activated charcoal was placed in the storage vessel to reduce organic content and milky appearance. Twig samples were weighed before and after the distillation procedure to determine water content.

4.3 Precipitation sampling

Precipitation was collected using a PVC collector mounted to a T-bar. The PVC collector consists of a vertical PVC tube with open top and bottom attached to a funnel. The funnel channels precipitation into a tygon tube that runs to a gallon glass collection jug. A hole the size of the tygon tubing was drilled in the lid of the collection jug and the

tubing was run to the bottom of the jug. Mineral oil was placed in the jug so as to prevent evaporation of precipitation collected.

4.4 Stable Isotopes

Isotopes can be separated into stable and radioactive isotopes. Radioactive isotopes decay over time and can be used to date materials in which enough information is known while stable isotopes maintain the number of neutrons in their nucleus. This discussion will focus on stable isotopes.

Isotopes are atoms of the same element that have varying atomic weights due to a different number of neutrons in their nuclei. An element's chemical property is dictated by its charge balance which is directly related to the number of protons in the nucleus. All isotopes of the same element have the same number of protons in their nucleus and thus behave the same in chemical reactions. However, due to the different masses arising from having different numbers of neutrons, isotopes proceed through physical processes slightly differently, especially those where kinetic energy is important. The equation for kinetic energy is

Equation 1

$$KE = \frac{mv^2}{2}$$

Where KE is kinetic energy, m is mass and v is velocity. Different isotopes in the same conditions will on average have equal kinetic energy, leading to heavier isotopes having lower velocities. This will dictate how they proceed through a physical reaction such as a

phase change. This difference is what allows us both to make inferences from as well as measure isotopic abundances.

Processes that cause the abundance of an isotope in some material to change are said to fractionate them. This refers to fractioning or partitioning the original isotopic distribution within some substance to some new distribution, often split between two phases. The most common form of fractionation for water is evaporation.

Craig [1961] collected precipitation samples all around the world and established the global meteoric water line (GMWL), a trend line upon which precipitation samples can be expected to plot. This line is given by $\delta D = 8*\delta^{18}O + 10$.

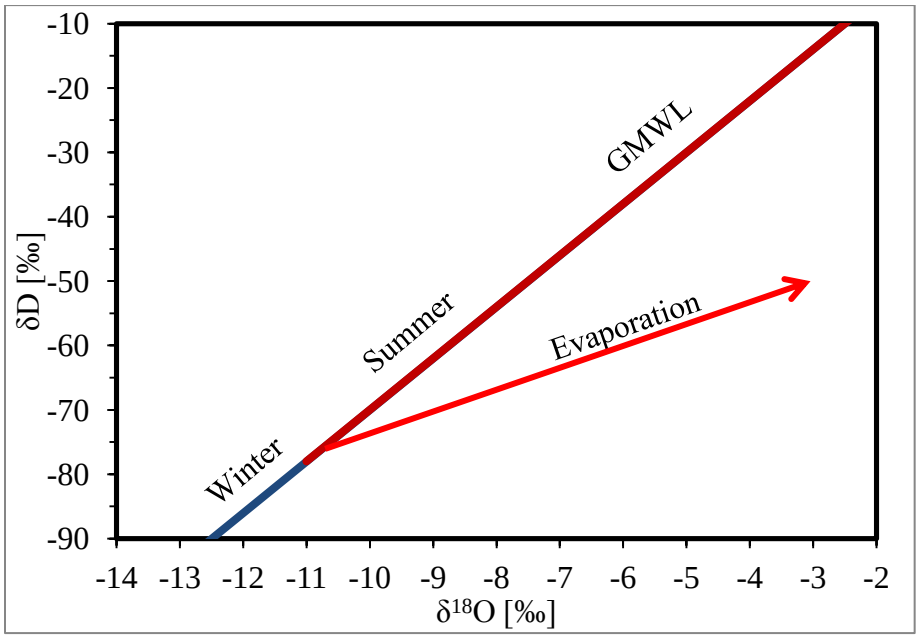

Figure 23: The global meteoric water line (GMWL) and a typical evaporation trend line on a $\delta^{18}O$ vs. δD plot. The upper right portion of the line is red and labeled summer to distinguish it from lighter winter precipitation values. The transition between these two types of precipitation will vary with location.

Dansgaard [1964] identified the difference between equilibrium and kinetic processes as well as several factors that contribute to the isotopic composition of precipitation. Among them are condensation temperature, amount of rain per event and elevation. Important to this study are the kinetics that lead to a deuterium excess, elevation effects and seasonal differences caused by condensation temperature.

4.4.1 Stable isotope analysis

Extracted water samples were analyzed on a Picarro Cavity-Ring-Down Spectrometer for the abundances of the stable isotopes of hydrogen and oxygen. Isotopic values are reported in delta notation (δ) as per mil (‰) values (parts per thousand). δ values are defined as

Equation 2

$$\delta = \left(\frac{R_x - R_{std}}{R_{std}}\right) * 1000$$

where R is the ratio of the heavy isotope to the light isotope, *x* is for the sample and *std* is the standard. For oxygen, R is $^{18}O/^{16}O$, the number of ^{18}O atoms divided by the number of ^{16}O atoms. The standard is commonly standard mean ocean water (SMOW). δ values then, are the abundances of a particular isotope in a sample compared to that of SMOW. Standard deviation for measurement on this method is 0.14 ‰ for $\delta^{18}O$ and 0.70 ‰ for δD on this machine.

4.4.2 Spectral Interference

Spectral interference is a complication associated with stable isotope analysis using isotope ratio infrared spectroscopy (IRIS). This method of analysis uses photo absorption of an infrared laser by H2O molecules to calculate the isotopologues of water via spectroscopy. The bonds between heavier isotopes of hydrogen or oxygen have different bond energies that can be detected with different laser frequencies. Organic compounds present in distilled tree and soil samples can interfere with this process and cause erroneous calculated isotope abundances. Spectral interference can cause deviations as large as 15.4 ‰ and 46 ‰ for $\delta^{18}O$ and δD respectively [*West et al.*, 2010].

Spectral interference was analyzed using the procedure recommended by the manufacturer (Picarro, Inc.). Inner cavity H_2O level data was used to identify injections. Injections were identified as periods when inner cavity H_2O levels were above some minimum value (15,000 ppmv). This value is on the slope of the injection peak so injection peaks were further refined by eliminating 13 time steps after that minimum value was achieved in order to examine only the peak levels of the injection. The end of the injection interval was determined by flagging the same minimum value and eliminating 2 time steps backward in time, toward the injection peak. With the injection peak identified, standard deviation residuals were examined during these peaks. The standard deviation residuals of the 5 calibration samples were averaged and used to compare the quality of other injections. Each subsequent injection was divided by that

average and variation of 30% or more (values outside the range of 0.7 to 1.3) were flagged as having spectral interference and that injection data was thrown out.

4.5 Sap flow sensors

In watershed and ecological studies, sap flow is useful in many respects. It can be used to develop an estimate of transpiration, to understand how trees respond to precipitation inputs, to monitor seasonal trends or simply to monitor individual tree health. For this particular study it was chosen in order to develop an understanding of residence time within an individual tree. Understanding residence time helped to determine when markedly different precipitation inputs such as summer monsoon events may manifest in twig samples.

Theory

Granier style sap flow sensors operate under the assumption of conservation of thermal energy. A known amount of energy is introduced to the system and under no flow conditions, a pure thermal gradient is established. This pure thermal gradient is used as a boundary condition in calibration. Variations from this pure thermal gradient are generated as sap flow begins to advect thermal energy out of the system. By understanding some of the thermal properties of the tree material and calibrating to known sap flow velocities, in situ sap flow velocities can be monitored.

Temperature differences are measured with copper-constantan thermocouple pairs. The system consists of two thermocouples, one with a heat generating coil, wired together such that only the temperature difference between them is recorded by way of millivolts. Sensors are placed in a tree 10 cm apart, the heating coil above the reference sensor.

Construction

Sensors were constructed based on the instructions provided by Center for Embedded Networked Sensing, UCLA (http://www.cens.ucla.edu/pub/EnvironmentalSolutions/Sapflow_Tutorial.html). To quickly review, holes approximately 10 mm from the base of hypodermic needles were produced with a file before the needle was cut to 21 or 11 mm with a needle disposal box. The end was then filed down smoothly and the needle scoured out.

A 36 gauge copper-constantan thermocouple wire was soldered together in approximately 15 cm lengths to form thermocouples. Thermocouples were then inserted, loose ends first into the end of the cut hypodermic needle until the thermocouple was near the hole filed at10 mm from the base. A drop of runny superglue was then applied to the hole where it fixed the thermocouple wire in place. Superglue was also applied to the base of the needle to further secure the thermocouple. Heat producing sensors were constructed in the same way with the addition of a 60 cm constantan wire into the needle with the thermocouples. The constantan heating wire was then coiled tightly around the needle to

the base where it entered the base of the needle via a hole made by another hypodermic needle. It was secured with super glue similarly to the sensor with only thermocouples.

Installation

Appropriately sized holes (2 mm for heated sensors and 1 mm for reference sensors), were drilled in trees. The larger hole (approximately 10 cm above the smaller hole) was fitted with an appropriately sized aluminum sleeve. The heated sensor was covered in thermally conductive silicone heat sink compound and placed in the sleeve in the upper hole. The reference sensor was placed in the lower hole and the constantan wires of the two sensors in the pair were soldered together. The copper wires were then soldered onto a wire running to a data logger (Campbell Scientific CR10 and CR10X). The constantan heating wires were soldered to wires running to a constant current circuit supplied with 12 V from the data logger. The current was adjusted according to the resistance of the circuit to deliver 0.2 W.

The installation was covered with reflective thermal insulation wrapped around the tree and secured with duct tape. Power to the data logger was supplied by a 12 V marine battery that was maintained by a 10 W solar panel. The data logger was set to collect average differential voltages [mV] over 20 minute and 1 hour intervals.

Differential voltages were converted to temperatures which, in turn, were converted to sap flux (J_s; g m^{-2} s^{-1}) using Granier's empirical calibration [*Granier*, 1974] as follows

Equation 3

$$J_s = 119k^{1.231}$$

where:

Equation 4

$$k = \frac{(\Delta T_m - \Delta T)}{\Delta T}$$

and ΔT_m is the predawn temperature difference when sap flow is assumed to be zero. This maximum temperature value was taken from more than a single day (usually 3 days) so as to account for days when some nocturnal transport process was active.

5 RESULTS

To understand where trees derive their water supply, it is important to understand the sources available. Regional groundwater and precipitation trends were discussed in the study area section and will not be covered here. This section will present and discuss soil water data from distilled bulk soil samples, passive-wick soil water samples and tree-water samples in the context of the regional precipitation trends presented earlier. Symbols used for data presentation are shown in Table 1, soil descriptions in Table 2, paired plot sampling locations in Table 3 and tree descriptions in Table 4.

Table 1: Symbols used in presentation of results

Bulk Soil Water	▲
PCAPS Water	■
Tree Water	♦
Soil Moisture/ Precipitation	●

Table 2: Soils

Sample	Location	Position	Texture
VB 1- 10	Thinned Plot	Upper Slope	Sandy Clay Loam
VB 1- 25			Sandy Clay Loam
VB 1- 40			Sandy Clay
VB 2- 15	Thinned Plot	Lower Slope	Clay Loam
VB 2- 25			Clay
VB 2- 40			Clay
VB 2- 55			Clay
VB 2- 65			Clay
VB 3- 20	Control Plot	Upper Slope	Sandy Clay Loam
VB 3- 35			Clay
VB 3- 50			Clay
VB 3- 75			Clay
VB 3- 95			Clay
VB 5- 30	Control Plot	Lower Slope, Above Spring	Sandy Clay Loam
VB 9- 25	Unthinned Area	Bottom of Draw	Silty Clay Loam
VB 9- 45			Clay Loam
VB 9- 65			Clay Loam
VB 9- 85			Clay Loam
RT 2- 5	Control Plot	Upper Slope	Clay Loam
RT 2- 20			Silty Clay Loam
RT 2- 30			Clay
RT 2- 40			Clay Loam

RT 3- 15	Control Plot	Upper Slope	Sandy Clay Loam
RT 3- 30			Sandy Loam

VB- Valley-bottom sites as.
RT- Ridge-top sites
Numbers refer to sample depths in cm.

Table 3: Paired plot locations

Pair Plots				
	Easting	Northing	Elevation [m]	Elevation [ft]
VB Control	444013	3640770	2379	7805
	444073	3640700	2379	7805
	444005	3640640	2405	7892
	443946	3640710	2398	7866
VB Thinned	444111	3640630	2378	7802
	444150	3640550	2372	7783
	444069	3640510	2391	7845
	444030	3640590	2406	7892
RT Control	443116	3640200	2565	8417
	443180	3640140	2548	8358
	443117	3640070	2549	8362
	443053	3640130	2573	8441
RT Thinned	443196	3640280	2565	8416
	443261	3640220	2542	8340
	443198	3640150	2544	8346
	443133	3640210	2565	8416

Coordinates give four corners of the experimental paired, control and thinned plots. More specific sampling locations within the plots can be found in Figure 21 and Figure 22. VB denotes valley bottom and RT denotes ridge top. Easting and Northing are UTM coordinates.

Table 4: Tree descriptions and color coding for data points.

Tree	Location	Position	Tree Type	DBH* [cm]	Height** [m]	Tree Density [/hect]	Color-Desc.	Color
VB 1	Thinned Plot	Upper Slope	Douglas Fir	35	15	10	Open, Red Border	
VB 2	Thinned Plot	Lower Slope	Douglas Fir	35	15	10	Open	
VB 3	Control Plot	Upper Slope	Douglas Fir	10	4.5	2964	Black	
VB 4	Control Plot	Lower Slope, Above Spring	Douglas Fir	8	1.5	2964	Cyan	
VB 5	Control Plot	Lower Slope, Next to Spring	Douglas Fir	60	18	2964	Cyan, Black Border	
VB 6	Control Plot	Mid Slope, Above Spring	Douglas Fir	8	4.5	2964	Not Used	
VB 7	Valley Floor	Next to Collection Pond	Douglas Fir	15	6	2	Brown	
VB 8	Unthinned Area	Below Spring	Douglas Fir	8	4.5	2964	Magenta	
VB 9	Unthinned Area	Bottom of Draw	Western White Pine	15	7.5		Yellow, Black Border	
RT 1	Control Plot	Upper Slope	Douglas Fir	25	12	1482	Not Used	
RT 2	Control Plot	Upper Slope	Douglas Fir	13	4.5	1482	Blue	

RT 3	Control Plot	Upper Slope	Douglas Fir	20	12	1482	Not Used	
RT 4	Control Plot	Upper Slope	Douglas Fir	5	3	1482	Green	
RT 5	Control Plot	Upper Slope	Ponderosa Pine	5	3	1482	Not Used	
RT 6	Control Plot	Upper Slope	Douglas Fir	15	7.5	1482	Purple	

* Diameter at Breast Height

** Heights were estimated and should not be used to make further inferences.

5.1 Spring Water

To determine the source of tree uptake, the end members must be characterized. Spring discharge is often used as a proxy for groundwater. Spring water samples collected in Three L Canyon plot in a group on the groundwater trend line near its intersection with the local meteoric water line (Figure 24).

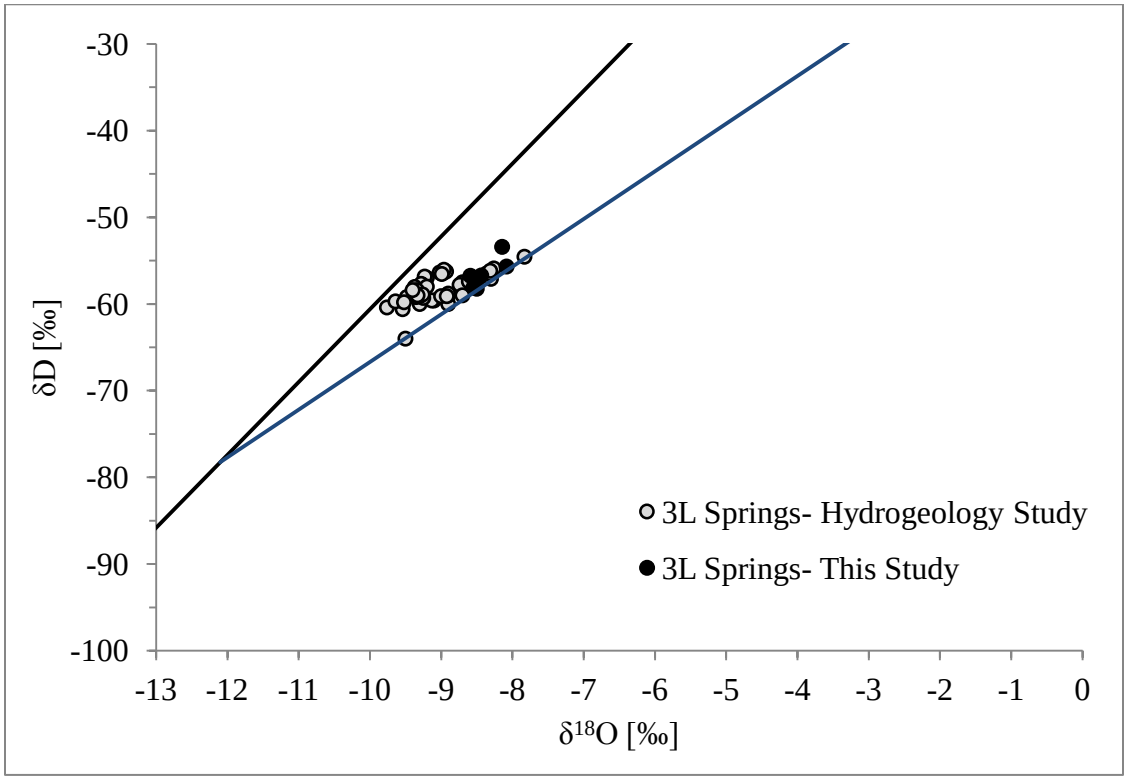

Figure 24: Spring water samples collected in Three L Canyon plotted on a $\delta^{18}O$ vs. δD plot. Spring samples from 2007 to present are shown in the hydrogeology study data and samples collected in 2011 for this study are shown. Spring water values plot near the intersection of the groundwater trend line with the LMWL. Spring samples from Three L Canyon have not plotted heavier than -7.5 ‰ with respect to $\delta^{18}O$ since 2007.

The tight grouping of spring samples collected in Three L Canyon demonstrates the stability of the groundwater system. The location on the groundwater trend line near the intersection with the LMWL shows little evaporation. This is consistent with the high mountain location of the watershed and the findings of Newton et al. [2012] who reported that isotopic enrichment increases along regional flow paths. This watershed's high elevation location in the recharge area has not allowed for significant evaporation along the flow path. Further plots will continue to show the groundwater trend line but it should be kept in mind that groundwater from this watershed plots near the intersection with the LMWL.

5.2 Bulk Soil Water

5.2.1 Data

To determine where trees derive their water for transpiration, soil-water end members must be constrained. It is important to understand both spatial and temporal variability as well as to identify common trends. Several soil profiles were sampled during this study by both collection of bulk soil and by passive capillary wick water extraction. Moisture content and isotopic abundances were measured and their results will be presented in such a way as to compare spatial and temporal variability with an emphasis on comparisons between ridge-top (RT) and valley-bottom (VB) locations as well as thinned vs. control plots. The more illustrative results will be presented here and all results can be found in Appendix II.

Comparison between ridge-top and valley-bottom soils is important because of the underlying geology. The different geologies give reason to suspect that recharge mechanisms and vegetative usage patterns may be different. This comparison is complicated by the different range of depths to which samples can be recovered. Ridge-top soils are shallow, generally 40 cm or less. Ridge-top soil pits were often started by removing large stones, which rendered near surface samples unavailable.

Comparison between thinned and control plots is important because we aim to build an understanding of the changes caused by tree thinning. We will start by presenting all soil

samples and building generalizations from them. We will then examine some individual profiles and categorize the different trends encountered.

The $\delta^{18}O$ and δD values for all distilled bulk soil samples are shown in Figure 25. These values tend to plot together below and to the right of both the LMWL and the groundwater trend line.

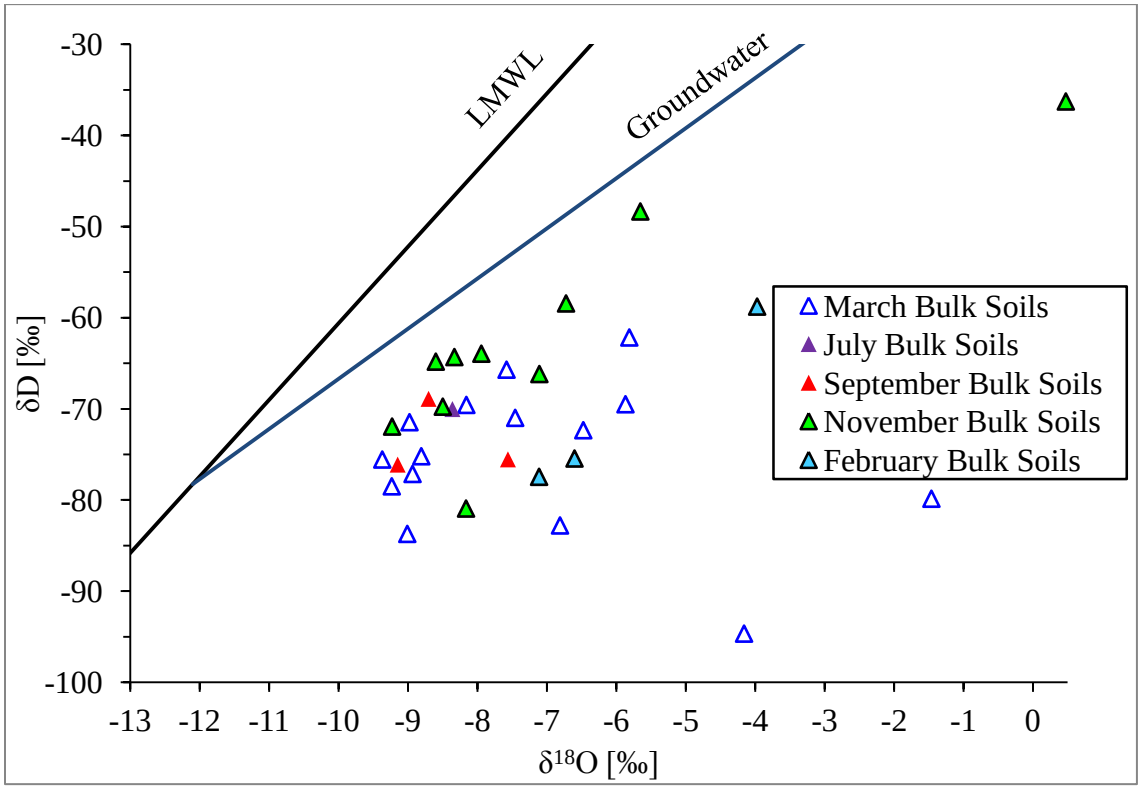

Figure 25: Bulk soil samples plotted by time of sample collection on a $\delta^{18}O$ vs. δD plot. Symbol sizes are approximately equal to the error associated with analysis (± 0.14 ‰ for $\delta^{18}O$ and ± 0.70 ‰ for δD). Most of this data tends to group together in a distinct region. The local meteoric water line (LMWL) and groundwater trend line are shown for reference.

Regardless of sampling time or location, bulk soil water samples tend to plot in the same general area suggesting that spatial and temporal variability is low relative to that of

precipitation [*Dansgaard*, 1964; *Newton et al.*, 2012]. Values tend to fall within the range of -10 to -5 for $\delta^{18}O$ and -85 to -60 for δD. The field within which bulk soil waters tend to plot suggests evaporation from an isotopically light meteoric origin. This grouping gives confidence that more sampling would yield similar results. We will now examine soils based on timing of sample collection.

March 2011

Much can be gained through examination of individual depth profiles. Here we will examine them both by depth and on $\delta^{18}O$ vs. δD plots. The soil profiles seen in Figure 26 exhibit a pronounced decrease in gravimetric moisture content and a slight increase in isotopic values toward the surface. The data in Figure 27 exhibit a strong linear trend.

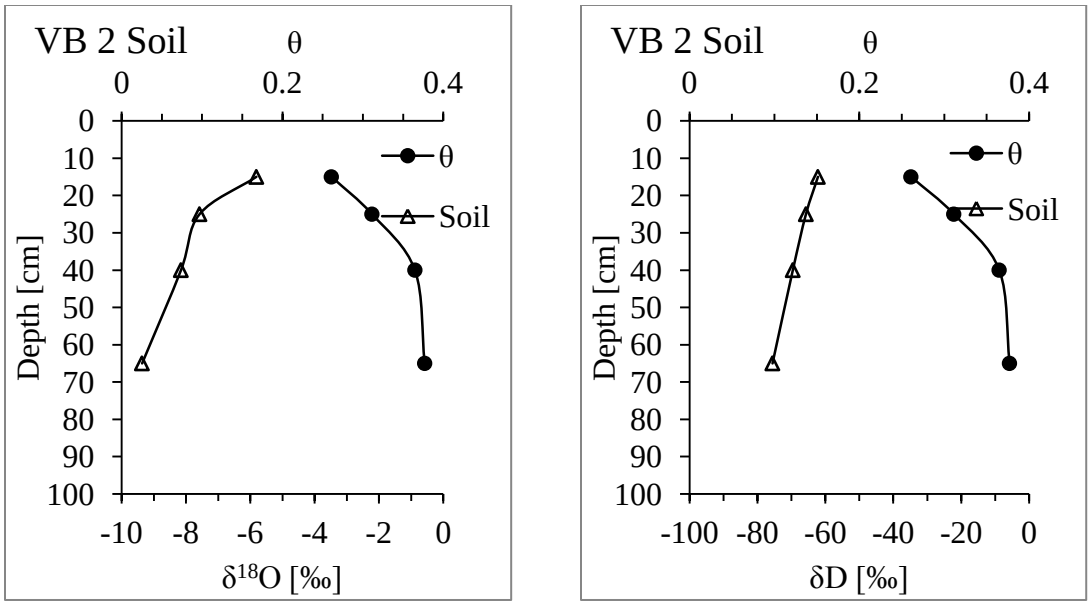

Figure 26: Gravimetric moisture content (θ) and stable isotope values (δ) vs. depth for bulk soil samples taken from VB 2 in March 2011. Corresponding tree water isotope values are also shown as diamonds. Gravimetric moisture content is plotted on the upper x-axis while soil and tree water isotope data is plotted on the lower x-axis. The plot from which these samples were taken has been thinned and has a tree density of 10 trees/hectare. Isotopic enrichment and decreased soil moisture are seen near the surface.

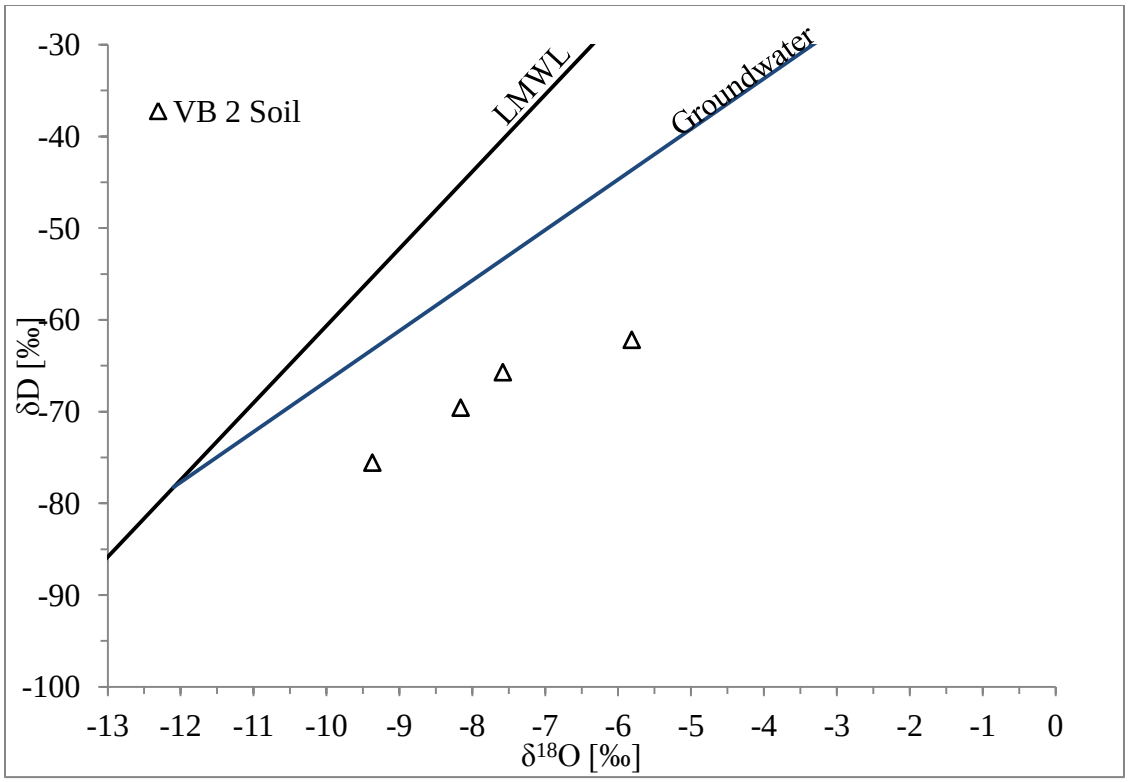

Figure 27: Tree water and bulk soil water isotope data from the VB 2 location sampled in March 2011 plotted in $\delta^{18}O$ vs. δD space. The symbol sizes are approximately equal to the error associated with analysis (± 0.14 ‰ for $\delta^{18}O$ and ± 0.70 ‰ for δD). The local meteoric water line (LMWL) and groundwater trend line are shown for reference.

The pronounced decrease in gravimetric moisture content with a corresponding increase in isotopic values toward the surface is consistent with evaporative depletion of moisture from the upper soil profile causing isotopic fractionation and subsequent enrichment in that region. The highly linear trend on the $\delta^{18}O$ vs. δD plot indicates evaporation of water from a single source.

This location, being on a thinned plot, is exposed to high solar radiation and consequential high evaporative demand. This form of the depth profile indicates that no new precipitation inputs were introduced for a period of time sufficient to develop this

profile. This is significant because it suggests that snowmelt infiltrated a substantial amount of time previous to sampling which is consistent with in situ soil moisture data (Appendix II,). The time required for such a profile to become established depends on the soil type as well as the environmental conditions [*Barnes and Allison*, 1988].

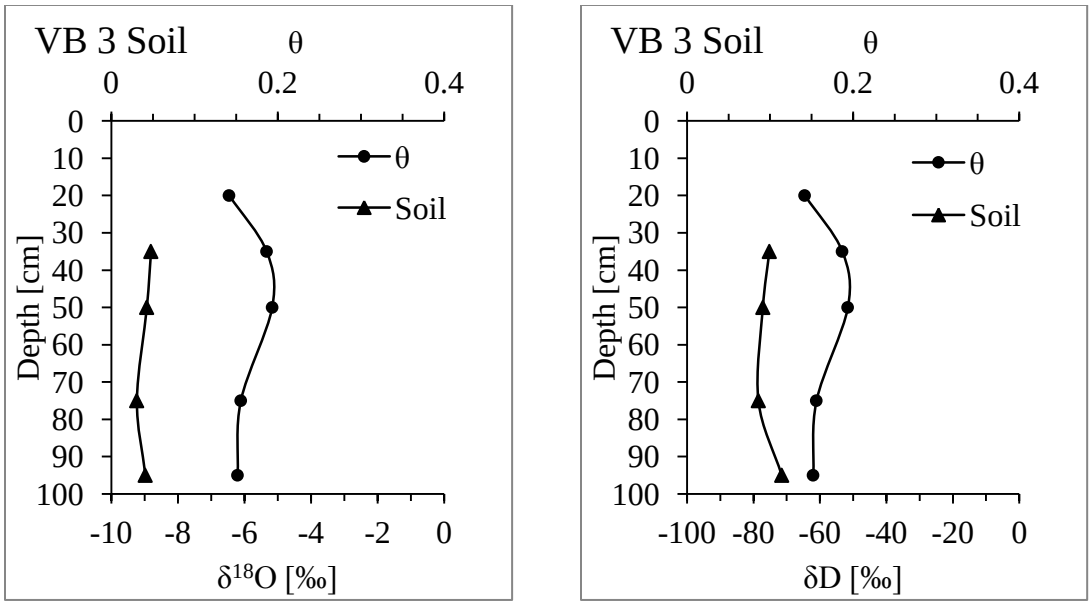

Figure 28: Gravimetric moisture content and stable isotope values vs. depth for bulk soil samples taken from VB 3 in March 2011. The inconsistency between the number of soil moisture and isotopic data points is due exclusion of data points based on spectral interference. The plot from which these samples were taken has a tree density of 2964 trees/hectare.

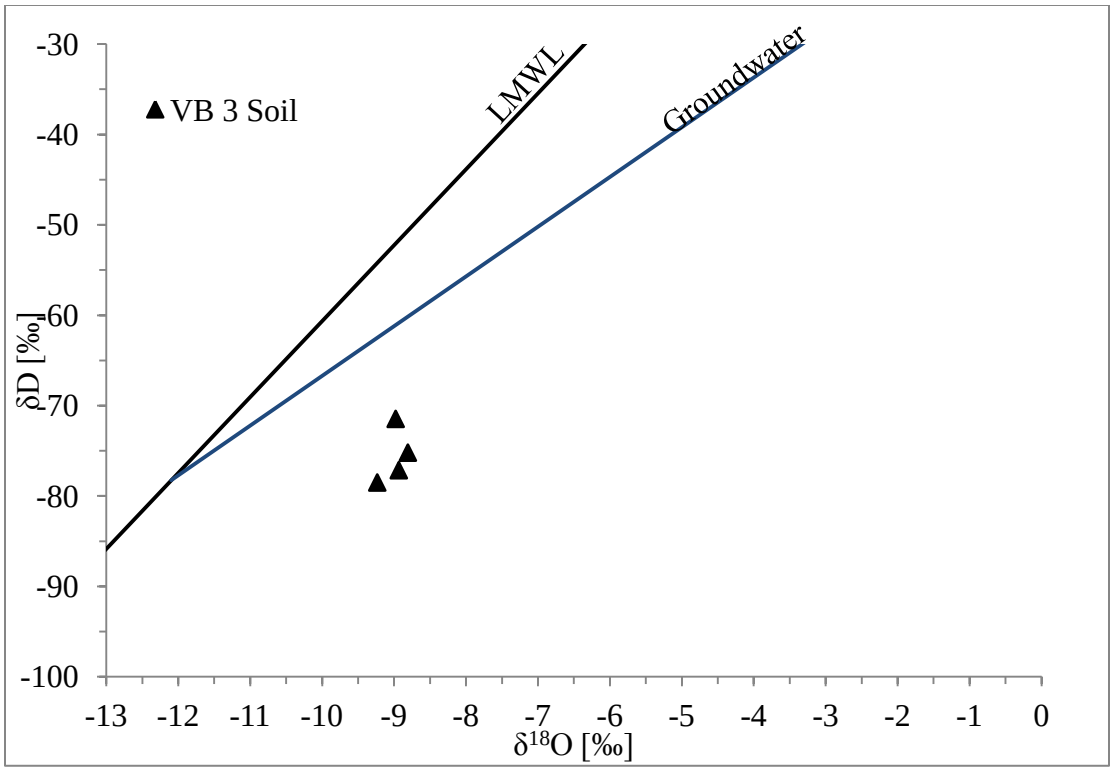

Figure 29: Bulk soil water isotope data for samples collected at the VB 3 location in March 2011 plotted in $\delta^{18}O$ vs. δD space. The symbol sizes are approximately equal to the error associated with analysis. The local meteoric water line (LMWL) and groundwater line are shown for reference.

The soil profile seen in Figure 28 exhibits a pronounced pulse of increased moisture content beginning at about 35 cm depth. Both $\delta^{18}O$ and δD exhibit fairly stable values with depth and slightly heavier values at the bottom of the profile. On the $\delta^{18}O$ vs. δD plot (Figure 29), no linear trend is evident and bulk soil water values plot quite close together.

The pulse observed in soil moisture is likely a manifestation of infiltrating snowmelt moving slowly through a high-clay-content layer. Light isotope values observed in the upper portion of the profile (Appendix 1, Table 6) agree with recent snowmelt and the low permeability clay-rich soil at this location explains the water pulse being held near

the surface. The shallow depth of the moisture pulse suggests that snow melted recently, and by comparison, later than at the VB 2 location. Canopy coverage at the VB 3 location reduces solar radiation and snow cover should be able to persist longer than in the open configuration of VB 2.

The slight increase in isotope values seen at the bottom of the VB 3 profile may suggest the presence of heavier antecedent bulk soil water below the advancing snowmelt pulse. On the $\delta^{18}O$ vs. δD plot (Figure 29), the data point corresponding to the deepest sample (the highest point) deviates from the linear trend line expected from evaporation. This heavier value at the bottom of the profile suggests that a lighter snowmelt pulse overlaid a heavier antecedent bulk-soil water at the time of sampling.

The absence of the typical profile exhibiting enriched isotopic values toward the surface is likely due to several factors, primarily greater shading due to greater tree density. This causes profile development to be slower. As was mentioned before, the time requirement for establishment of such a profile depends on several factors. In addition to possible later snowmelt at the VB 3 location, leaving less time for development, canopy cover, lower solar radiation and the resultant lower evaporation rate will all contribute to increased time required to develop characteristic vertical profiles. Additionally, the relatively large depth of the shallowest sample obtained may have truncated part of the profile that exhibited enrichment towards the surface.

The VB 2 and VB 3 depth profiles were selected because of their depth and their distinguishing characteristics; VB 2 with its evaporative enrichment curve and VB 3 with its moisture pulse. Figure 30 shows moisture content for all soil profiles sampled in March. VB 1 and VB 2 have the highest moisture contents, though their forms are quite different.

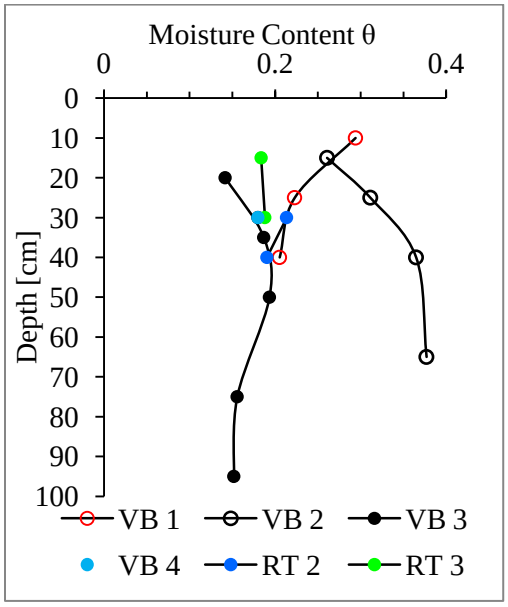

Figure 30: Soil gravimetric water content (θ) vs. depth for all bulk soil profiles sampled in March 2011. Thinned plots are represented with open symbols and control plots with closed symbols. For supplemental plots, see Appendix II.

VB 1 and VB 2 valley bottom thinned plot locations have the highest moisture content likely due to increased effective precipitation associated with tree thinning. This increase is due to the absence of canopy interception by tree branches. All samples from control plots, VB 3, VB 4, RT 2 and RT 3, have similar moisture content which is likely a reflection of the natural moisture levels for non-thinned forest soils in the area.

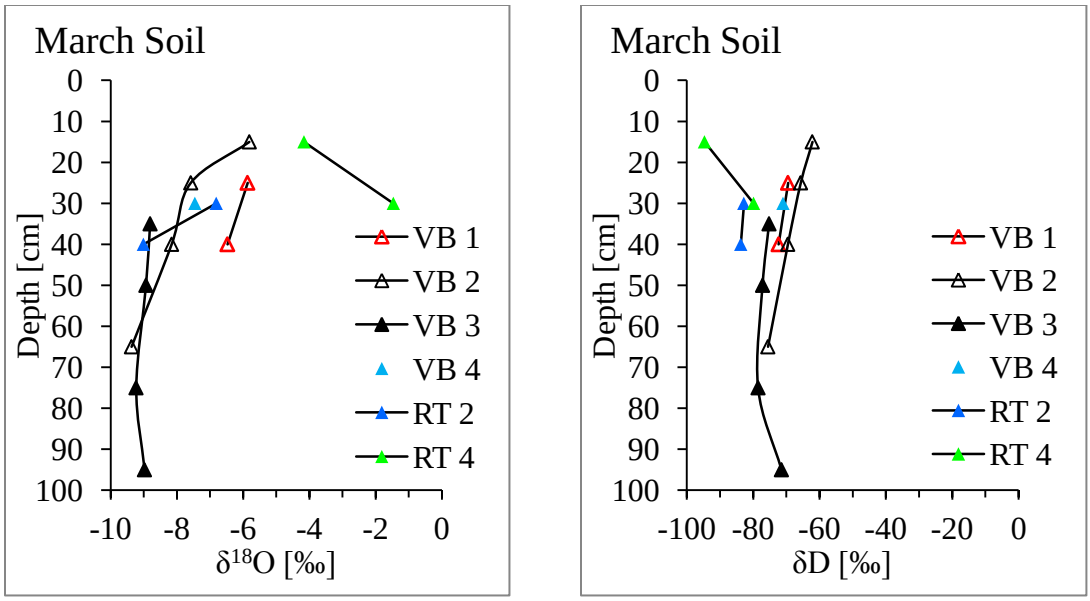

Figure 31: Stable isotope values vs. depth for all bulk soil samples taken in March 2011. More enriched isotopic values can be seen near the surface. Aside from the RT 4 location with respect to $\delta^{18}O$, VB 1 and VB 2 have the most enriched values. These samples were taken from the valley bottom thinned plot while the rest represent profiles that lie on a control plots.

Examining all profiles on a single plot (Figure 31), a general trend of isotopic enrichment towards the surface is evident. This reflects the fact that after snowmelt, water evaporates at most locations throughout the watershed. It is also interesting to note that enrichment tends to be more pronounced on thinned plots. This is likely due to fractionation induced by the higher evaporation rates associated with higher solar radiation.

We have now seen two of the main types of profiles identified in this study: 1) an evaporative profile with characteristic vertical profile development and 2) undeveloped reflecting insufficient time for development such a profile. This may also be due to the

soil material and evaporative environment. The third profile type which we have not yet seen is created by mixing of multiple waters.

Examining all March profiles on a single $\delta^{18}O$ vs. δD plot (Figure 32), a general region in which bulk soil waters tend to plot becomes evident, similar to that seen in Figure 25. Despite some significant scatter, most of the values plot in the range of -10 to -5 with respect to $\delta^{18}O$ and within -85 to -65 with respect to δD. Examining samples grouped by ridge-top or valley-bottom location, grouping is stronger in valley-bottom bulk-soil samples than ridge-top (Figure 33). Ridge top soil waters display values that are lighter with respect to deuterium, heavier with respect to $\delta^{18}O$ and more scattered.

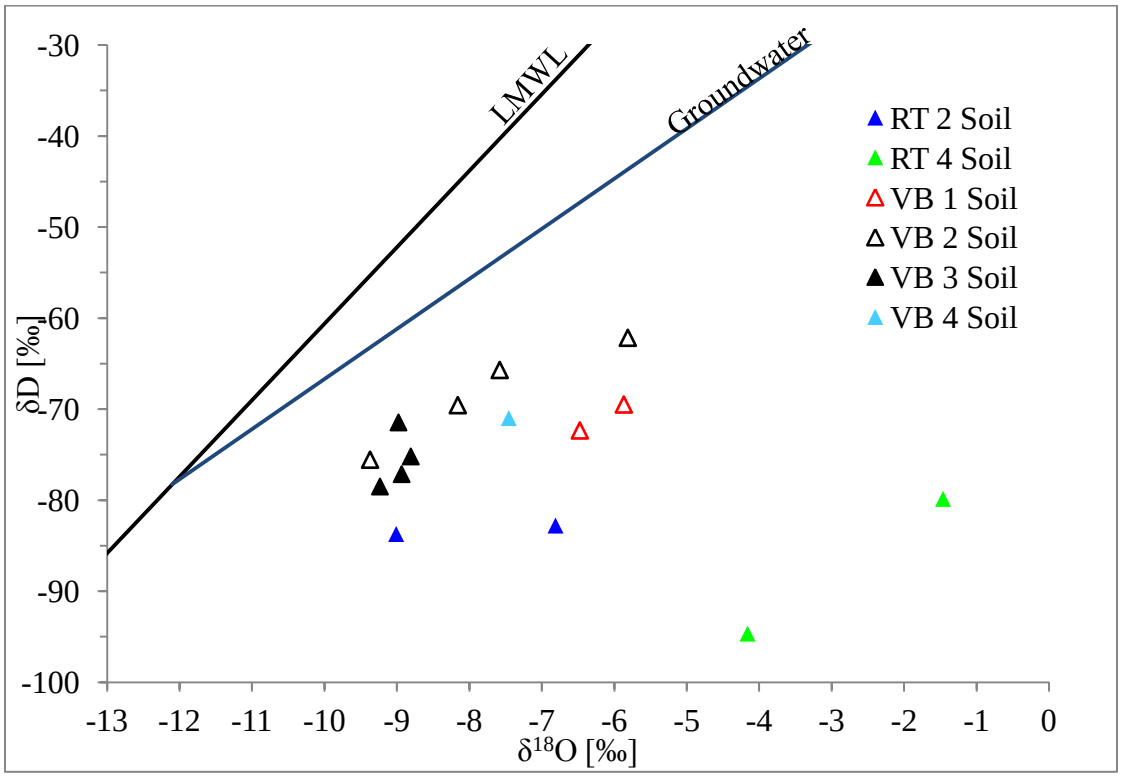

Figure 32: Bulk-soil water isotope data plotted in $\delta^{18}O$ vs. δD space for samples collected in March 2011. The symbol sizes are approximately equal to the error

associated with analysis. The local meteoric water line (LMWL) and groundwater line are shown for reference.

This grouping is likely due to much of the water stored in soils being from a common source and similar processes that drive evolution from that source. A spatial understanding of both the variability between precipitation inputs and the processes that drive isotopic evolution becomes apparent when valley-bottom soils are compared with ridge-top soils as in Figure 33. The spatial variability observed between ridge top and valley bottom bulk soil water values is likely due to two factors: elevation effects on precipitation input and soil properties. The relief between the valley bottom and the ridge top is on the order of 350 m (1,000 ft) which may cause elevation, temperature or rain-out effects that lead to lighter precipitation on the ridge top. Additionally, ridge-top soils are generally more sandy and shallow, creating conditions that allow more air to penetrate the profile and consequently more evaporation. This evaporation leads to fractionation and the larger range of composition observed in ridge-top bulk-soil-water isotope data.

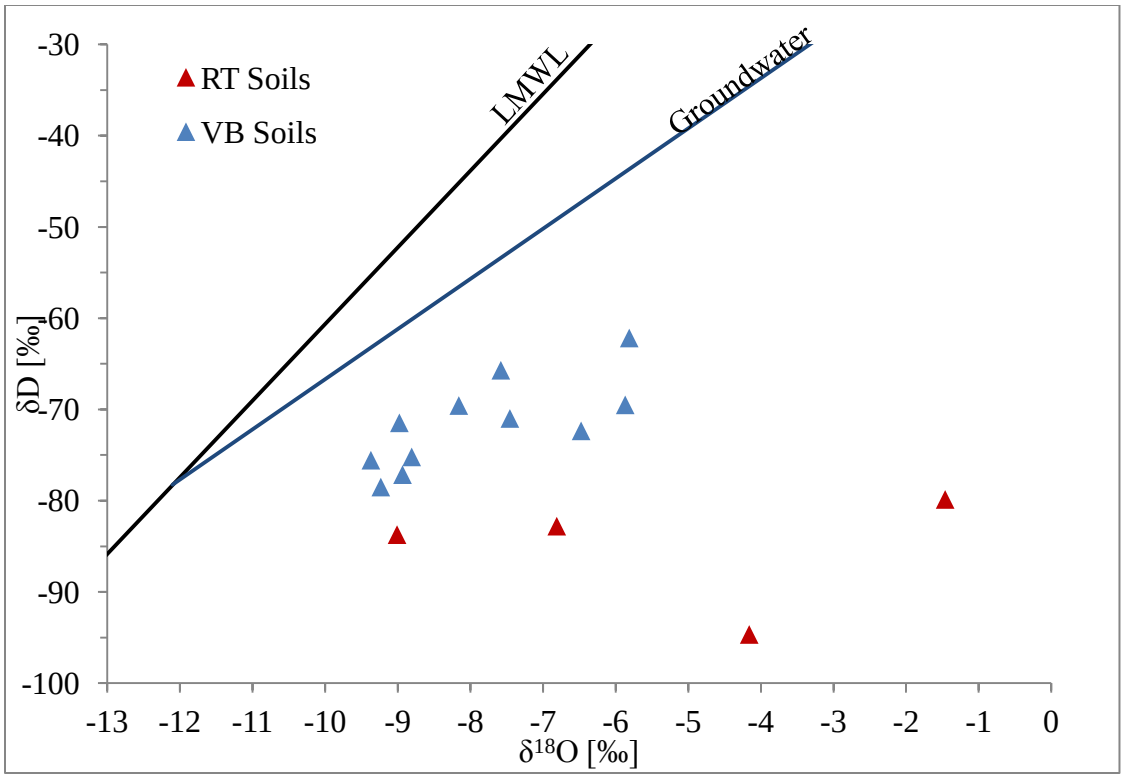

Figure 33: Bulk-soil-water isotope data plotted in $\delta^{18}O$ vs. δD space for samples collected in March 2011. The samples are grouped based on valley-bottom and ridge-top locations. The symbol sizes are approximately equal to the error associated with analysis. The local meteoric water line (LMWL) and groundwater lines are shown for reference.

September 2011

Soil sampling intervals were large due to constraints visiting the field site and ongoing development of experimental design. This sampling time was significant due to it being collected during the monsoon season. Monsoon rains typically have heavy isotopic compositions.

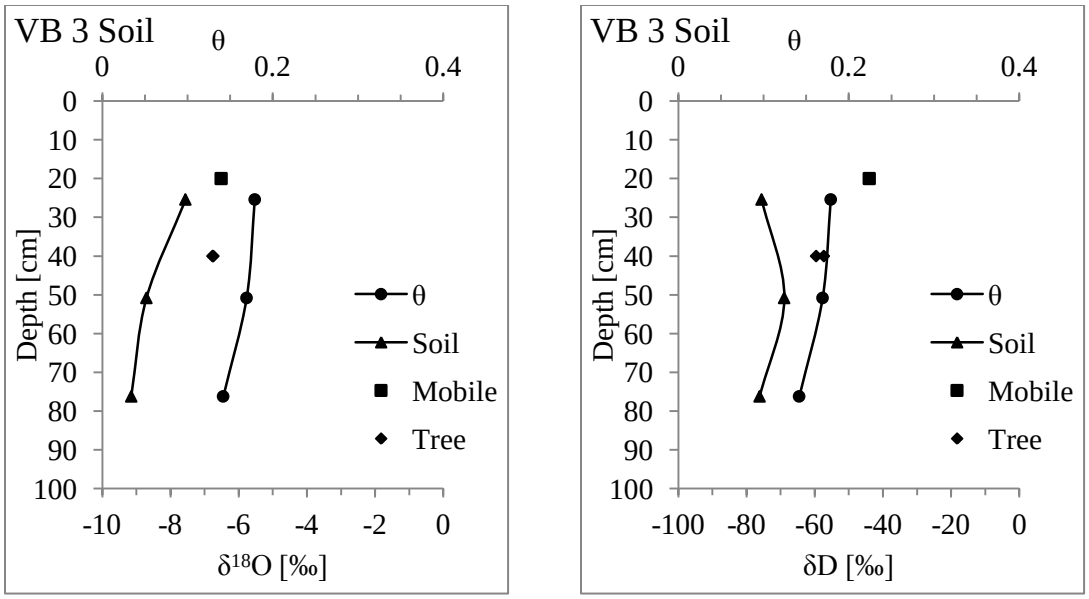

Figure 34: Gravimetric-moisture-content and stable isotope values vs. depth for bulk soil water collected from VB 3 in September 2011. Tree water and mobile soil-water-isotope values are also shown.

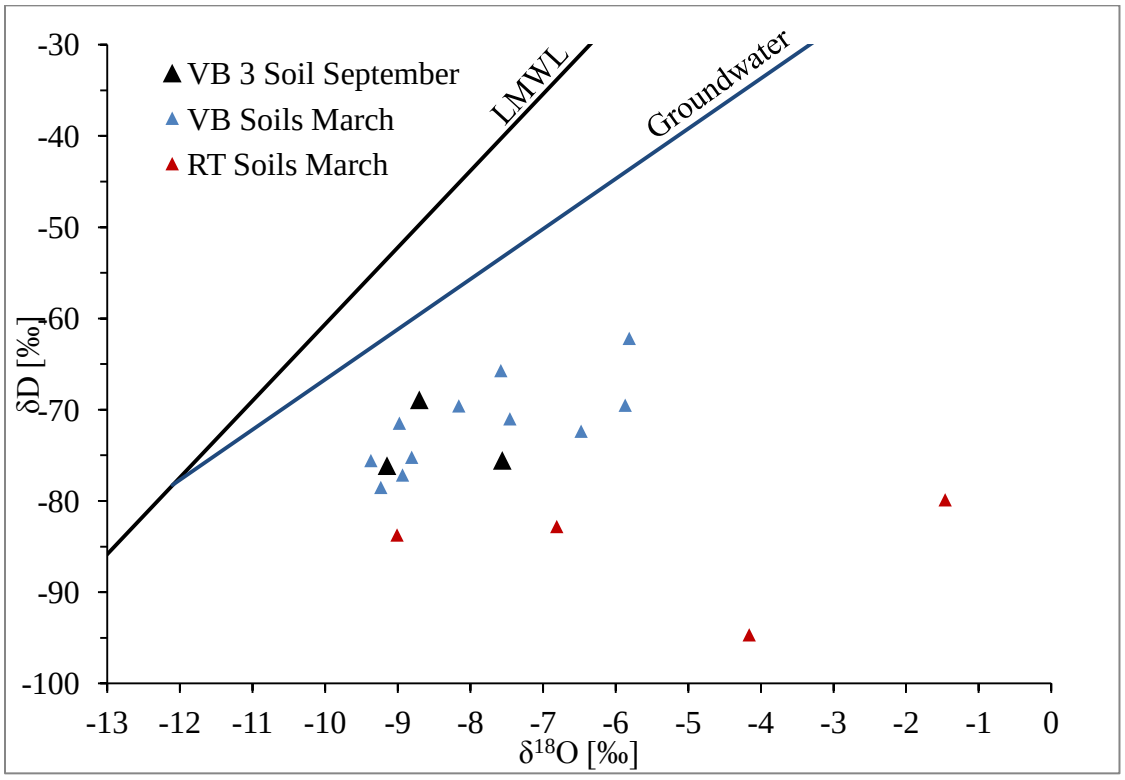

Figure 35: Bulk-soil-water isotope data from the VB 3 location plotted in $\delta^{18}O$ vs. δD space. These samples were collected in September 2011, near the end of the monsoon season. Bulk-soil-water data from March is shown for reference. Bulk soil samples from

the ridge top location were not collected at this time. The symbol sizes are approximately equal to the error associated with analysis. The local meteoric water line (LMWL) and groundwater line are shown for reference.

Gravimetric soil moisture content for VB 3 bulk soils sampled in September show a slight increasing trend towards the surface. The $\delta^{18}O$ depth profile gets heavier toward the surface while the deuterium profile becomes lighter (Figure 34). In Figure 35 we see that bulk soil water values exhibit no linear trend but plot within the previously observed valley bottom grouping.

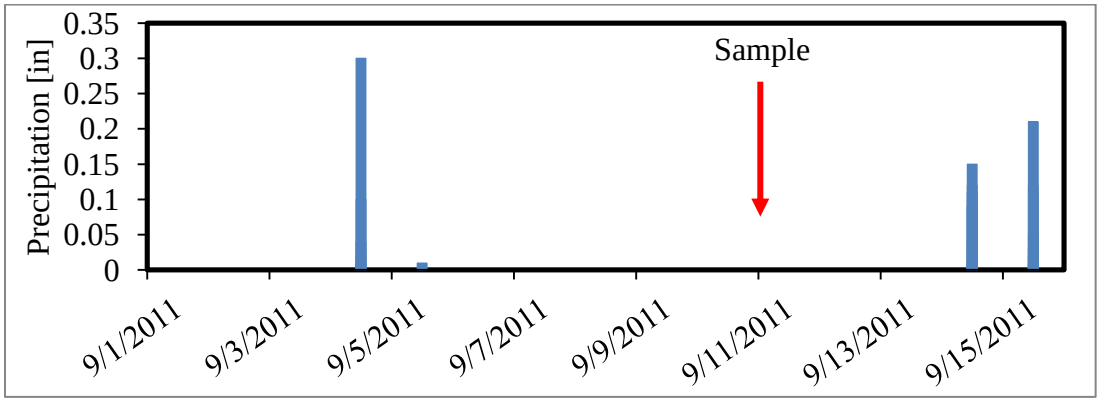

Figure 36: September 2011 precipitation data from a weather station located on the ridge that bounds Three L Canyon.

November 2011

The VB 2 soil profile seen in Figure 37 exhibits fairly high gravimetric moisture content near the surface and a sharp decrease at greater depth. The $\delta^{18}O$ isotope profile exhibits slightly heavier values toward the surface while the deuterium profile shows lighter values towards the surface. The trend of the VB 2 values on the $\delta^{18}O$ vs. δD plot is nonlinear (Figure 39). The VB 9 soil profile seen in Figure 38 exhibits fairly low

gravimetric moisture content and a slight decrease toward the surface. Both isotope profiles exhibit enrichment toward the surface. These data points form a linear trend on the $\delta^{18}O$ vs. δD plot (Figure 39).

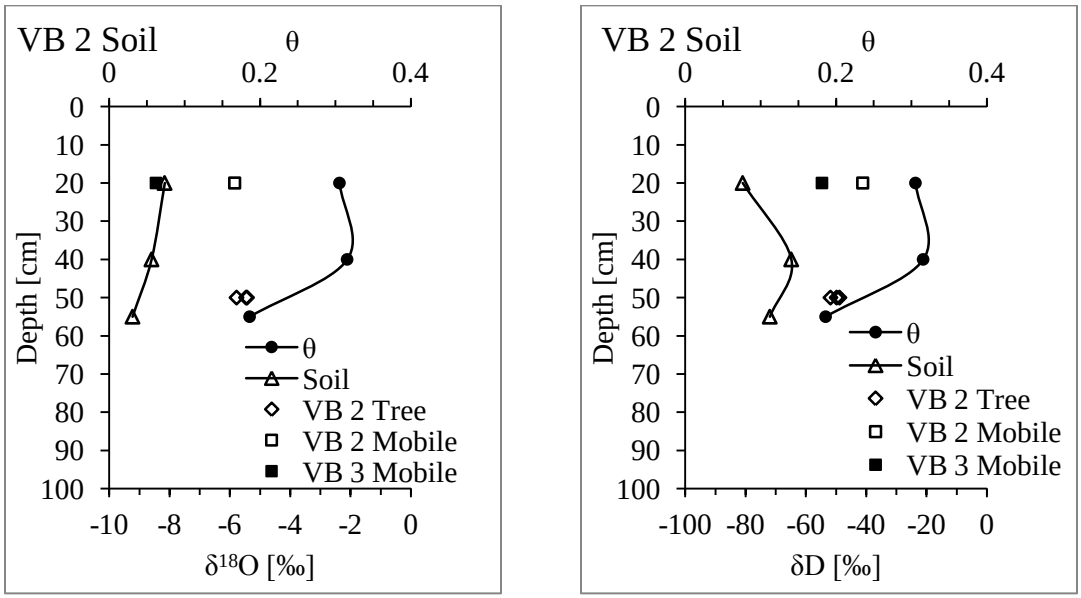

Figure 37: Gravimetric moisture content and stable isotope values vs. depth for bulk soil water collected from VB 2 in November 2011. Tree water and mobile soil water isotope values are also shown.

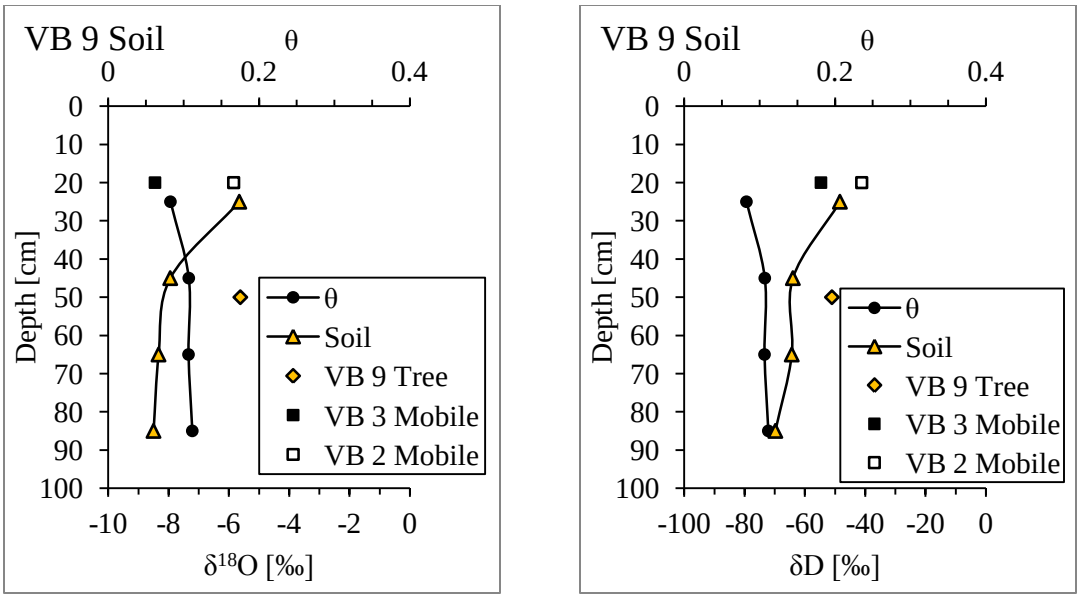

Figure 38: Gravimetric moisture content and stable isotope values vs. depth for bulk soil water collected from VB 9 in November 2011. Tree water and mobile soil water isotope values are also shown. This profile lies in the watershed outlet drainage.

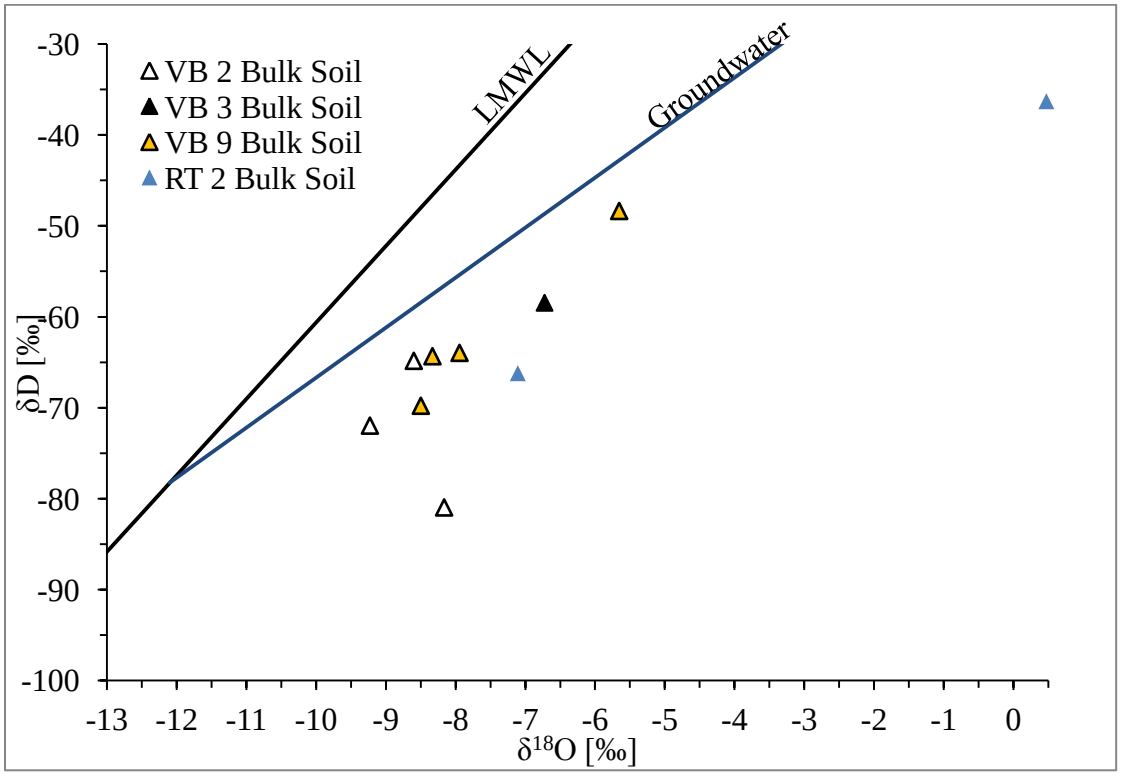

Figure 39: Bulk soil water isotope data for samples collected in November 2011 plotted in $\delta^{18}O$ vs. δD space. These samples were collected in November 2011, after the monsoon season. The symbol sizes are approximately equal to the error associated with

analysis. The local meteoric water line (LMWL) and groundwater line are shown for reference.

The VB 2 $\delta^{18}O$ isotope profile exhibits slightly heavier values toward the surface but the concavity in this curve is in the opposite direction of evaporation curves. The lighter values towards the surface in the deuterium profile are more instructive and likely reflect a small, late October snowmelt whose deuterium values were lighter than the antecedent soil water. This is consistent with the high moisture content values near the surface. Additionally, the highly nonlinear pattern on the $\delta^{18}O$ vs. δD plot suggests multiple water sources within this profile.

The corresponding decrease in moisture content and enrichment in isotopes toward the surface of the VB 9 soil profile suggests significant evaporation. The low moisture content values in this profile can likely be attributed to the sandy material (Table 2). Sandy soils tend to be better drained which also decreases the time required to establish a characteristic vertical profile. The deeper depth to which enrichment is evident is also a product of the sandy nature of the soil at this location near the watershed outlet. Sandy soil allows for the combined effects of vapor and liquid diffusion to penetrate further into the soil profile thus extending the characteristic curve further into the profile [*Barnes and Allison*, 1988]. The linear trend on the $\delta^{18}O$ vs. δD plot suggests evaporation-dominated isotopic evolution from fairly uniform initial water. The position of the linear trend closer to the ground water trend line is likely a reflection of the sandy nature of the soil and the lower water retention. With less water retained in the profile due to its sandy composition, recent precipitation has a larger effect on bulk soil water isotopic values.

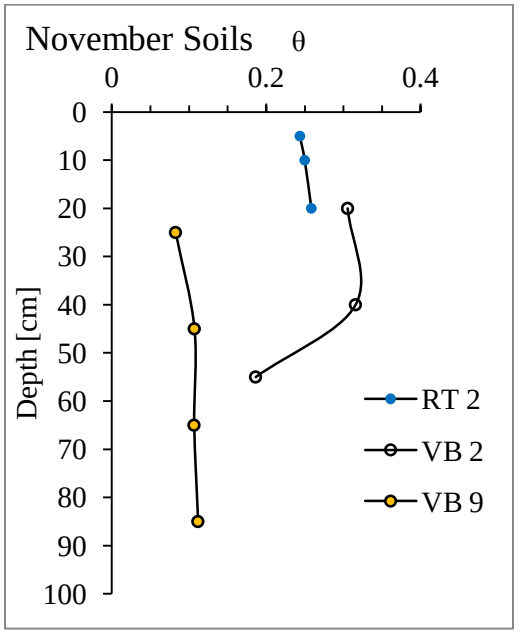

Figure 40: Gravimetric water content for soils sampled in November 2011. The increased moisture content at the VB 2 location is likely correlated with increased effective precipitation on a thinned plot.

February 2012

The soil profile seen in Figure 41 exhibits fairly low gravimetric moisture content with a slight increase toward the surface. Both isotope profiles exhibit enrichment toward the surface and appear to be stabilizing at depth. A linear trend is observed on the $\delta^{18}O$ vs. δD plot in Figure 42.

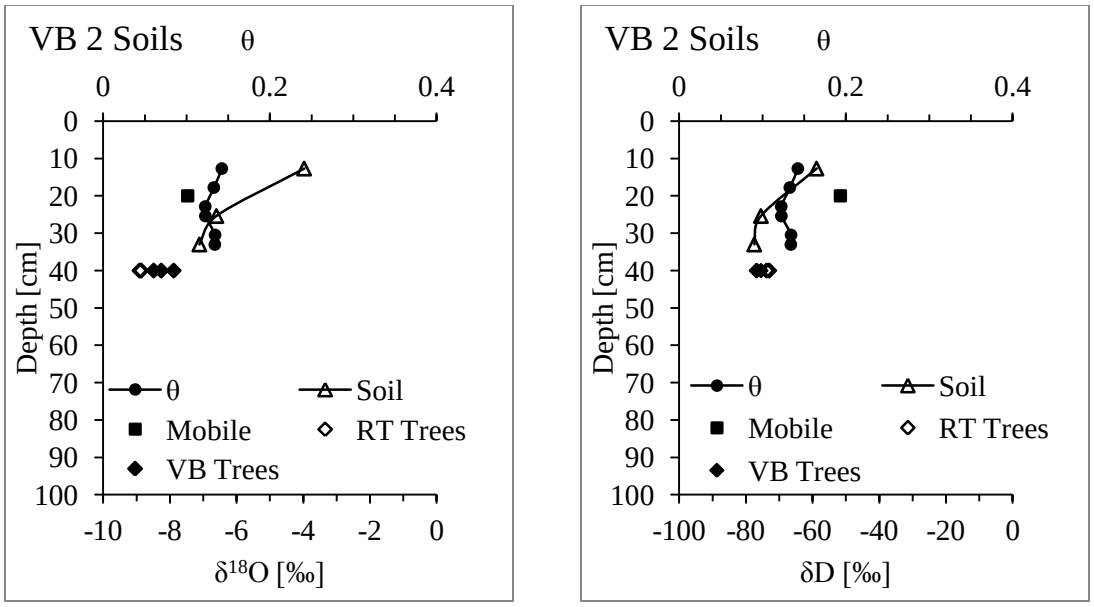

Figure 41: Gravimetric moisture content and stable isotope values vs. depth for bulk soil water collected from VB 2 in February 2012. Tree water and mobile soil water isotope values are also shown. This profile lies on a valley bottom control plot.

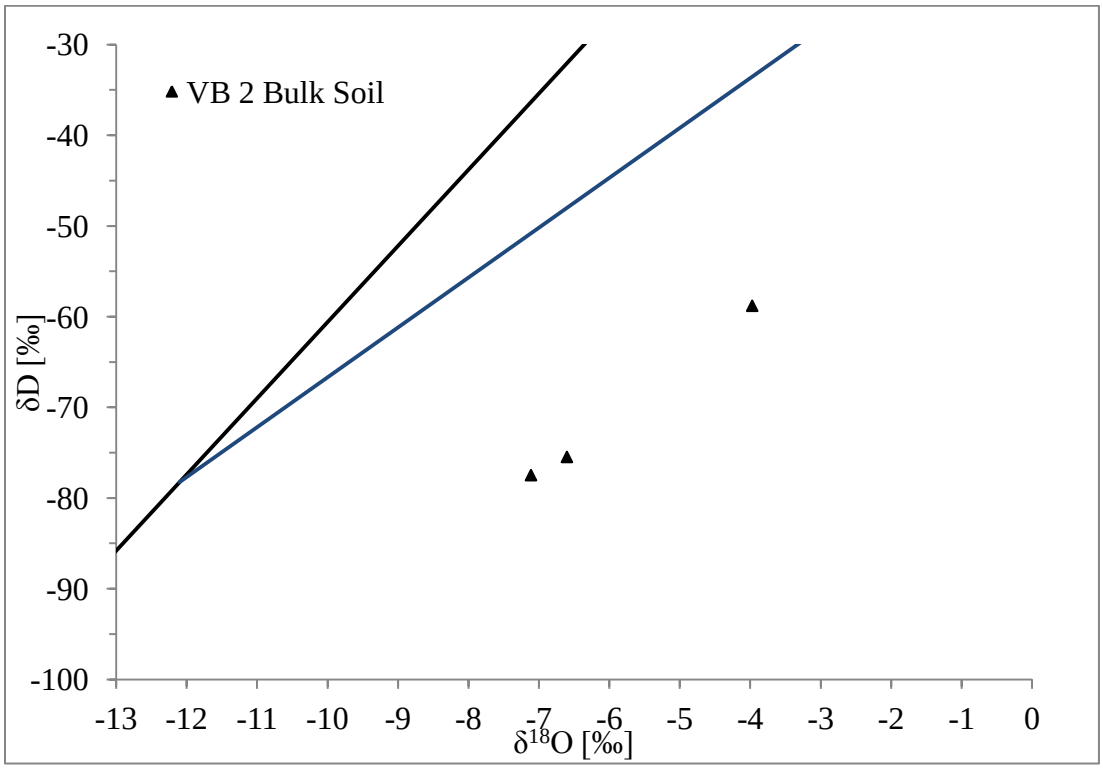

Figure 42: Bulk soil water isotope data from VB 2 plotted in $\delta^{18}O$ vs. δD space. These samples were collected in February 2012 after snowmelt. Bulk soil samples from the ridge-top location were excluded due to spectral interference. The symbol sizes are

approximately equal to the error associated with analysis. The local meteoric water line (LMWL) and groundwater line are shown for reference.

The enrichment towards the surface observed in the isotopic profiles suggests evaporation from the profile but the soil moisture profile does not agree. This may be due to isotopic enrichment of snow equilibrating with atmospheric water vapor before snowmelt [*Earman et al.*, 2006]. Such enrichment could contribute enriched water at the time of snowmelt causing heavier values near the surface and the corresponding increased moisture content. The sampling interval is fairly small but the observed trend would be expected to stabilize at depth with a slightly lighter isotopic value. The linear trend on the $\delta^{18}O$ vs. δD plot indicates evaporation from a uniform source, such as would be expected from the recent snowmelt.

5.2.2 Discussion

Isotopic depth profiles for bulk soil water undergoing evaporation have been proven to exhibit characteristic vertical evaporation profiles like those seen in Figure 15 [*Barnes and Allison*, 1988]. Soil water isotopic values are controlled by the water sources as well as evaporation processes. As water evaporates from the surface, lighter isotopes evaporate preferentially, creating enrichment near the surface. The characteristic exponential shape is a result of both, evaporation from the surface as well as water transport to the surface via liquid and vapor diffusion.

Barnes and Allison [1988] did their study on lab columns where conditions were well constrained. However, conditions in the field are variable and processes that develop such profiles are often interrupted. Soils are often layered, evaporation rates change or the entire process may be reset as new precipitation is introduced. These changes create overprinting on partially equilibrated profiles, cause deviation from characteristic depth profiles and complicate interpretations. For this study, further complications arise due to sampling constraints on maximum attainable depth and infrequent sampling. However, several profiles were observed that do exhibit expected evaporation trends. These profiles were more common on thinned plots that had ample time for development. These locations, with their lack of canopy and high solar radiation, have high evaporative-demand environments. Profiles sampled shortly after precipitation did not display this trend. Instead, these profiles displayed evidence of mixing of multiple sources, likely antecedent bulk soil water with recent precipitation.

Bulk Soil Water Origin

Examining bulk-soil isotopic values in $\delta^{18}O$ vs. δD space we see a different trend for bulk soil water than for the groundwater evaporation trend line. Figure 43 shows VB 2 bulk soil water samples with a best-fit linear regression through them. This best-fit line intersects the LMWL in the winter precipitation region below the groundwater trend line. It is also interesting to note that the late season snow sample plots very close to this line.

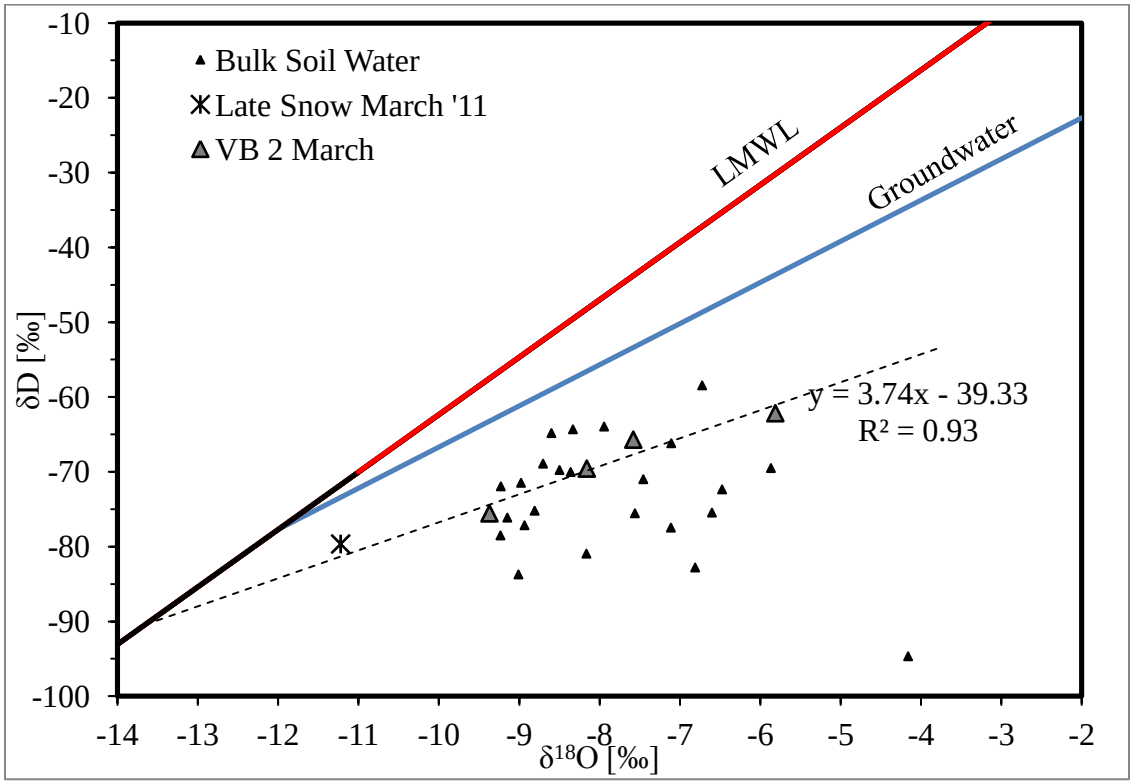

Figure 43: Bulk soil water and late snow isotope data plotted in $\delta^{18}O$ vs. δD space. The VB 2 March profile was used to fit a linear regression and trace back to the local meteoric water line (LMWL). This is often used to determine the origin of natural waters that have undergone evaporation. This method indicates that the origin of this bulk soil water is lighter than that of groundwater, indicating that the majority originates as winter precipitation or snowmelt [*Campbell et al.*, 1996]. Comparing the trend line intersection for this profile with that of the groundwater trend line indicates that soil water and groundwater have different origins.

The light isotopic signature of bulk soil water indicates that snowmelt is stored in the smallest pore spaces of the soil. Soils become well saturated during snowmelt due to the slow nature of water delivery which allows for ample infiltration. The fairly consistent composition of bulk soil samples throughout the year suggests that once these small pore spaces are filled with snowmelt water, that water is preferentially sequestered. Further inputs will then have to be stored in larger pore spaces that have less capillary tension.

Later precipitation inputs will have only slight effects on the composition of bulk soil water [*Brooks et al.*, 2009].

Variability

In order to examine the significance of spatial variations, the March bulk soils dataset was examined and compared to the entire dataset to determine the applicability of the standard deviations and confidence intervals calculated. For the March dataset, mean values of -7.06 and -75.05 ‰ with standard deviations of 2.22 and 8.31 were calculated for $\delta^{18}O$ and δD respectively. The confidence intervals on these values were determined to be -5.53 to -8.59 and -69.33 to -80.77 ‰ for $\delta^{18}O$ and δD and can be seen in Figure 44.

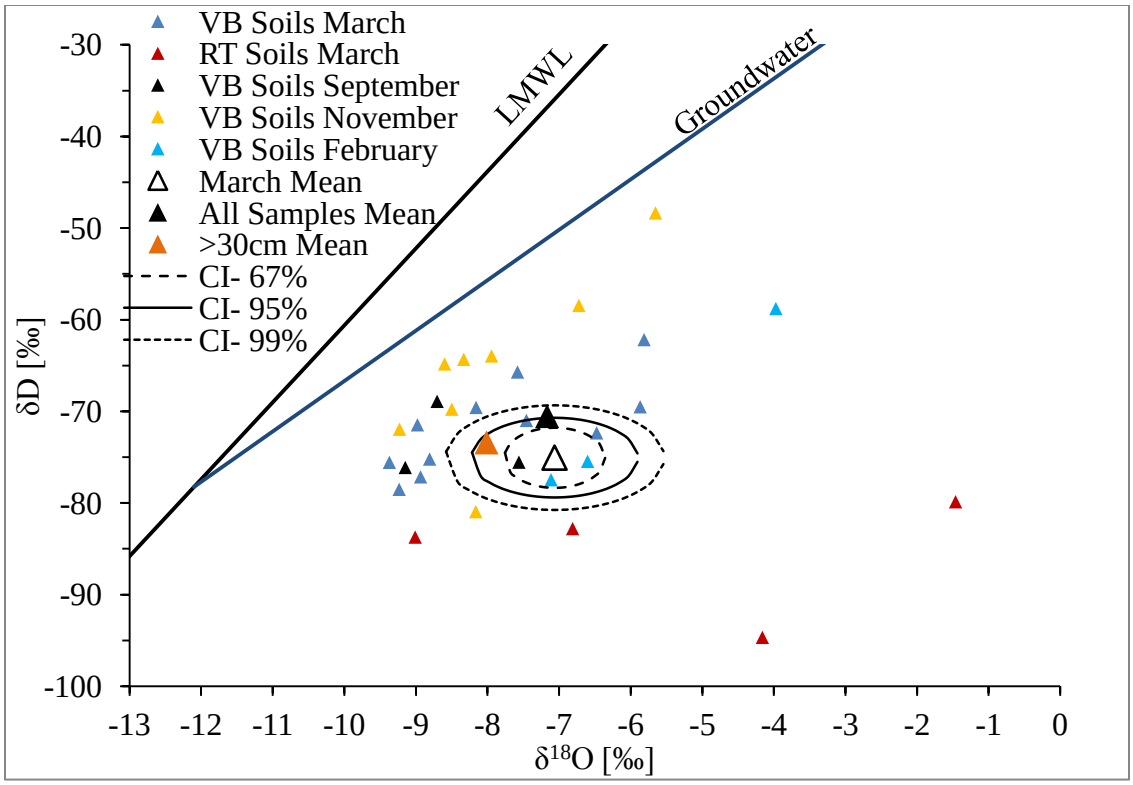

Figure 44: Bulk-soil-water values, sample means and population mean confidence intervals based on the sample mean for March bulk soil water isotopic values plotted in $\delta^{18}O$ vs. δD space. Sample means of the entire dataset as well as for samples collected at or below 30 cm are also shown.

The entire dataset was then used to calculate a mean of -7.17 and -70.52 ‰ for $\delta^{18}O$ and δD which is illustrated in Figure 44. Samples collected from 30 cm deep or greater were also grouped and their sample mean was calculated to be -8.01 and -73.39 ‰ for $\delta^{18}O$ and δD. Both of these groupings plotted within the 95% confidence interval calculated from the March dataset. This consistence suggests that the spatial and temporal variations of bulk-soil-water isotopic values are insignificant and can be assumed to remain in a fairly well-constrained area on a $\delta^{18}O$ vs. δD plot despite changes in timing or location of sampling.

5.3 Passive Wick Soil Water

Many previous studies investigating soil water dynamics have found evidence of multiple soil water reservoirs [*Brooks et al.*, 2009; *Landon et al.*, 1999; *Mathieu and Bariac*, 1996; *Newman et al.*, 1998]. In order to assess our field area and build a more complete understanding of the soil water dynamics, we installed passive wick samplers. Passive wick soil water samples are collected when soils became saturated to a point at which the matric potential of the soil (ψ_{soil}) is less negative than that of the passive wick sampler (ψ_{wick}). This threshold potential is approximately equal in magnitude to the length of the wick employed (commonly -60 cm in this study).

5.3.1 Data

The stable isotopes of $\delta^{18}O$ and δD in precipitation display seasonal variability [*Craig*, 1961; *Dansgaard*, 1964; *Newton et al.*, 2009]. This seasonal variability in the stable isotopic composition of precipitation can be seen clearly in Figure 45. The seasonal variability can be seen in Figure 46 as a trend moving along the LMWL towards heavier values during the monsoon season (July through September), then shifting back towards lighter values in the winter (November and February) as temperatures drop. This is consistent with seasonal/temperature effects reported by Dansgaard [1964]. A dampened form of this seasonality is observed in the passive wick soil water values as well (Figure 45 and Figure 46).

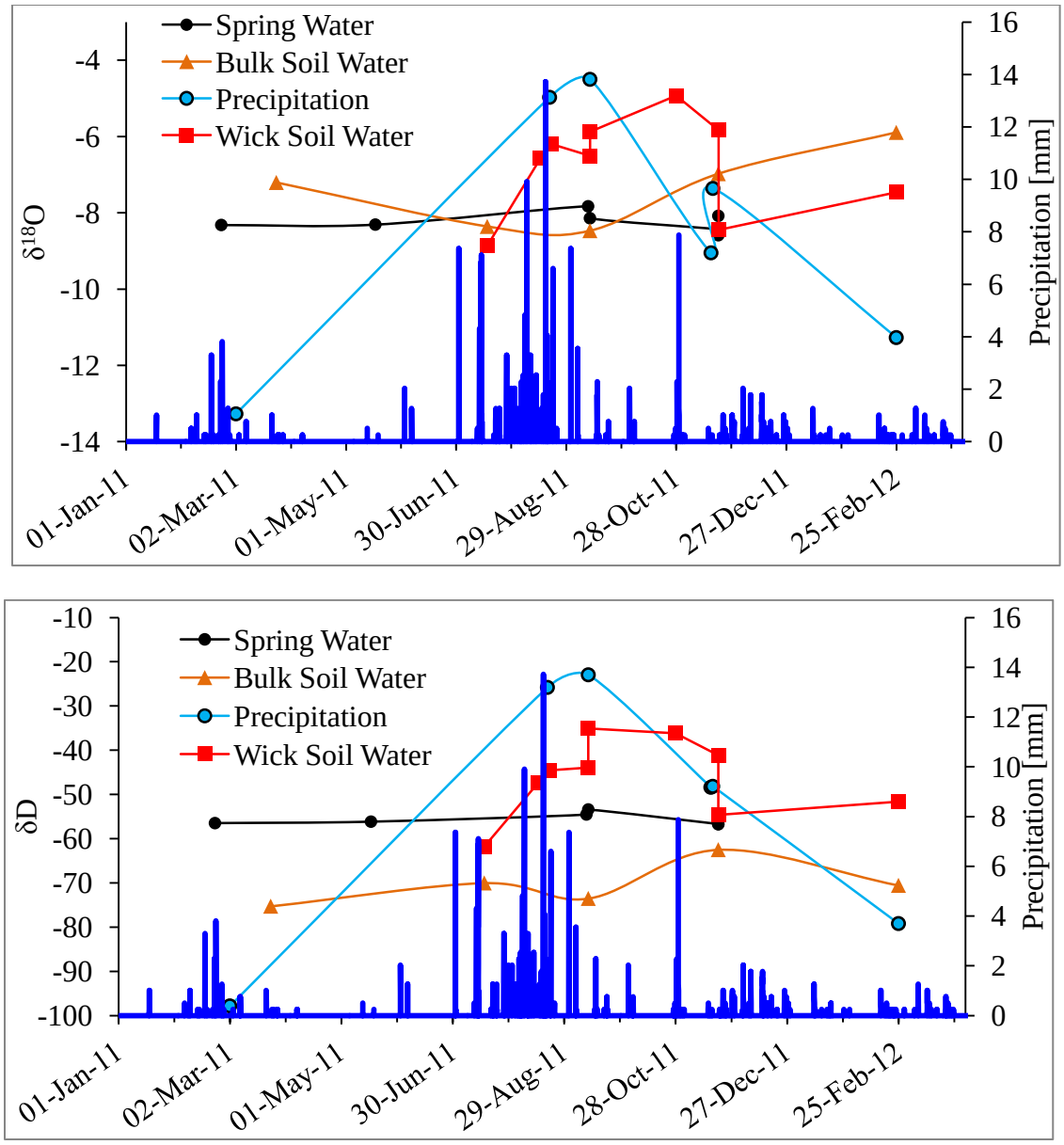

Figure 45: Time series data showing spring water, bulk-soil-water averages, passive-wick soil-water and precipitation isotope data. Note the attenuated seasonal trend in passive-wick soil-water samples.

Passive-wick soil-water isotope values are heavier than those of bulk soil water for both $\delta^{18}O$ and δD (Figure 45 and Figure 46). Passive-wick soil water also tends to plot on the groundwater evaporation trend line (Figure 46).

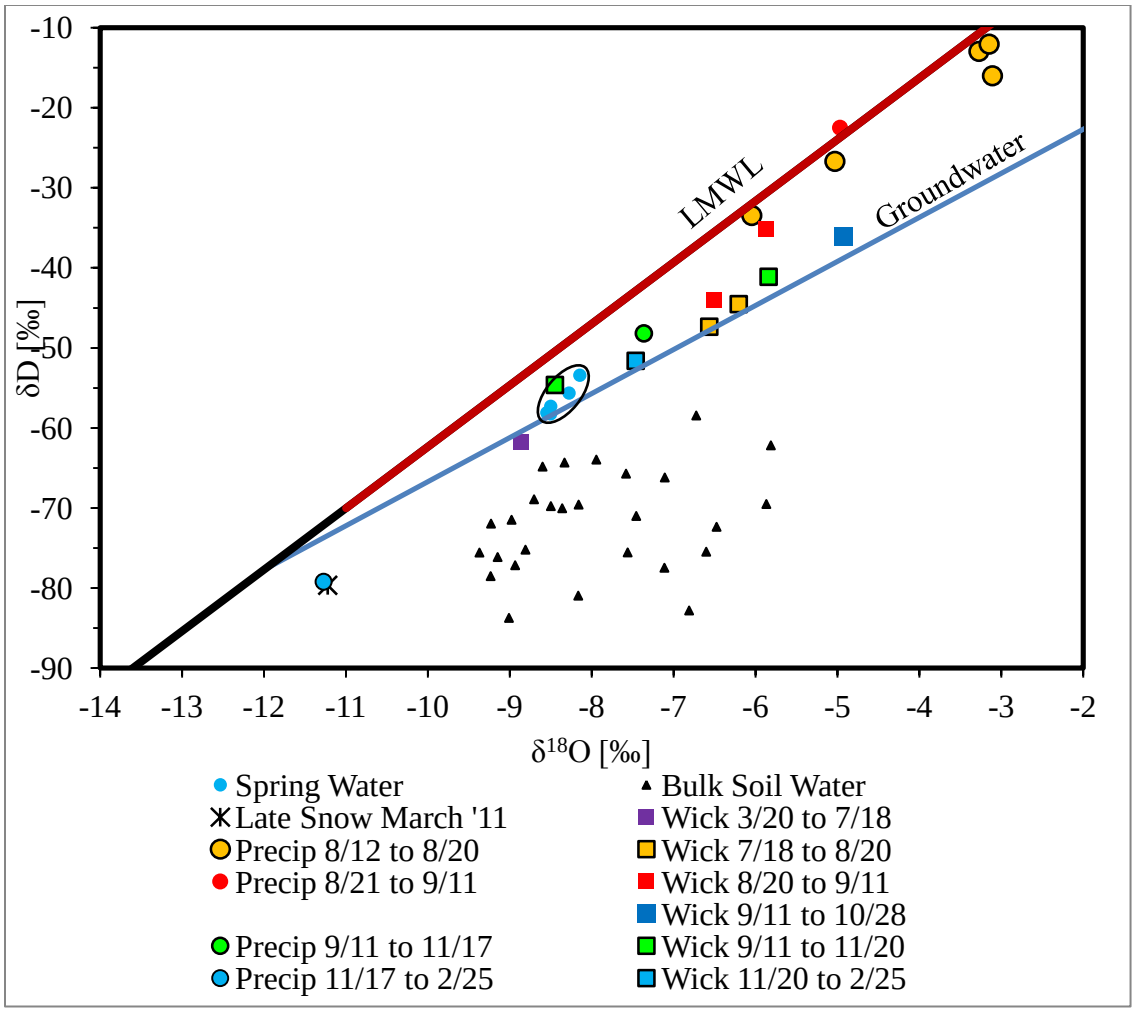

Figure 46: Passive wick soil water, bulk soil water, local spring water, precipitation and late-snow isotope data plotted in $\delta^{18}O$ vs. δD space. Both precipitation and passive-wick soil-water samples are time-integrated or, a cumulative sum of all the water since the previous sample collection. An oval grouping spring samples is shown to eliminate confusion between local spring water and wick samples that may plot on the regional groundwater trend line. The symbol sizes are approximately equal to the error associated with analysis. The local meteoric water line (LMWL) is depicted in two parts, red corresponding to summer and black corresponding to winter precipitation.

The dampened seasonal variability observed in passive-wick soil water is due to precipitation mixing with antecedent soil water. As was demonstrated, bulk soil water values change little with time and even less so with increasing depth [*Tang and Feng*, 2001]. Figure 45 and Figure 46 show that passive-wick soil water samples generally plot

between bulk-soil-water samples and the precipitation samples that correspond in time. The location of passive wick soil water samples in $\delta^{18}O$ vs. δD space between these two end members identifies them as the product of mixing between them.

The seasonal variability of passive-wick soil-water isotopic composition appears to mimic seasonal precipitation. When compared with the relative stability of bulk soil water composition, it becomes clear that water collected by passive-wick samplers is more mobile than bulk soil water. The presence of these two soil water reservoirs suggests that preferential flow is dominant in this system [*Brooks et al.,* 2009; *Landon et al.,* 1999; *Mathieu and Bariac,* 1996; *Newman et al.,* 1998].

The large change in the composition of passive-wick soil water over relatively short time intervals indicates that there is turnover, if not complete replacement, in this more mobile soil water reservoir while the absence of observed change in bulk-soil-water samples suggests a relatively immobile soil water reservoir. This data seems to indicate some sort of flushing mechanism that controls the composition of passive wick soil water.

The isotopic composition of the first passive wick soil water sample collected in July resembled that of the of the surrounding bulk soil (Figure 45 and Figure 46). As the monsoon season progressed, the isotopic composition of PCAPS soil water samples began to resemble that of local precipitation more closely (Figure 45 and Figure 46). In July, very little rain had fallen since the spring. Due to the lack of precipitation input to the system, it is assumed that there had been no recent water movement and any water

present in the soil profile, whether in the mobile or immobile reservoir, had ample time to equilibrate with bulk soil water. As the first rains began to fall, this water began to be mobilized. As the monsoon season progressed, water was flushed through more rapidly allowing relatively little time to equilibrate with bulk soil water.

5.3.2 Analytical Model

We developed a model to estimate the potential recharge of mobile waters and to investigate the composition of effluent as compared to samples collected. To model this mobile-soil-water flushing phenomenon, a simple ordinary differential equation was used. The equation describes the composition of outflow from a water reservoir with constant input. The equation is

Equation 5

$$\frac{d\delta_{reservoir}}{dt} = \frac{\phi_{in}\delta_{rain} - \phi_{out}\delta_{soil}}{V_o}$$

Where $\delta_{reservoir}$ is water flowing out of the reservoir, in this case the volume of the wick sampler. ϕ is the flux in or out, δ_{rain} is the average isotopic composition of monsoonal precipitation inputs, δ_{soil} is the composition of bulk soil water, in this case the initial reservoir composition and V_o is the volume of the wick sampler. The solution to the equation is

Equation 6

$$\delta_{reservoir} = \delta_{rain} + (\delta_{soil} - \delta_{rain}) exp\left(\frac{\phi_{out} * t}{V_o}\right)$$

The initial condition is at time zero, $\delta_{reservoir}$ equals that of antecedent bulk soil water and the initial time is the onset of the monsoon season.

The model assumes a well mixed system with flux in equal to flux out. It is therefore steady state with respect to water storage but transient with respect to isotopic composition. The first assumption is good due to the wicking properties of the fiberglass wick material that creates different flow velocities thus mixing different waters that may be present within the wick. The second assumption is not strictly valid due to naturally occurring transitions from low to high soil-matrix potentials which interrupt sampler collection. However, at low soil-matrix potential under which wick samplers function, the wick discharges as much water as it absorbs, which can be considered a temporary steady state.

The model uses a cumulative sum to calculate the isotopic compositions of the collection reservoir because the passive-wick soil-water samples collected were not discrete measurements of water leaving the wick but rather an integrated sample of this effluent. Isotopic values observed from passive-wick samples collected at the VB 2 passive wick installation are then used to calibrate the model. The fluxes are adjusted until modeled values similarly match those observed. The removal, collection of sample and placement of collection vessels is not considered in the model.

The model-predicted flux is then compared to precipitation data observed during that time period to determine percent recharge. Percent of precipitation contributing to recharge is calculated by dividing the cumulative sum of flux this model predicted by the cumulative sum of precipitation observed over the time period during which the model is run. The calculated recharge rates of 0.70 and 0.56 mm/day during the monsoon season constitute recharge percentages of 25.4 and 20.3 % for $\delta^{18}O$ and δD respectively. A calibrated result is shown in Figure 47.

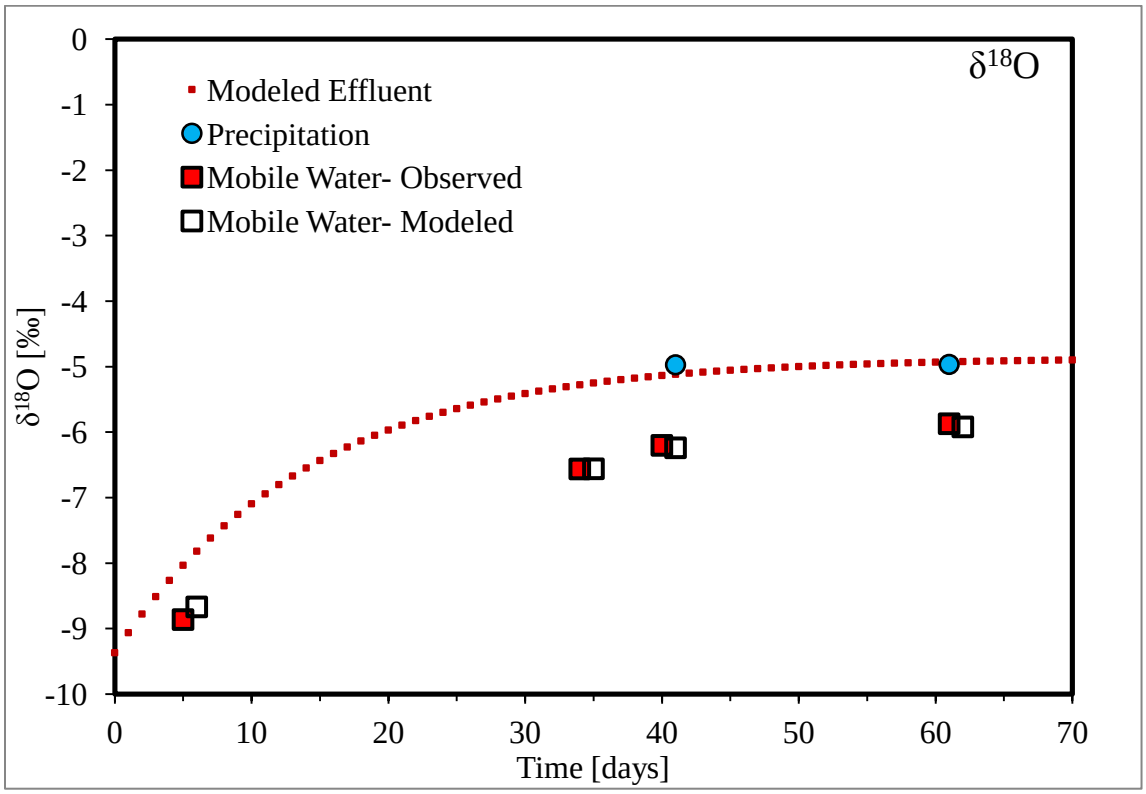

Figure 47: Model results calibrated to VB 2 $\delta^{18}O$ passive wick sample values (δD calibration not shown). An initial composition of bulk soil water was assumed with an input of monsoonal precipitation values to predict recharge rates. The modeled effluent collected by a wick sampler was used to calculate a cumulative sample composition. Recharge rates were then varied to calibrate modeled mobile soil water values to those observed. A single day difference between the modeled and observed was used to make the calibrated results more visible.

Figure 47 indicates that, due to mixing in the collection vessel, the wick sample produced does not reflect that of the actual effluent. The stable isotopic composition of the actual effluent required to produce these values is more similar to that of precipitation. Considering the saturation requirements that must be satisfied for this type of sample to be collected, it seems reasonable that as this water is being collected, the effluent would become more and more similar to precipitation.

This section provides a conceptual model consistent with observed data and supports the hypothesized flushing of mobile waters through the soil matrix. It also supports the hypothesis that water that is able to percolate through the soil profile will likely bear an isotopic composition similar to that of precipitation. This is supported by Landon et al. [1999] who stated: "The isotopic results of this study indicate that, during infiltration events, soil water collected by wick samplers is more representative of the composition of mobile water that is likely to recharge ground water during or soon after an infiltration event, than soil water collected from suction lysimeters or soil cores."

5.3.3 Discussion

The dampening of seasonal variation by antecedent bulk soil water results in passive-wick soil-water values that plot near the groundwater evaporation trend line. Some samples could even be confused with local spring water (Figure 46). However, at the depths from which passive-wick soil waters were collected, groundwater is not present and could not have been collected by the wick samplers.

Conceptual Model- Preferential Flow

Due to the intensity of water delivery during monsoonal storms, high saturation conditions develop and macropores begin to conduct water, transporting it through the soil profile or to intermediate depths within (Figure 48). The presence of macropores and dominance of preferential flow is supported by the large differences observed between bulk soil water samples and passive wick soil water samples [*Brooks et al.*, 2009; *Gee et al.*, 2009; *Landon et al.*, 1999; *Mathieu and Bariac*, 1996; *Newman et al.*, 1998].

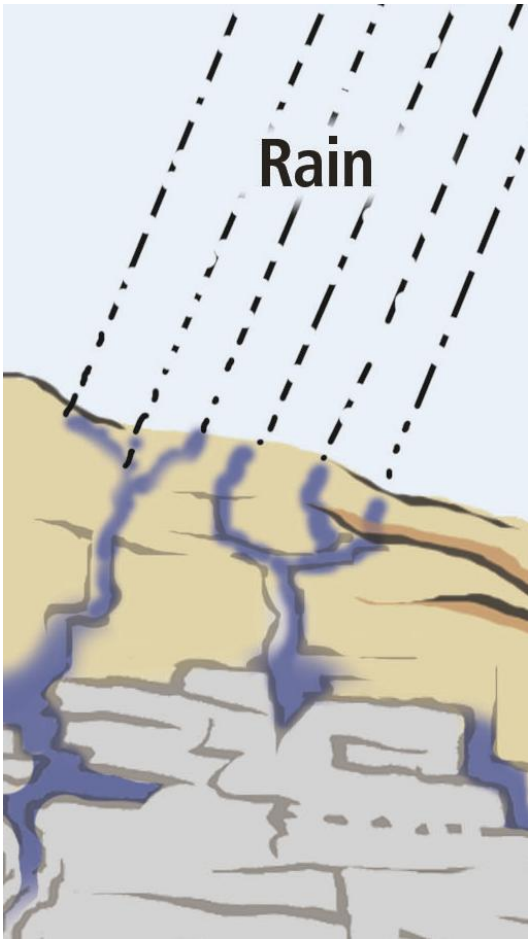

Figure 48: Conceptual depiction of preferential flow through macropores. High-intensity precipitation can deliver abundant water that exceeds the infiltration capacity of the soils at which point macropores may begin to transmit water.

This rapidly percolating water manifests itself as mobile water while passing through soil profiles and it is this water that is collected by wick samplers [*Frisbee et al.*, 2008; *Gee et al.*, 2009; *Landon et al.*, 1999; *Mathieu and Bariac*, 1996]. Although wick samplers collect water from within the soil, not the water exiting the bottom of the profile, they provide insight regarding the composition of water accumulating in the underlying epikarst reservoir [*Landon et al.*, 1999]. For the purposes of this study, it is assumed that the composition of the epikarst reservoir is similar to that of mobile soil water collected by wick samplers.

Additional qualitative information gained from wick samplers includes knowledge about spatial distribution of preferential flow paths and insight into different infiltration mechanisms. The valley-bottom thinned plot installation tended to collect the most water. Also, the two locations that produced mobile-soil-water samples most frequently were located in clay-rich profiles found in the valley bottom.

Clay-rich soils generally have high capillary tension, which would require wick samplers be designed with more capillary force to extract samples. However, Gee et al. [2009] noted that in highly aggregated fine soils or those that contain macropores, passive-wick collectors work much as they do in coarser soils. Because of the frequency with which these clay-rich profiles produced water, it becomes apparent that preferential flow is dominant in these areas.

Direct evidence for preferential flow was observed when testing a PCAPS installation. Approximately 3 gallons of water was poured onto the forest floor immediately above the RT 3 wick sampler. The water pooled on the surface momentarily indicating possible hydrophobicity, before infiltrating the soil. No wetting front was observed in the open soil pit exposing the PCAPS installation but instead, water began to discharge from two discrete macropores. This observation, combined with the fact that only one ridge-top PCAPS installation ever produced passive-wick soil-water samples, indicates that most of the ridge top PCAPS installations were bypassed by preferential flow paths.

The other relevant observation gained from the implementation of wick samplers has to do with the single ridge-top PCAPS sample that was collected. This installation is located on the ridge-top thinned plot and collected water only one time after a small, mid fall snow melt. This sample collection being just after a small snow melt lead to the development of a conceptual model regarding the nature of the dual infiltration mechanisms. One mechanism is that of the preferential flow paths that appear to be active throughout the watershed. The other mechanism is the slow, even distribution of snow melt. By delivering water to the soil profile over a long period of time, the soil matrix is able to absorb more water than in the case of short-duration, intense precipitation inputs such as monsoons. These mechanisms differ in that snowmelt infiltrates the entire matrix and does not exploit preferential flow paths because infiltration capacity is not exceeded. Monsoonal inputs exceed infiltration capacity and begin to exploit preferential flow paths.

Wick samplers have been extremely eye opening in this study. They have helped us to identify and characterize the mobile and immobile soil water reservoirs as well as given us insight into the different infiltration mechanisms that ultimately control groundwater recharge. They also have helped to develop an idea of the stable isotopic composition of water recharging aquifers and epikarst features through soil profiles.

5.4 Tree Water

With the understanding we have developed of soil water dynamics and the dual reservoirs that coexist, we are now prepared to examine tree-water sources. First, all tree data will be presented by sampling time. Then we will focus on individual samples in order to build an understanding of the dynamic sources of tree water in the study area.

5.4.1 Data

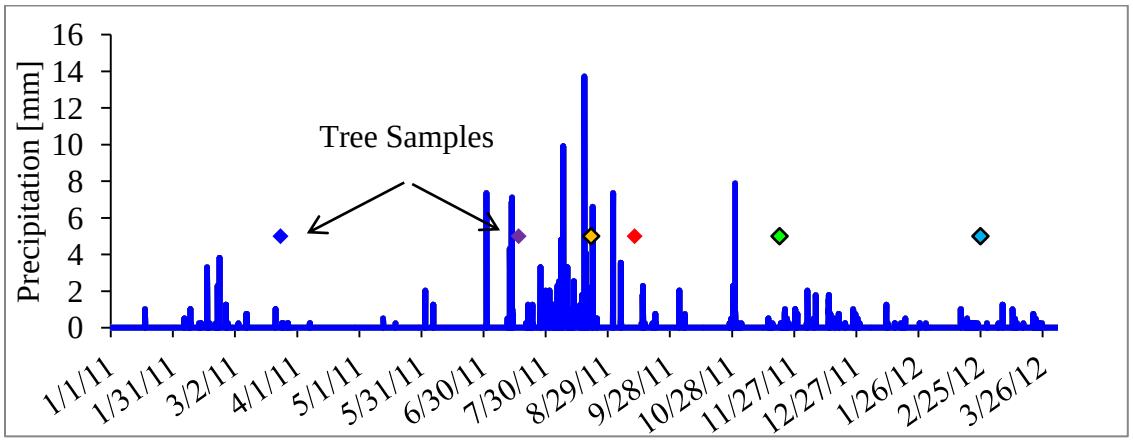

Figure 49: Precipitation data with color coded tree sample dates.

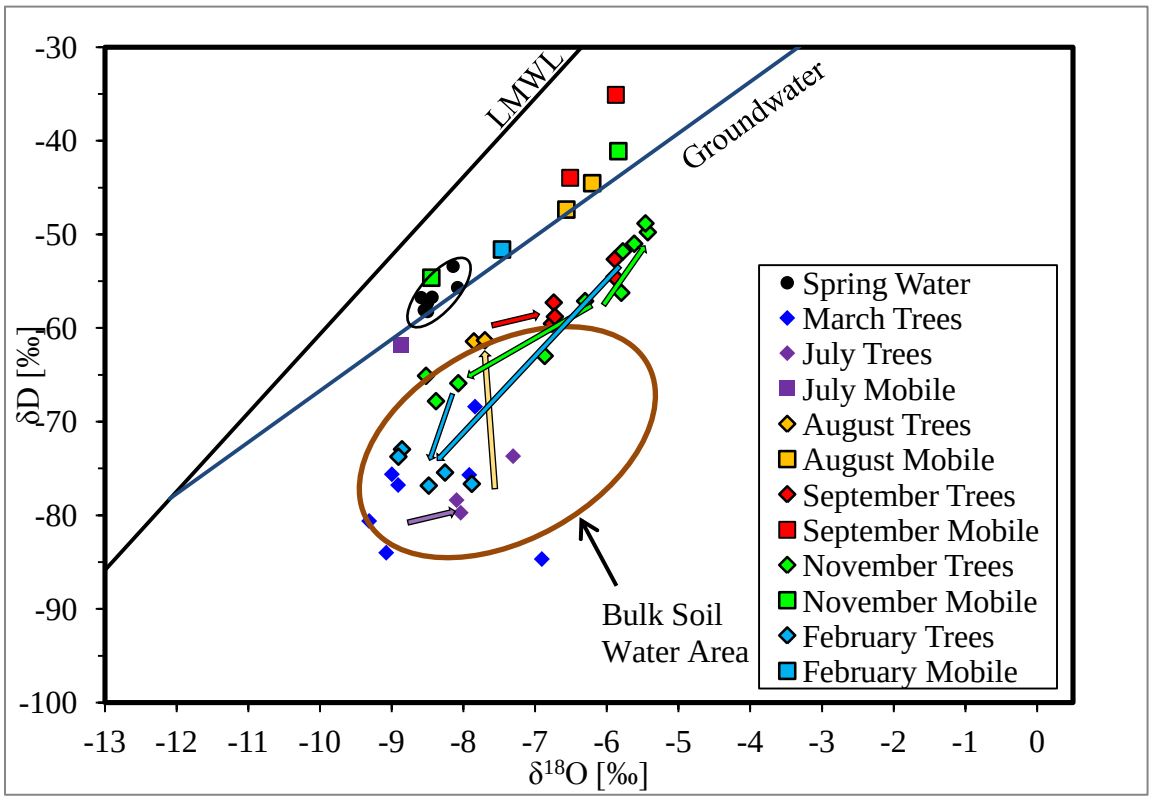

Figure 50: Local spring water, tree water and passive-wick-soil water isotope data grouped by sampling time on a $\delta^{18}O$ vs. δD plot. Local spring water has been grouped to eliminate confusion about mobile soil waters that may plot on the regional groundwater trend line. Arrows are color coded such that the transition from one point in time to the next is guided by an arrow with the same color as the next sample. It starts with March tree samples on the bottom left. Symbol sizes are approximately equal to the size of the error associated with measurement.

Tree water started out plotting in agreement with bulk soil water in March and this continued in July. In August there was a shift toward the groundwater trend line and slightly toward the passive wick soil water values observed. September tree-water values plotted outside of the typical bulk-soil-water zone and towards the observed passive-wick-sample values. November showed a division between tree water values that plotted in the bulk-soil-water region and outside it towards the passive-wick sample values. February tree values plotted in the bulk-soil-water field.

March

RT 2 tree isotope values show good agreement with soil water values for this sampling time (Figure 51). RT 4 tree isotope values show good agreement with respect to deuterium but exhibit deviation from $\delta^{18}O$ values. VB 1 tree isotope values plot slightly lighter than corresponding soil water values with respect to $\delta^{18}O$ and with δD (Figure 51). Despite the slightly lighter values that tree-water isotope values exhibit, they appear to be on a common linear trend line. VB 2 tree isotope values plot among soil water values along a linear trend line. Unfortunately, VB 3 tree-water samples had to be excluded due to spectral interference. However, VB 4 & 5 tree waters plotted in good agreement with VB 3 bulk-soil-water values and in fair agreement with the VB 4 bulk soil sample.

Samples from thinned-plot locations (open symbols in Figure 51) appear to exhibit linear trends with more enriched $\delta^{18}O$ and δD values.

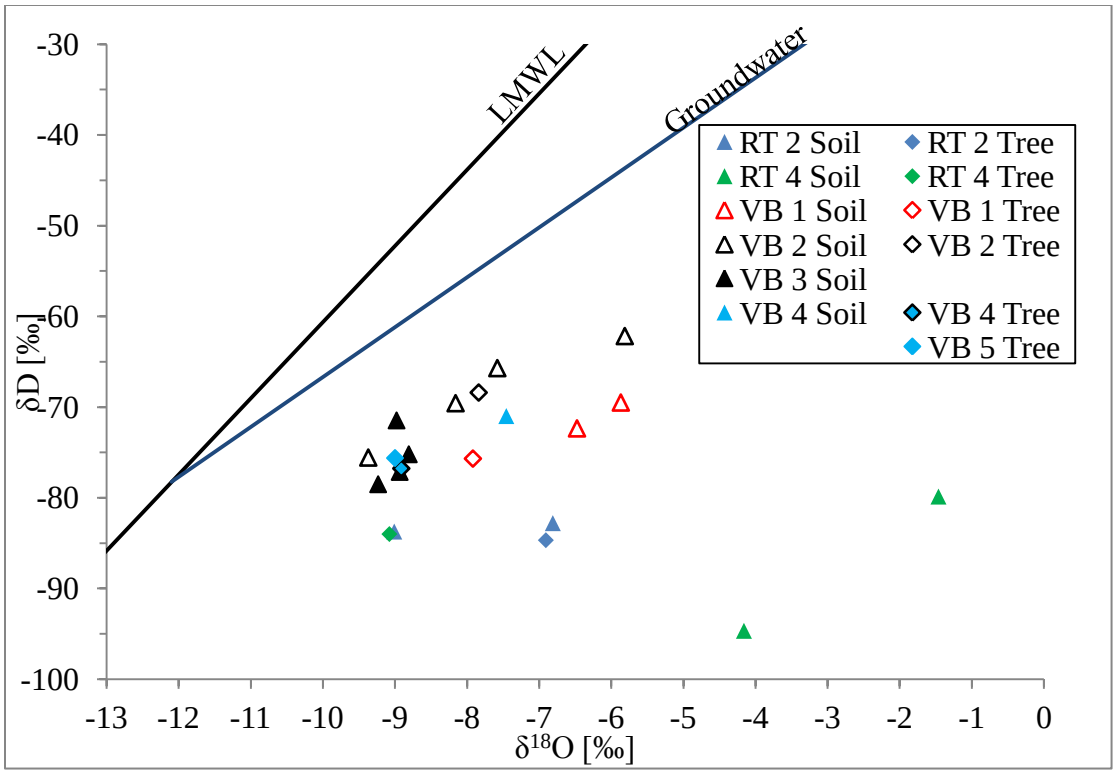

Figure 51: Isotopic values for bulk-soil-water and tree-water samples collected in March 2011 plotted on a $\delta^{18}O$ vs. δD plot. Data is presented such that bulk soil and tree water values are color coded by location. Open symbols represent thinned-plot locations.

The good agreement between RT 2 tree-water and soil water values indicates soil water usage at this time. The deviation from $\delta^{18}O$ values observed in RT 4 tree water could be due to a number of factors but is most likely explained by spatial heterogeneity of bulk soil water and insufficient sampling to capture the range of that variability. As was mentioned before, soil sampling at the ridge-top location was complicated by frequency of rocks encountered and the shallow depths attainable. The disagreement between the soil water values from the shallow samples obtained and the tree-water values suggests a usage of soil water that was deeper than was obtained in this sampling or possible usage of water from another source.

VB 1 tree isotope values being slightly lighter than bulk soil water values is likely due to insufficient depths sampled. The tree water values plot on the same linear trend indicating sources along a common evaporation trend line. Evaporation is likely considering the sandy soil composition at this location (Table 2).

VB 2 tree isotope values show good agreement with soil water values indicating soil water usage at this time. The linear trend line upon which both tree water isotope values and those of soil water plot suggests evaporation. The depth of this profile allowed for a range of soil values that was able to encompass the tree water values as opposed to the previously examined samples where soils were too thin for thorough sampling.

VB 4 & 5 tree waters plotting in good agreement with VB 3 bulk soil water suggesting soil water usage. Based on the limited sampling at the VB 4 soil pit and the discussion of statistical variance in bulk soil water data, these values are generally in agreement with bulk soil water samples.

Examining the thinned plot data vs. the control plots, it appears that the values are more enriched with respect to both $\delta^{18}O$ and δD and that the linear evaporation trend is more pronounced. The higher solar radiation due to absence of canopy cover creates a higher evaporative demand that is observed in the tree water through soil water trends.

Just as with bulk soil water samples, ridge top and valley bottom tree samples group separately (Figure 52). Ridge top samples tend to plot lighter with respect to deuterium

and with a larger range in $\delta^{18}O$. Valley bottom samples plot a bit heavier with respect to deuterium and tend to group tighter than the ridge top samples. The tree values from each area tend to plot well with their respective soil samples.

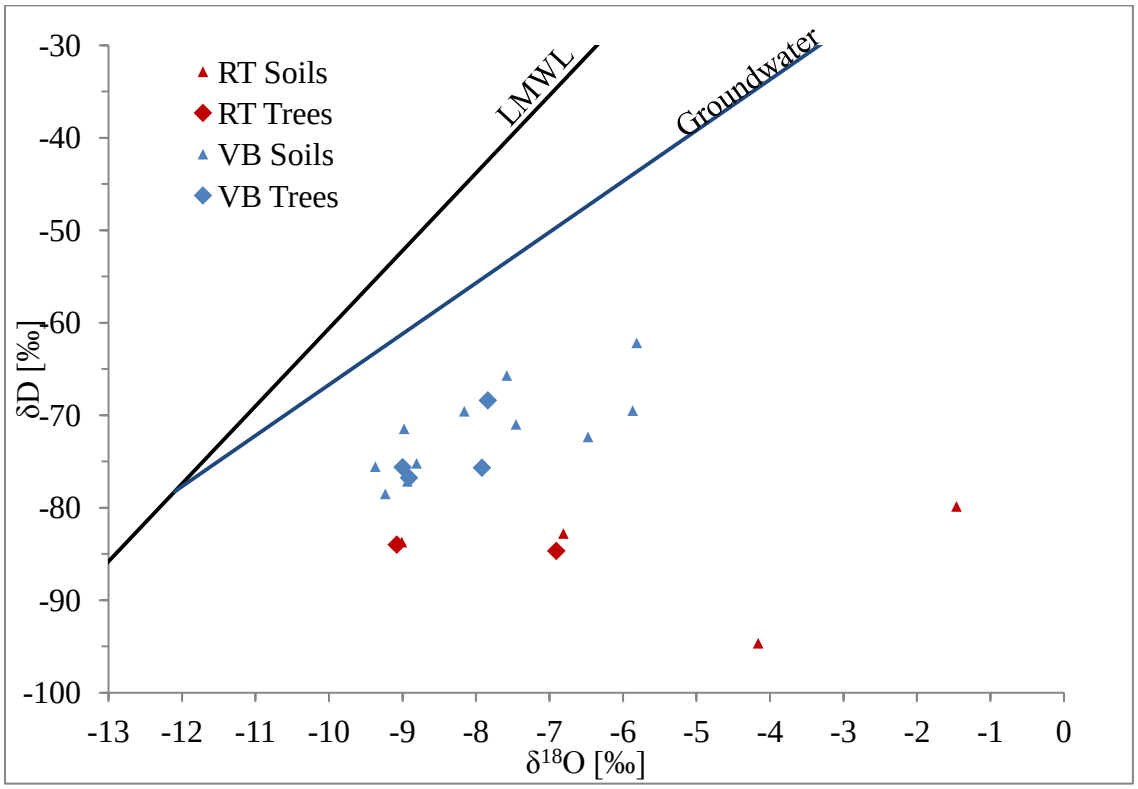

Figure 52: Isotopic values for bulk-soil-water and tree-water samples collected in March 2011 plotted on a $\delta^{18}O$ vs. δD plot. Data is presented such that ridge-top and valley-bottom locations are color coded.

March tree-water and bulk-soil-water samples exhibit good agreement suggesting use of bulk soil water at that time. Valley-bottom and ridge-top trees are both using bulk soil water which indicates that the mechanisms in the two settings are operating similarly. Conceptually, soils are likely near field capacity due to infiltration of recent snowmelt providing ample moisture for transpirative demands.

Summer 2011

Changes were observed in a series of tree samples collected over the summer of 2011. In March, June and July, tree-water values were in agreement with bulk-soil-water values. August tree-water samples displayed a shift toward heavier values with respect to deuterium. Tree waters sampled in September displayed more variation from bulk-soil-water values, this time with a shift toward heavier $\delta^{18}O$ values.

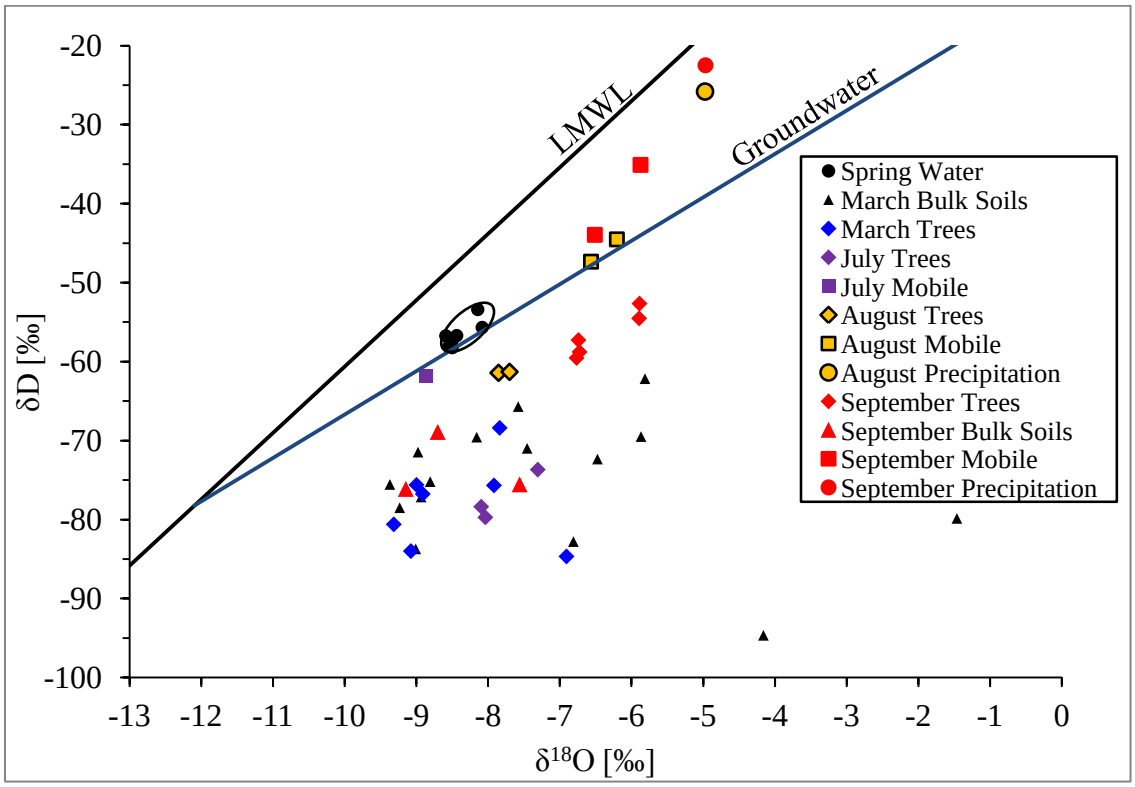

Figure 53: Isotopic values for local spring water, March 2011 bulk-soil-water samples, summer passive-wick samples, summer trees, September passive-wick soil water and September tree water plotted on a $\delta^{18}O$ vs. δD plot. Because bulk soils were not sampled in the summer, March soil values are shown here as a reference (see bulk-soil-water variability section above). Note that the y-axis scale is different than in other plots in order to encompass precipitation values.

March soil values are shown in Figure 53 for reference because summer soils were not sampled. March values were chosen based on the assumption that bulk-soil-water values change little with time (see statistical analysis above) so March values should be a fairly good representation of summer bulk soil values.

Early-summer tree-water isotope values (June and July) display good agreement with presumed bulk-soil-water values. Later-summer tree-water isotope values (August and September) display poor agreement with bulk-soil-water values. The temporal evolution of the tree-water values appears to mimic that of the mobile-soil-water samples, which in turn mimic seasonal precipitation values.

September

VB 2, VB 3 and RT 2 tree isotope values show poor agreement with bulk-soil-water values and with passive-wick soil-water samples. The tree values tend to plot together in a region that is in between the bulk-soil-water and passive-wick soil-water samples.

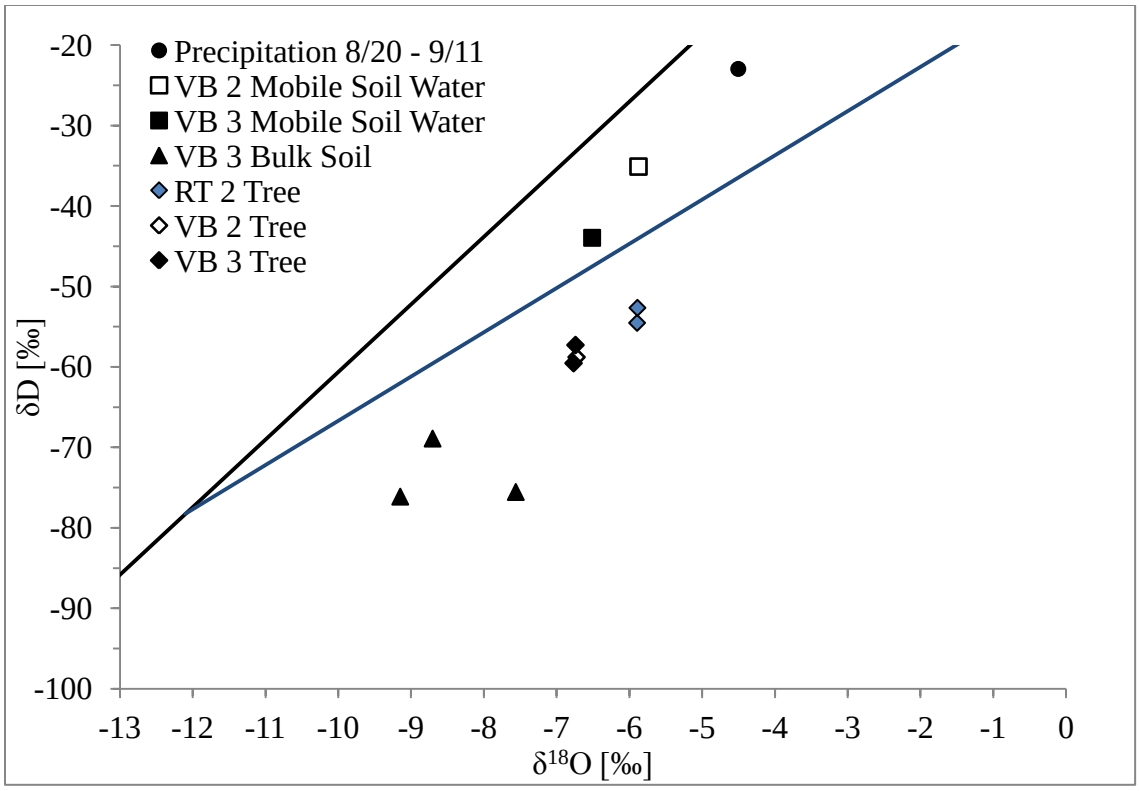

Figure 54: Precipitation, tree-water, bulk-soil-water and passive-wick soil-water isotope data collected in September 2011 plotted in $\delta^{18}O$ vs. δD space. Note that the y-axis scale is different than in other plots in order to encompass precipitation values. These samples were collected in September 2011, near the end of the monsoon season. The position of the precipitation and passive-wick water samples makes them seem a likely end member for possible tree-water sources.

All tree-water isotope values show poor agreement with bulk-soil-water and passive-wick soil-water values. However, when examining tree-water isotope values with bulk-soil-water, passive-wick soil-water and precipitation values, a mixing pattern becomes evident. It appears that at this time dual usage of bulk soil water and passive-wick soil water was occurring.

This passive-wick soil water i.e., or mobile soil water, was likely being derived from a shallow epikarst feature. Additionally, if trees were using recent precipitation preferentially from soils, a pronounced increase in uptake following precipitation events would be expected. Figure 55 shows that this did not occur in August during the peak of the monsoon season.

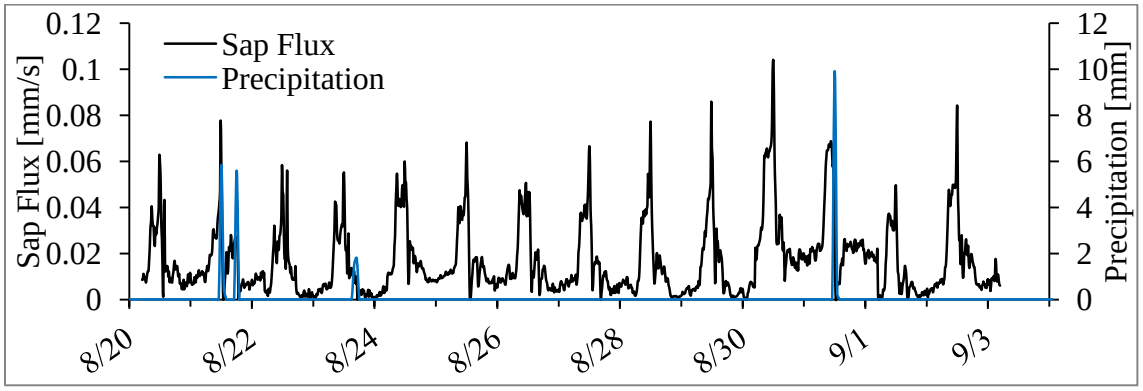

Figure 55: Sap flux and precipitation from August 2011. There seems to be no correlation between precipitation and increased sap flux. The absence of increased transpiration following precipitation events and their introduction of available water seems to indicate that trees have some other reliable water source from which they derive mobile water.

The tree water isotopic signature indicates that trees were deriving water from two isotopically distinct sources. Their insensitivity to precipitation inputs suggests that they are not deriving that water from the soil matrix and that there must be an alternative and reliable source. This is in conflict with the hypothesis that increased sap flow would be observed following monsoonal storms.

In their study examining vegetative water use near streams, Brooks et al. [2009] found that trees in their watershed did not use water from recent precipitation inputs. Rather, trees used water that had initially wet soils in the beginning of the rainy season and was retained in the smallest pore spaces throughout the rainy season. Though this is not exactly the same situation, it does provide an example of trees do not respond to recent precipitation due to use of a more reliable water source.

November

Tree isotope values from VB 7 & 8 appear to be in good agreement with bulk soil water values (Figure 56). VB 9 tree isotope values appear to be in good agreement with the more enriched bulk-soil-water values. Both RT 2 and RT 6 tree isotope values show fair agreement with soil water values but there does seem to be a slight variation toward mobile-soil-water values. VB 2 tree water values are not in agreement with bulk-soil-water values or passive-wick samples.

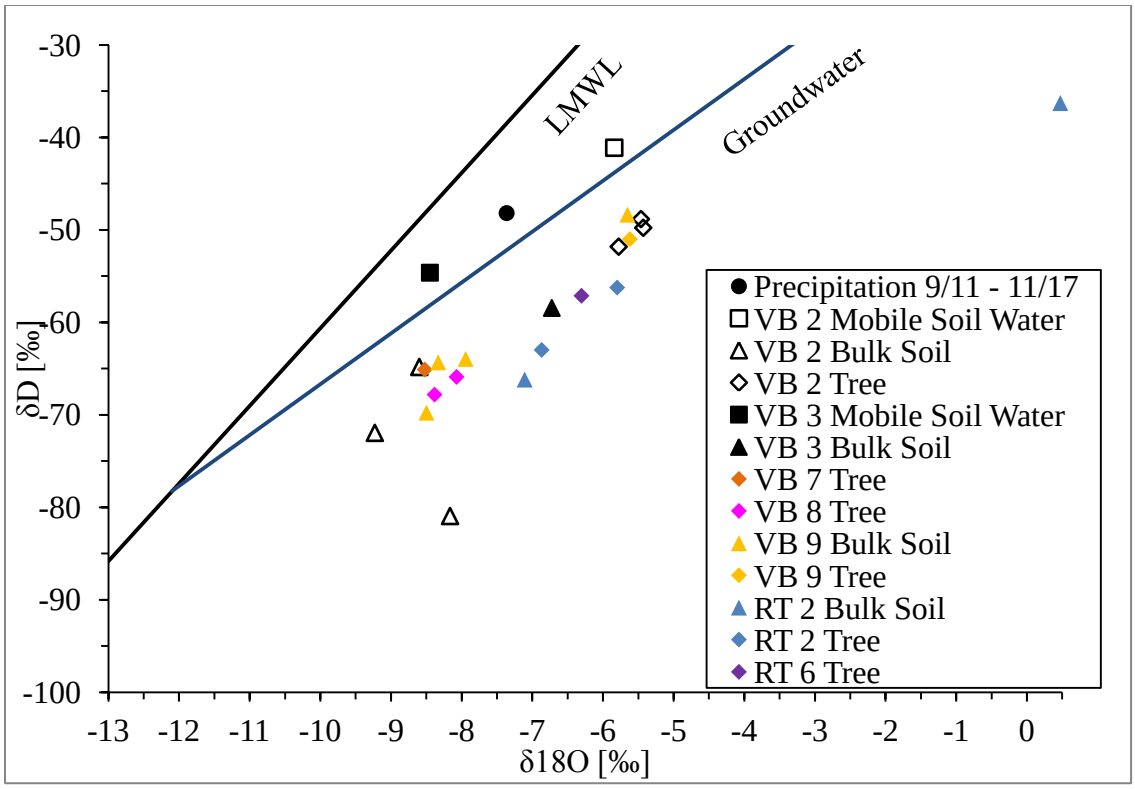

Figure 56: Precipitation, tree-water, bulk-soil-water and passive-wick soil-water isotope data plotted in $\delta^{18}O$ vs. δD space. These samples were collected in November 2011, after the monsoon season.

Tree-isotope values from VB 7 and VB 8, a tree located next to a collection pond and just below a spring discharge, show good agreement with soil water values suggesting bulk-soil-water usage. VB 9 tree-isotope values appear to be in good agreement with shallow, evaporated bulk soil water. This is supported by noting the small size of the tree sampled (Table 4) and assuming the tree to have a shallow root system.

Both RT 2 and RT 6 tree-isotope values show enough agreement to say that they are using bulk soil waters though there may be some influence from mobile soil water. This location, being on the ridge top where soils are thin and fractured bedrock quite shallow, is a likely setting for dual use of bulk soil water and mobile soil water collected in

underlying fractures. With the shallow soils, it is likely that water passing through the soil via preferential flow paths would be relatively unaltered from its original composition when it fell as precipitation.

The VB 2 tree samples however, exhibit mixed use of bulk soil water and mobile soil water. These values are quite similar to those observed in September though they are a bit heavier with respect to both $\delta^{18}O$ and δD. In September, it was tempting to interpret this as preferential use of recent precipitation as it moved through soil profiles. However, the precipitation inputs for November do not appear to be an eligible end member for tree-water values. Instead, this data suggests storage of mobile soil water. This storage could be in the soil profile or in the shallow fractured bedrock underlying the soils as suggested by Newton et al., [2009].

To summarize November samples, tree use was one of two categories: bulk soil water usage or mixed bulk soil water and mobile water usage. With the exception of VB 2, trees had switched back to primarily using bulk soil water. VB 2 tree-water values indicate that a mobile-soil-water source was still being used. This difference in tree water usage at the same sampling time is quite revealing for the spatial distribution of epikarst and its differential drainage rates.

February 2012

Trees sampled in February were in good agreement with bulk soil waters if the assumption that lighter bulk-soil-water values would have been encountered at greater depth (Figure 57). This is similar to results from samples collected in March 2011, the previous year, when trees were determined to be using bulk soil water.

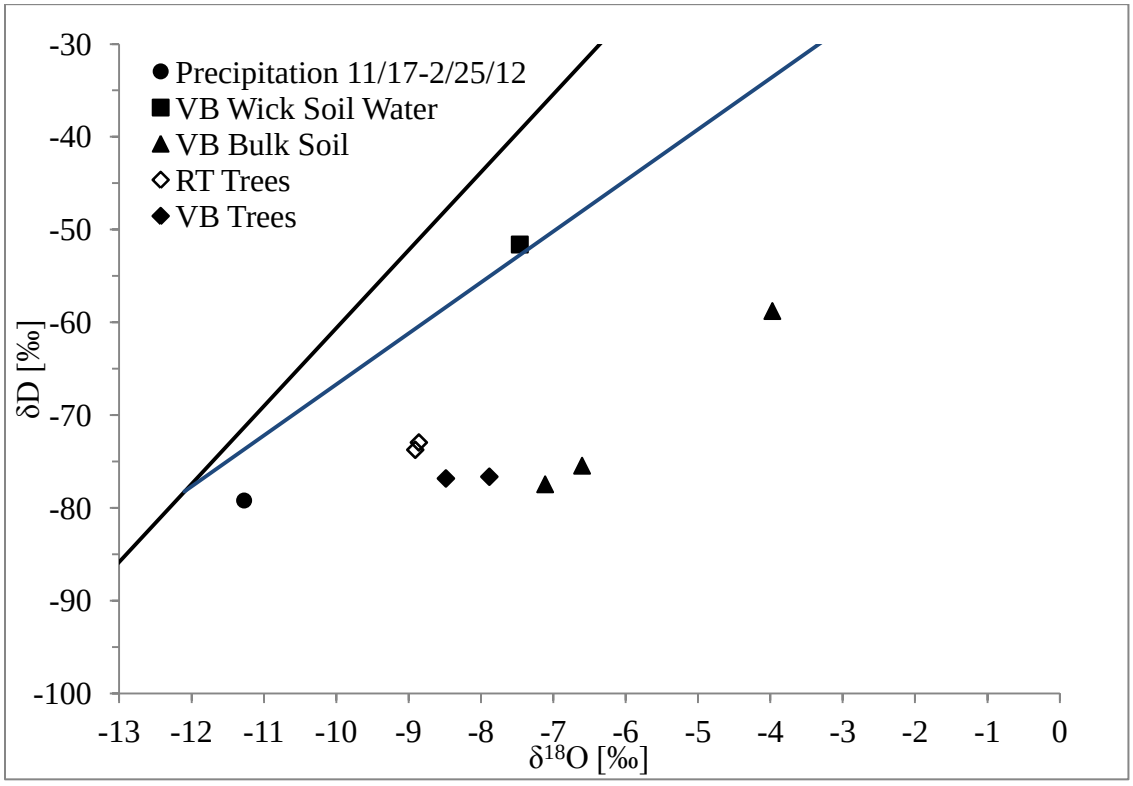

Figure 57: Tree water, bulk-soil-water and passive-wick soil water isotope data plotted in $\delta^{18}O$ vs. δD space. These samples were collected in February 2012 after snowmelt. This plot has bulk-soil-water values from a samples taken in the valley bottom and tree water values from both valley-bottom and ridge-top trees. The local meteoric water line (LMWL) and groundwater line are shown for reference.

Comparing ridge-top and valley-bottom samples on the $\delta^{18}O$ vs. δD plot, we see that the ridge-top tree-water samples have lighter values. This is likely due to the different

influences of recent snowmelt between the two locations. The ridge top likely had less antecedent water at the time of snowmelt and so the influence of this depleted input would be more prevalent in the bulk soil water isotopic values. In valley-bottom soils that retain more water due to their higher clay content, the influence of the light snowmelt is more strongly attenuated by antecedent water.

5.4.2 Analytical Model

A model to describe the evolving isotopic composition of a bedrock fracture filling with water through the monsoon season was developed to help understand the epikarst reservoir as a potential water source for trees. Precipitation data observed in the watershed was used to determine how much water was input into the system. The precipitation was partitioned into five periods correlated with five collections of passive-wick samples. The amounts of observed precipitation associated with these periods were taken as the cumulative sums of observed precipitation between collection times. These were assumed to have the composition of the passive-wick samples collected at that time. This information was used to calculate the fracture-reservoir composition based on the relative inputs from the five periods. The equations to describe the calculations are as follow.

Composition July

Equation 7

$$\delta_{total} = \frac{P_{June-July}}{P_{total}} * \delta_{June-July}$$

$$P_{total} = P_{June-July}$$

Composition August

Equation 8

$$\delta_{total} = \frac{P_{June-July}}{P_{total}} * \delta_{June-July} + \frac{P_{July-AugA}}{P_{total}} * \delta_{July-Aug}$$

$$P_{total} = P_{June-Aug}$$

…

Composition October

Equation 9

$$\delta_{total} = \frac{P_{June-July}}{P_{total}} * \delta_{June-July} + \frac{P_{July-AugA}}{P_{total}} * \delta_{July-AugA} + \frac{P_{AugA-AugB}}{P_{total}} * \delta_{July-AugB} + \frac{P_{AugB-Sept}}{P_{total}} * \delta_{AugB-Sept} + \frac{P_{Sept-Oct}}{P_{total}} * \delta_{Sept-Oct}$$

$$P_{total} = P_{June-Oct}$$

Where P is precipitation taken from observed data and δ is the isotopic composition of passive wick samples.

The main assumptions of this model are that 1) mass balance of precipitation was preserved as if the fracture had no soil cover and 2) that isotopic changes induced by passing through the soil profile produced effluent with the composition of passive wick samples. The results can be seen in Figure 58.

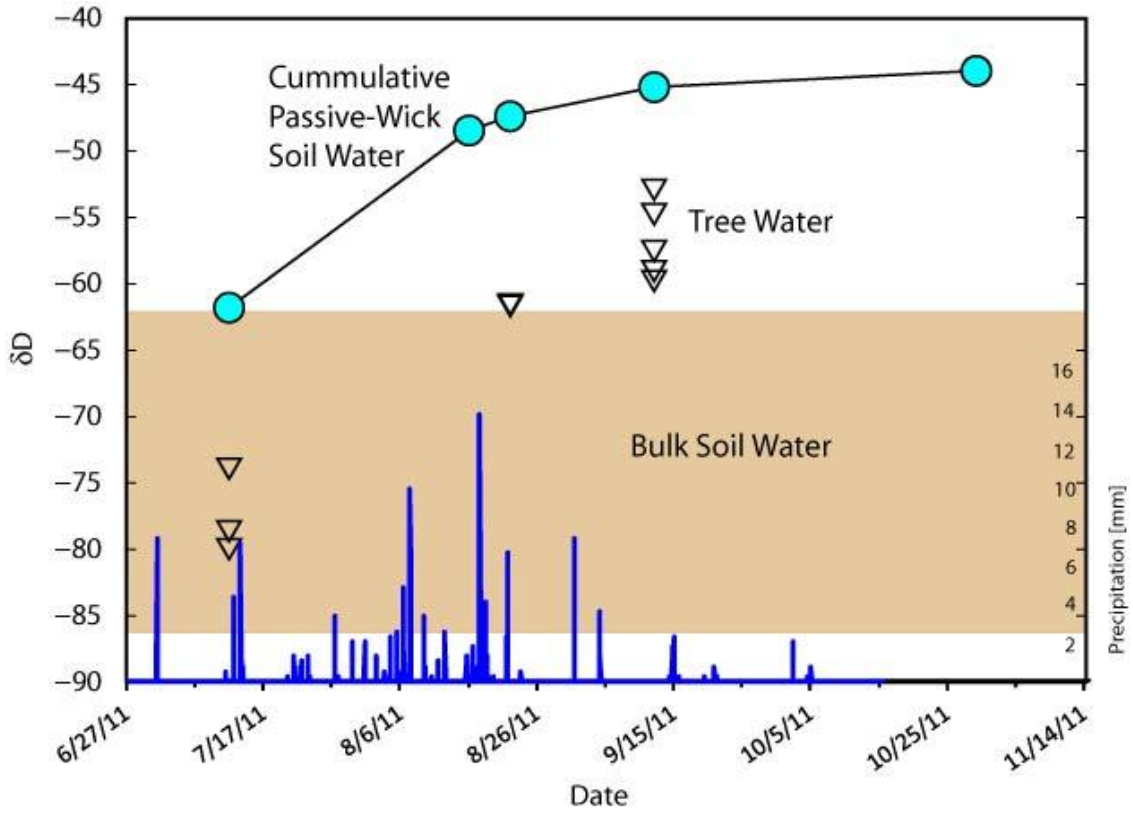

Figure 58: The modeled isotopic composition of a fracture filling with effluent exiting the bottom of soil profiles. Precipitation, the range of bulk soil water observed and tree-water isotopic data are also shown. This model assumes that 1) no water is retained in the soil matrix, 2) the composition of effluent leaving the bottom of the soil profile is the same as water collected by passive wick samplers, and 5) there are only five discrete inputs as the fracture fills.

As can be seen in Figure 58, tree water values tend to mimic the modeled composition of cumulative passive-wick soil water through the monsoon season. Tree-water values for samples collected in September were completely out of the range of observed bulk soil water values. This deviation from observed bulk soil water values suggests tree use of a water source similar to the modeled composition of epikarst reservoir water.

Spatial Variability

In November, most trees had returned to exclusive use of bulk soil water suggesting that the epikarst reservoir was no longer available. At this time, the VB 2 tree continued to use a mobile soil water component suggesting some epikarst-reservoir water was still available at that location. This helps us to understand the spatial distribution of the epikarst feature and the relationship it has with tree water usage. This type of information is important in determining the effects of tree thinning on the hydrological system because it affords us a glimpse into the subsurface.

Temporal Variability

Tree-water values were in good agreement with bulk-soil-water values up until the onset of the monsoon season at which point tree-water composition began to move toward mobile-soil-water composition (Figure 50). This data set suggests trees were using a mixture of bulk soil water and mobile water as mobile water became available. Absence of increased uptake following recent precipitation suggests that the source of this mobile water was more reliable than would be expected of excess water passing through the soil profile. Continued use of this mobile water source in November suggests that there is some longer term storage that trees are able to use after monsoon rains have stopped and precipitation signatures have changed.

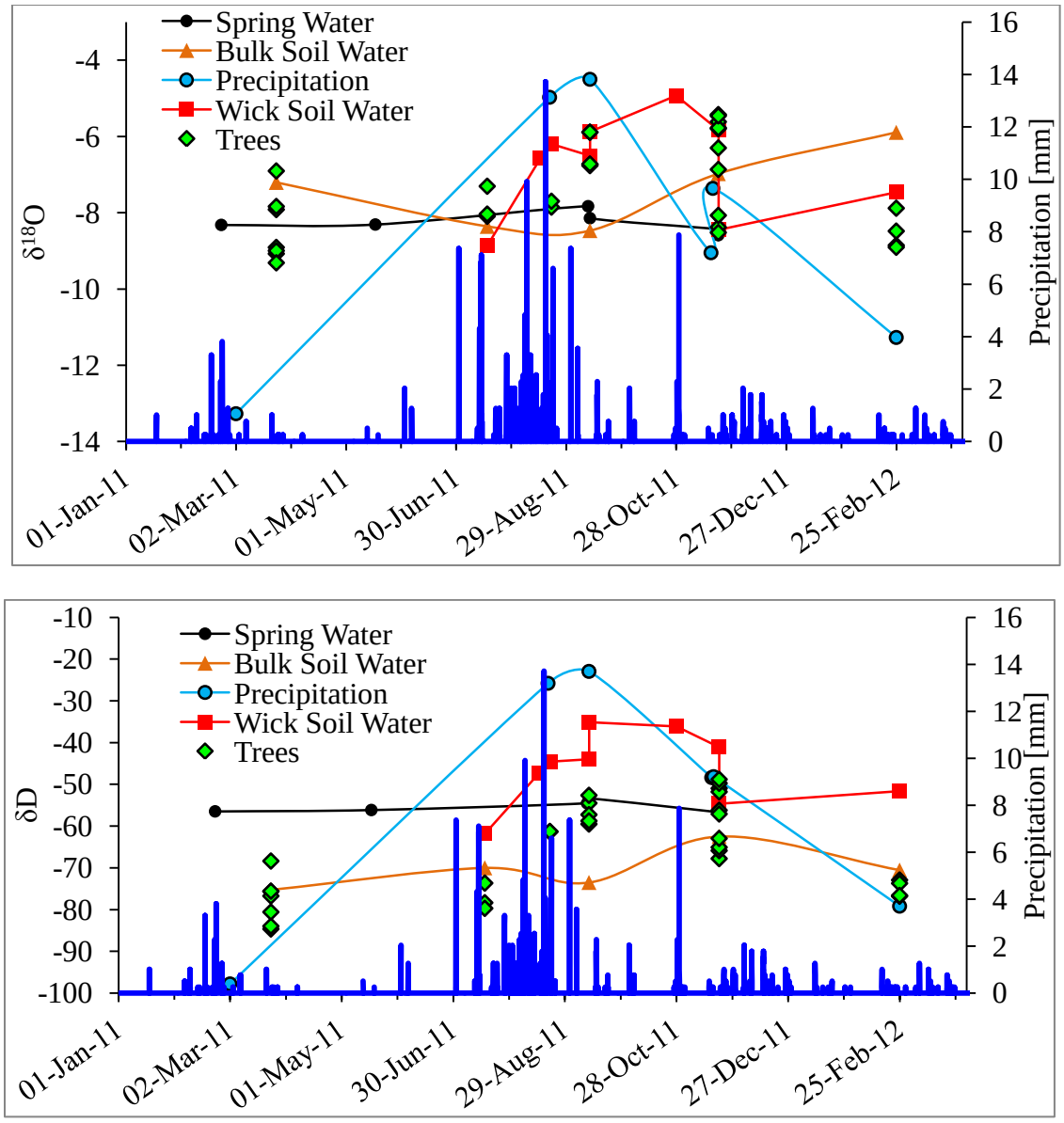

Figure 59: Time series showing stable isotope values for spring water, bulk soil water, passive-wick soil water, precipitation and tree water. Average values were used for bulk soil water. The deviation of tree-water values from bulk-soil-water values correlates well with the heavy precipitation input of the monsoon season.

5.4.3 Discussion

Trees used bulk soil water after spring snowmelt and until the onset of the monsoon season when tree water indicated mixed usage of mobile and bulk soil water. Aside from

differences that can be attributed to different bulk-soil water isotopic compositions, there was no pronounced difference in tree-water sources between ridge-top and valley-bottom locations. There was no evidence of trees using groundwater and no increase in sap flow following monsoonal precipitation events. Changes observed in the isotopic composition of precipitation between September and November combined with the lack of change in tree-water signature suggests storage in soil and an epikarst component. Some of the trees had switched back to primary usage of bulk soil water in November (VB 7, VB 8, VB 9 & RT 2 Figure 56) while others were still using some amount of mobile soil water (VB 2 Figure 56). The spatial distribution of trees continuing to use mobile soil water vs. those that had switched back to exclusive use of bulk soil water is suggestive to spatial variation and variable drainage rates of the epikarst feature.

Conceptual Model- Trees

In March, bulk soil waters met the transpirative demands of trees in the watershed. Recent snowmelt provided enough water for trees to derive their water from near-surface root systems. This can be seen conceptually in Figure 60.

With the assumptions that we know the composition of water in the underlying epikarst reservoir, the source of tree water from the September data set appears to be a mix of bulk soil water from the soil profile and water derived from the underlying epikarst reservoir. This would suggest a bimodal root configuration with a superficial root network and a deeper tap root network as is seen in Figure 60. Bimodal root

configurations in Douglas Fir were reported by McMinn [1963]. The superficial root network derives water from bulk soils and the deeper tap root network derives water from the epikarst reservoir. The depth of this reservoir need only be as shallow as the deepest extent of trees in the area. In a bibliographical study supplemented by their own data set, Foxx and Tierney [1986] reported an average evergreen tree root depth of 336 cm with a range from 10-6096 cm.

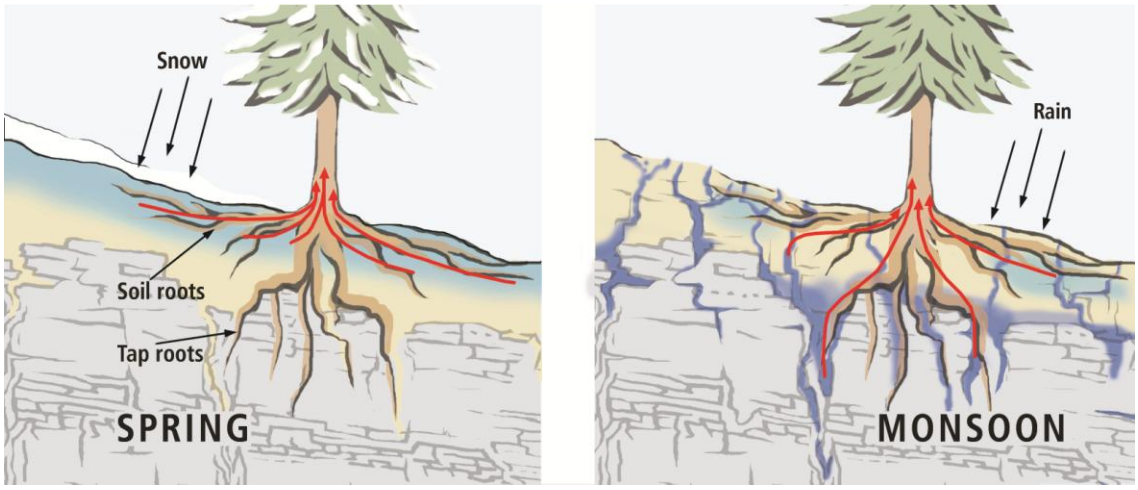

Figure 60: Conceptual models for tree water use in the spring and the monsoon seasons. In the spring, snowmelt evenly wets the soil matrix, providing the water for tree usage. Deeper tap roots are inactive at this time due to the availability of shallow soil water. During the monsoon season, heavy rains create preferential flow conditions that allow water to flow through macropores and quickly pass through soil profiles where it can accumulate in underlying fractured bedrock. As this alternative source becomes available, deeper tap roots become active to derive part of the trees' water demand from this epikarst reservoir.

It is possible that trees derive mobile water directly from macropores in the soil as it is passing through the soil profile. However, the absence of uptake spikes following precipitation events does not support this and suggests use from some type of reliable storage of mobile soil water. Further support for storage of mobile soil water is seen by

trees that continued to use water with an isotopic signature similar to that of monsoonal precipitation into November despite the seasonal change in the isotopic composition of the precipitation. Drainage of this reservoir is evidenced by tree water returning to bulk soil-water-composition during the November sampling.

In March, spring snowmelt had uniformly wetted soils and supplied sufficient water for tree use (Figure 60). With the onset of the monsoon season, intense precipitation events provide the conditions necessary for preferential flow and rapid, deep percolation that collects in epikarst features of the shallow, fractured carbonate bedrock (Figure 48). Trees then begin to derive part of their water needs from this epikarst reservoir (Figure 60). As this temporarily available water source drains, trees switch back to bulk soil water usage.

6 CONCLUSIONS

Both immobile waters and mobile soil waters are present in the study area. Immobile water appears to have evolved from winter precipitation that is lighter in stable isotopes than local groundwater. This winter precipitation is retained in the soil matrix through changes in seasonal precipitation input. It is rendered immobile due to the high capillary tension of the smallest pores where it is bound.

Mobile waters appear a mixture between seasonal precipitation and antecedent bulk soil water. The degree of mixing appears to change with time. As precipitation enters the soil, it inevitably mixes with water that is stored in small pores by specific retention. Mobile and immobile waters are distinguishable by isotopic analysis, which indicates that preferential flow is active within the system.

The varing degrees of mixing observed in mobile-soil water appear to be dependent on the amount of water introduced to the system. Early in the monsoon season mobile soil waters had isotopic compositions similar to bulk soil water and as more precipitation entered soils, mobile soil waters became more similar to precipitation. This evolution

toward the composition of rain water is a result of flushing of the mobile-water reservoir through soils via macropore networks, as precipitation inputs continue.

Mobile soil waters presumably are able to pass through thin soil profiles and recharge groundwater via fracture networks in the shallow bedrock. Water exiting soils also recharges the shallow epikarst reservoir, a system of fractures and conduits that is not well connected the larger groundwater system. While this may not contribute to groundwater recharge directly, the epikarst reservoir is activated by large events on a decadal scale [*Newton et al.*, 2012]. This reservoir appears to fill rapidly during the monsoon season and drain slowly thereafter.

Trees in the study area use bulk soil water throughout the year but show evidence of mobile-soil-water usage during the monsoon season. No groundwater usage was observed and no significant difference between ridge-top and valley-bottom tree-water usage was observed during this study. There also was no increase in sap flow observed following monsoonal precipitation events. We propose that the mobile-soil-water signature seen in tree water is derived from the underlying epikarst reservoir as it becomes available through the monsoon season (Figure 60). A shift back to complete usage of bulk soil is seen following the end of monsoon season's indicating that this reliable water source drains or is otherwise depleted. This shift was seen at different times for trees in different locations indicating epikarst drainage is spatially variable.

Based on the findings of this study, tree thinning should increase groundwater recharge in the study area. Tree usage of mobile soil water, even if only temporary, removes water from a part of the subsurface that is otherwise unaffected by evaporation. The mobile water being transpired had either already recharged local perched aquifers or would have been stored until the conditions required to mobilize epikarst water were met. Thinning will decrease this sink on shallow, perched aquifers or epikarst reservoir's leaving more water in the subsurface for regional groundwater recharge.

7 FUTURE WORK

To supplement the findings of this study, continued monitoring of tree water usage, bulk soil water and mobile soil water is recommended in conjunction with sap-flow monitoring and predawn leaf-potential measurement. Sap-flow monitoring will help to quantify tree water usage of both bulk soil waters and underlying epikarst reservoir waters. Continued monitoring of bulk and mobile soil water as well as trees will help to determine the relative proportions of them being used. This information will help to better understand the role trees play in the system as well as what impacts tree thinning may have. Due to its correlation with matric potential, predawn leaf potential will provide a better understanding of the subterranean environment from which trees derive their water. Consistent and/or low matric potentials during the monsoon season, in conjunction with isotopic evidence of mobile soil water use, would support the deep-tap-root epikarst-usage hypothesis.

8 APPENDICES

Appendix I Data Tables

Table 5: Soil Descriptions

	Color		Peds	Consistence			Structure				
Sample	Moist	Dry	Involvement	Gravels	Plasticity	Stickiness	Dry	Hardness	Texture	$CaCO_3$	Hf*
VB 1- 10	7.5 YR 2.5/1	7.5 YR 2.5/1	0	5	sp	ss	abk	s	SCL	-	hf
VB 1- 25	10 YR 2/2	10 YR 2/2	0	40	sp	ss	sbk	h	SCL	-	hf
VB 1- 40	10 YR 2/2	10 YR 3/3	0	60	p	ss	sbk	sh	SC	slight	hf
VB 2- 15	10 YR 2/2	10 YR 2/2	1	0	p	ss	sbk	sh	CL	-	-
VB 2- 25	7.5 YR 3/2	10 YR 4/3	2	0	vp	vs	sbk	sh	C	-	-
VB 2- 40	10 YR 4/4	10 YR 3/3	3	0	vp	vs	sbk	h	C	slight	-
VB 2- 55	7.5 YR 4/4	7.5 YR 4/3	3	10	vp	vs	abk	vh	C	slight	-
VB 2- 65	10 YR 3/6	7.5 YR 4/6	3	10	vp	vs	sbk	sh	C	slight (gravels)	-
VB 3- 20	10 YR 3/3	10 YR 3/1	1	0	sp	s	abk	h	SCL	-	-
VB 3- 35	7.5 YR 3/3	7.5 YR 2.5/3	1	0	vp	vs	sbk	h	C	-	shf
VB 3- 50	5 YR 3/3	2.5 YR 3/3	2	0	vp	vs	sbk	h	C	-	-
VB 3- 75	5 YR 3/3	5 YR 3/3	2	0	vp	vs	sbk	sh	C	-	-
VB 3- 95	10 YR 4/4	7.5 YR 3/3	2	0	vp	vs	sbk	sh	C	-	-

VB 5- 30	10 YR 3/3	10 YR 2/2	1	10	p	s	sbk	h	SCL	slight	hf
VB 9- 25	2.5 YR 2.5/1	2.5 YR 2.5/1	1	40	sp	ss	gr	-	SiCL	slight	hf
VB 9- 45	10 YR 3/3	10 YR 4/4	1	30	p	ss	sbk	h	CL	slight	hf
VB 9- 65	10 YR 2/2	10 YR 3/3	1	20	p	ss	sbk	s	CL	slight	hf
VB 9- 85	7.5 YR 2.5/2	10 YR	1	0	p	s	sbk	s	CL	-	hf
RT 2- 5	10 YR 3/1	10 YR 3/2	2	10	p	s	sbk	vh	CL	-	hf
RT 2- 20	10 YR 2/1	10 YR 4/1	2	10	vp	s	sbk	vh	SiCL	-	hf
RT 2- 30	10 YR 2/2	10 YR 3/2	3	10	vp	vs	abk	vh	C	-	hf
RT 2- 40	7.5 YR 2.5/2	7.5 YR 3/2	2	20	p	s	abk	vh	CL	-	hf
RT 3- 15	7.5 YR 2.5/2	10 YR 2/2	2	5	sp	s	sbk	h	SCL	-	hf
RT 3- 30	10 YR 2/2	10 YR 3/3	1	10	sp	ss	sbk	h	SL	-	hf

Hf is hydrophobicity
Gravels are measured as percent of total sample.

Plasticity	sp- slightly plastic; p- plastic; vp- very plastic
Stickiness	ss- slightly sticky; s- sticky; vs- very sticky
Dry Consistence	g- granular; abk- angular, blocky; sbk- sub-angular, blocky
Hardness	sh- slightly hard; h- hard; vh- very hard
Texture	SCL- sandy clay loam; SC- sandy clay; SL- sandy loam; CL- clay loam; SiCL- silty clay loam; C- clay
Hydrophobicity	shf- slightly hydrophobic; hf- hydrophobicity

Table 6: Bulk Soil Water Data

Bulk Soils					
Date	Sample	Interference*	$\delta^{18}O$	δD	θ**
3/17/2011	VB 1- 10	3.05	-8.90	-136.08	0.29
	VB 1- 25	NaN	-5.87	-69.50	0.22
	VB 1- 40	NaN	-6.47	-72.35	0.21
	VB 2- 15	NaN	-5.81	-62.17	0.26
	VB 2- 25	NaN	-7.58	-65.70	0.31
	VB 2- 40	NaN	-8.16	-69.57	0.36
	VB 2- 65	NaN	-9.37	-75.56	0.38
	VB 3- 35	NaN	-8.81	-75.20	0.19
	VB 3- 50	NaN	-8.93	-77.15	0.19
	VB 3- 95	NaN	-8.98	-71.47	0.15
	VB 5- 30	NaN	-7.45	-70.99	0.18
	RT 2- 30	NaN	-6.81	-82.79	0.21
	RT 2- 40	NaN	-9.01	-83.72	0.19
	RT 3- 15	NaN	-4.16	-94.66	0.18
	RT 3- 30	NaN	-1.46	-79.86	0.19
7/17/2011	VB 2- 20	NaN	-8.36	-70.03	0.33
9/11/2011	VB 3b- 25	NaN	-7.56	-75.55	0.18
	VB 3b- 50	NaN	-8.70	-68.91	0.17
	VB 3b- 75	NaN	-9.15	-76.12	0.14
	VB 3- 20	1.32	-8.49	-86.25	0.14
	VB 3- 70	NaN	-9.23	-78.51	0.16
11/20/2011	RT 2- 5	NaN	0.48	-36.28	0.24

	RT 2- 10	NaN	-7.11	-66.18	-0.73
	RT 2- 20	1.46	-3.66	-63.27	0.26
	VB 2- 20	NaN	-8.16	-80.94	0.31
	VB 2- 40	NaN	-8.60	-64.82	0.32
	VB 2- 55	NaN	-9.23	-71.95	0.19
	VB 3- 20	NaN	-6.72	-58.44	0.18
	VB 9- 25	NaN	-5.65	-48.35	0.08
	VB 9- 45	NaN	-7.94	-63.95	0.11
	VB 9- 65	NaN	-8.33	-64.32	0.11
	VB 9- 85	NaN	-8.50	-69.76	0.11
2/25/2011	VB 2b- 13	NaN	-3.97	-58.78	0.14
	VB 2b- 18	1.67	-7.21	-91.93	0.13
	VB 2b- 23	1.41	-7.41	-88.30	0.12
	VB 2b- 25	NaN	-6.60	-75.45	0.12
	VB 2b- 30	1.82	-9.66	-110.12	0.13
	VB 2b- 33	NaN	-7.11	-77.46	0.13
	RT Open	7.26	-12.74	-257.82	0.43
	RT Canopy	1.51	-2.93	-76.94	0.49

* Highlighted values were flagged for spectral interference and not used in interpreted data

** θ is gravimetric water content and is a percent measurement

Table 7: Passive Wick Soil Water Data

Passive Wick Samples			
Date	Location	$\delta^{18}O$	δD
7/17/2011	VB 2	-8.36	-70.03
8/15/2011	VB 2	-6.56	-47.35
8/21/2011	VB 2	-6.20	-44.53
9/11/2011	VB 2	-5.87	-35.10
	VB 3	-6.51	-43.96
10/28/2011	RT 3	-4.93	-36.14
11/20/2011	VB 2	-5.84	-41.11
	VB 3	-8.45	-54.63
2/25/2012	VB 3	-7.46	-51.61

Table 8: Tree Water Data

Date	Sample	Interference*	$\delta^{18}O$	δD
3/17/2011	VB 1	NaN	-7.92	-75.68
	VB 2- a	19.82	-43.61	-577.11
	VB 2- b	2.20	-10.72	-112.72
	VB 2- c	NaN	-7.84	-68.40
	VB 3	7.13	-20.18	-247.28
	VB 4	NaN	-8.91	-76.77
	VB 5	NaN	-9.00	-75.62
	RT 1	2.11	-10.13	-114.48
	RT 2	NaN	-6.91	-84.67
	RT 3	1.65	-10.58	-110.81
	RT 4	NaN	-9.08	-84.00
	RT 5	5.15	-17.30	-196.82
	VB 7	NaN	-9.31	-80.61
6/4/2011	VB 3- Small	19.21	-41.74	-545.66
	VB 3- Medium	3.03	-12.33	-137.28
	VB 3- Large	3.26	-13.29	-146.51
	VB 7- a	16.94	-38.66	-493.29
	VB 7- b	4.38	-15.89	-172.04
	VB 7- c	5.45	-17.34	-201.67
7/17/2011	VB 6- Morning- a	10.70	-25.35	-331.84
	VB 6- Morning- b	NaN	-7.31	-73.68
	RT 2- a	NaN	-5.99	-69.88

	RT 2- b	NaN	-7.26	-74.86
	RT 2- Phloem- a	5.89	-16.48	-210.93
	RT 2- Phloem- b	NaN	-7.62	-70.98
	RT 2- Xylem- a	NaN	-8.09	-78.38
	RT 2- Xylem- b	NaN	-8.04	-79.73
	RT 5	2.65	-6.22	-114.07
8/21/2011	VB 2- a	1.77	-10.38	-99.78
	VB 2- b	NaN	-7.85	-61.43
	VB 2- c	NaN	-7.70	-61.30
9/11/2011	VB 2- Xylem	NaN	-6.72	-58.79
	VB 2- a	NaN	-6.83	-56.92
	VB 2- b	NaN	-6.80	-55.82
	VB 3- Xylem a	NaN	-6.74	-57.28
	VB 3- Xylem b	NaN	-6.76	-59.54
	VB 3- Phloem	NaN	-6.50	-58.20
	RT 2- a	NaN	-6.04	-51.66
	RT 2- b	NaN	-6.47	-52.61
	RT 2- c	NaN	-6.49	-54.12
	RT 2- Xylem a	NaN	-5.89	-54.53
	RT 2- Xylem b	NaN	-5.89	-52.66
	RT 2- Phloem	NaN	-5.31	-48.73
11/20/2011	VB 3- a	NaN	-5.78	-51.81
	VB 3- b	NaN	-5.43	-49.77
	VB 3- c	NaN	-5.46	-48.83
	VB 7- a	NaN	-8.52	-65.10

	VB 7- b	15.80	-42.31	-526.47
	VB 8- a	NaN	-8.38	-67.81
	VB 8- b	NaN	-8.07	-65.90
	VB 9	NaN	-5.62	-51.00
	RT 2- a	NaN	-5.80	-56.23
	RT 2- b	NaN	-6.87	-62.98
	RT 6	NaN	-6.30	-57.12
2/25/2012	VB 2- Core	NaN	-8.26	-75.43
	VB 2- a	NaN	-8.48	-76.83
	VB 2- b	NaN	-7.88	-76.64
	RT 2- Core	NaN	-5.81	-76.13
	RT 2- a	NaN	-8.86	-72.95
	RT 2- b	NaN	-8.91	-73.74

* Highlighted values were flagged for spectral interference and not used in interpreted data

Appendix II Supplemental Data

The upper spring in Three L Canyon flows into a series of collection ponds where much of the water infiltrates the vadose zone and will eventually reenter the shallow-groundwater system. While it is exposed at the surface, water is subjected to evaporation and undergoes isotopic enrichment. Stable-isotope data resulting from this process is shown in Figure 61 and Figure 62 where stable-isotope values of water sampled along a surface flow path exhibit an evaporative enrichment trend. Also depicted in Figure 61 and Figure 62, a nearby spring exhibits an isotopic value that suggests a homogenized mixture of bulk groundwater. On the regional scale, this process is what leads to the evaporative signature in regional groundwater.

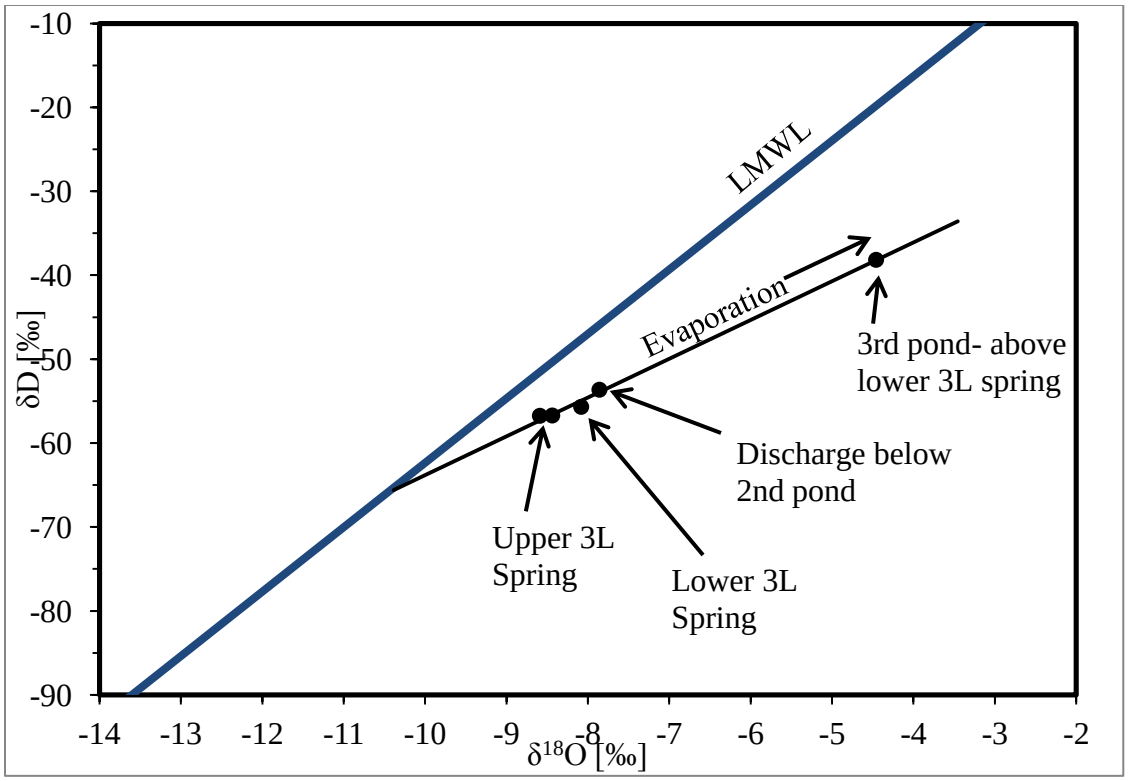

Figure 61: Isotopic values plotted in $\delta^{18}O$ and δD space for a surface flow path sampled in Three L Canyon. Water emerges from a spring and flows along a small stream, through three manmade collection ponds where it becomes evaporatively enriched before infiltrating and recharging groundwater.

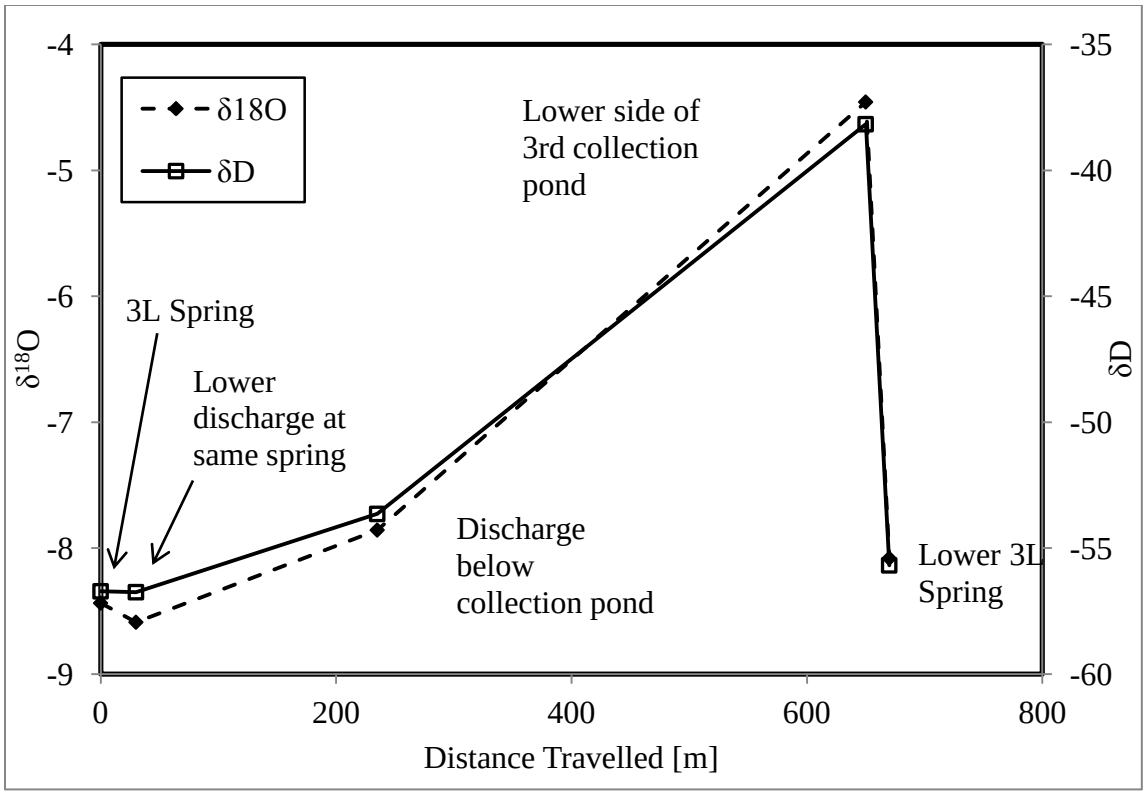

Figure 62: $\delta^{18}O$ and δD values for waters along a surface flow path in Three L Canyon. Water emerges from a spring and flows along a small stream, through three manmade collection ponds where it becomes evaporatively enriched before infiltrating and recharging groundwater.

This process of evaporative enrichment during surface exposure and reinfiltration is characteristic of the region and leads to the evaporation trend observed down regional flow paths.

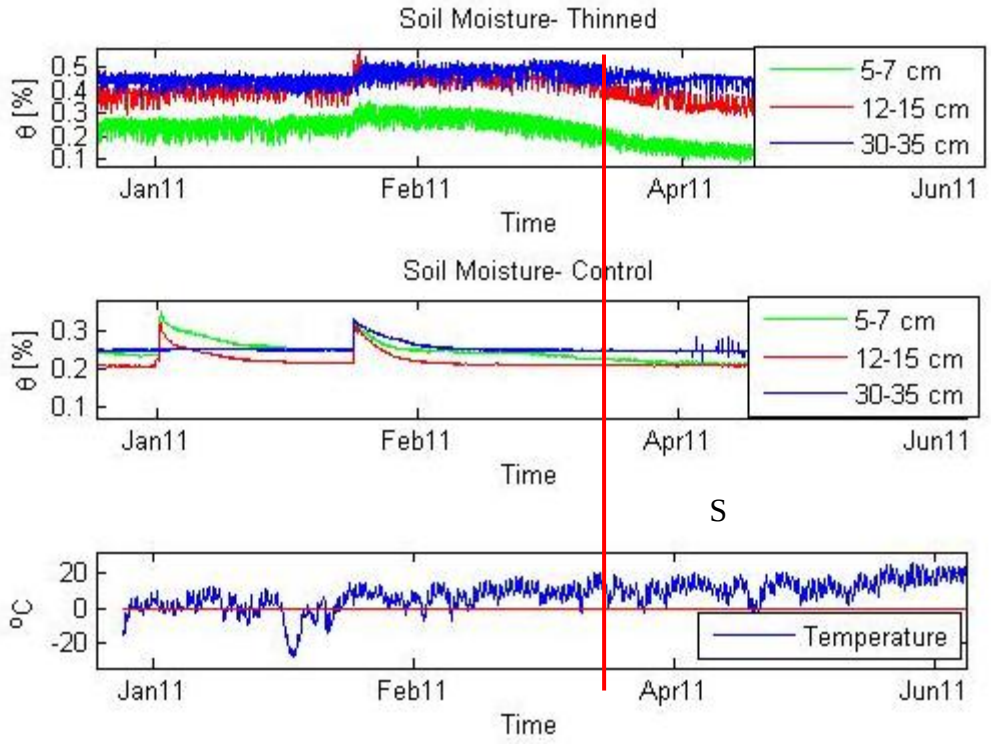

Figure 63: In situ soil-moisture data from the first part of 2011. The red line indicates the timing of March sampling. The data indicates that spring snowmelt was a significant amount of time previous to sampling allowing ample time for profile development. Data from personal communication with H.R. Garduño, (New Mexico State University).

March 2011

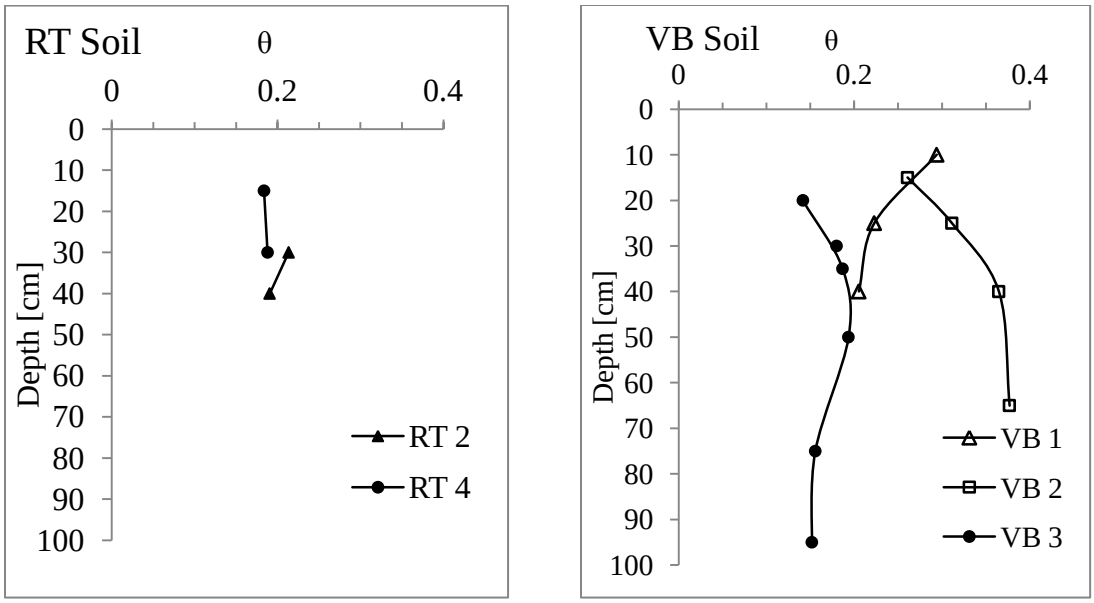

Figure 64: Soil gravimetric water content (θ) vs. depth for ridge top and valley bottom soil profiles sampled in March 2011. The ridge-top plot from which these samples were taken has an approximate tree density of 1482 trees/hectare. VB 3, located on a control plot, is shown with closed symbols while thinned plot sampling locations are shown with open symbols. Tree density on the control plot is 2964 trees/hectare while the thinned plot has 10 trees/hectare.

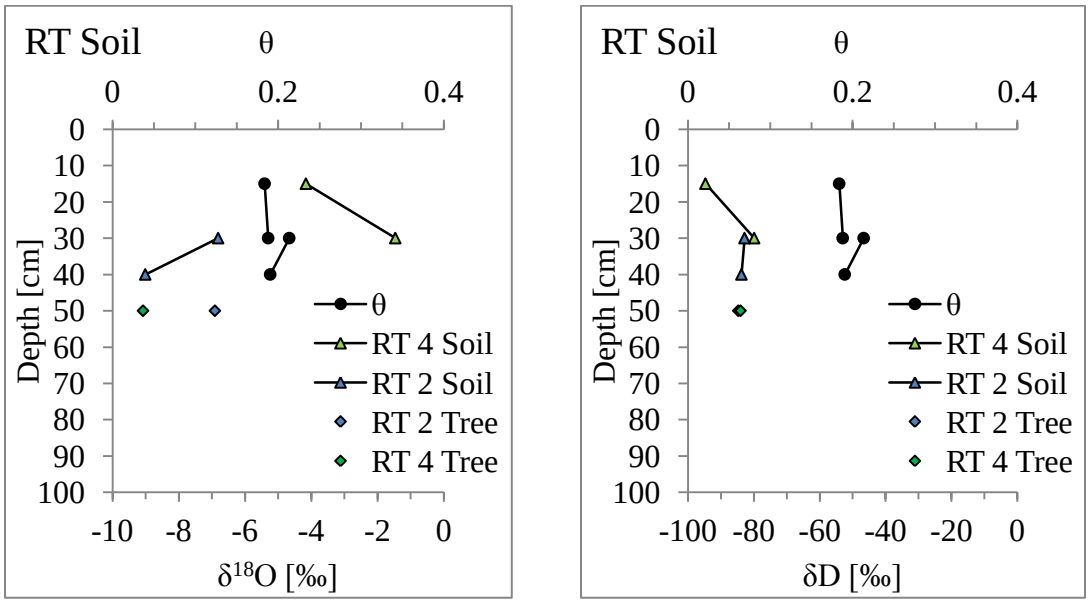

Figure 65: Gravimetric moisture content and stable-isotope values vs. depth for bulk-soil samples taken on a control plot located on the ridge-top in March 2011. Corresponding tree-water-isotope values are also shown. The plot from which these samples were taken

has an approximate tree density of 1482 trees/hectare. Enriched isotopic values can be seen near the surface.

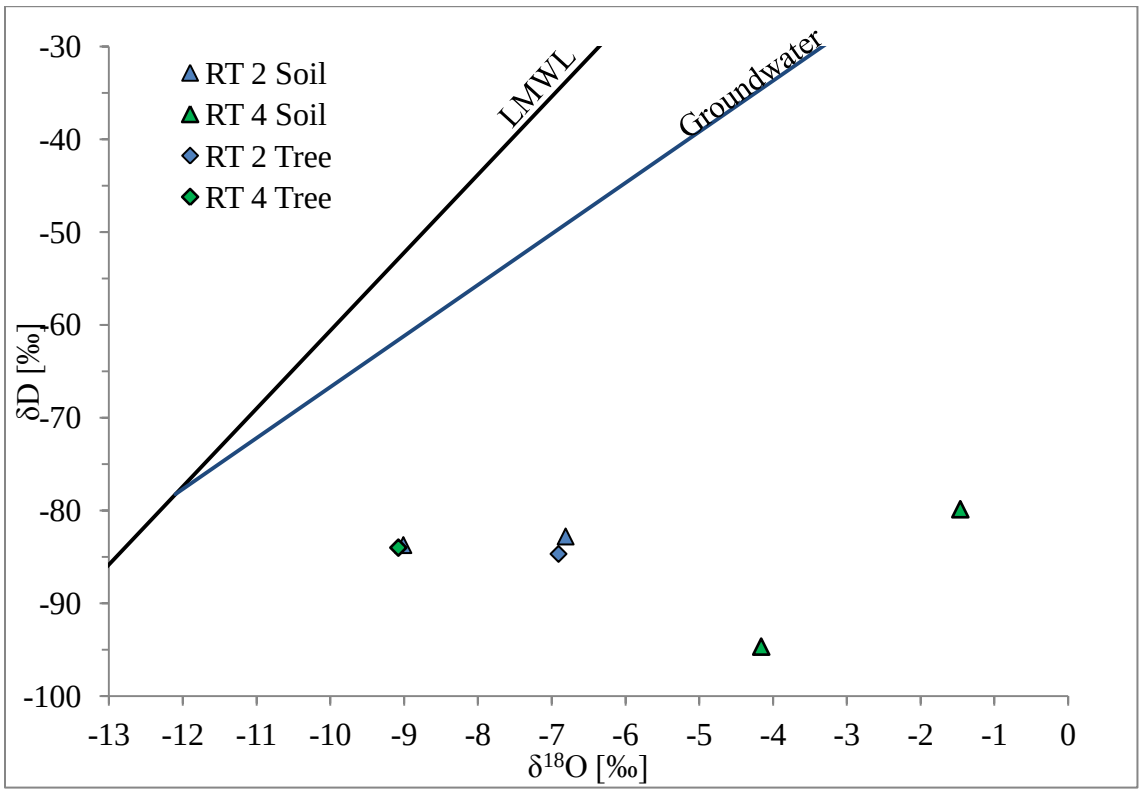

Figure 66: Tree water and bulk-soil-water-isotope data plotted in $\delta^{18}O$ vs. δD space. The symbol sizes are approximately equal to the error associated with analysis. The tree samples were taken from trees near the corresponding soil pits. The local meteoric water line (LMWL) and groundwater evaporation trend line are shown for reference.

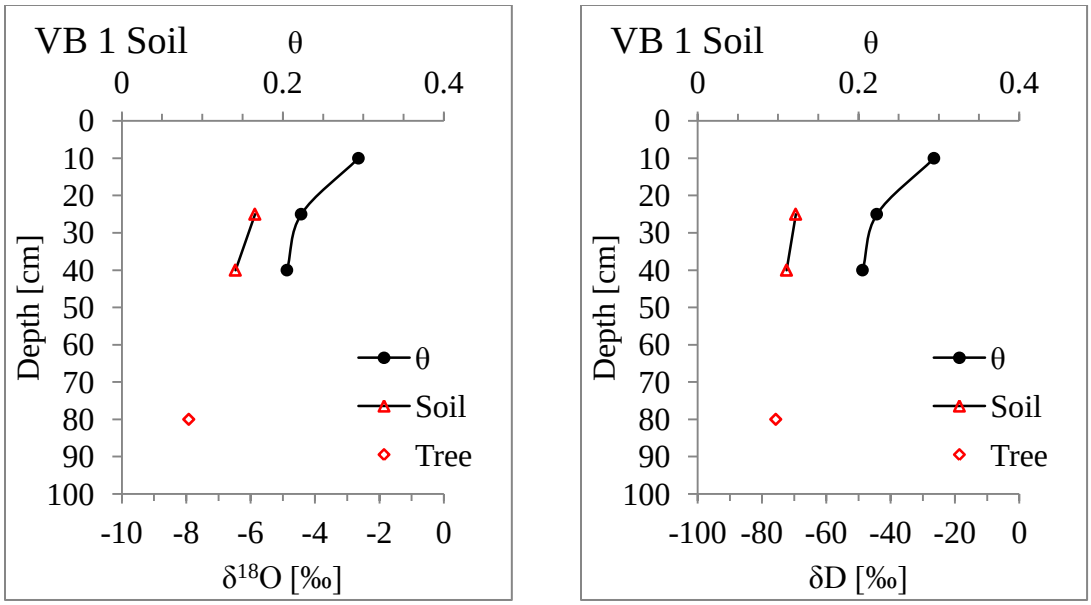

Figure 67: Gravimetric moisture content and stable-isotope values vs. depth for bulk-soil samples taken on a thinned plot located in the valley-bottom in March 2011. Corresponding tree-water isotope values are also shown. The plot from which these samples were taken has been thinned and has a tree density of 10 trees/hectare. The near surface soil-water isotope values were rejected due to spectral interference likely associated with the presence of organic matter in the sample.

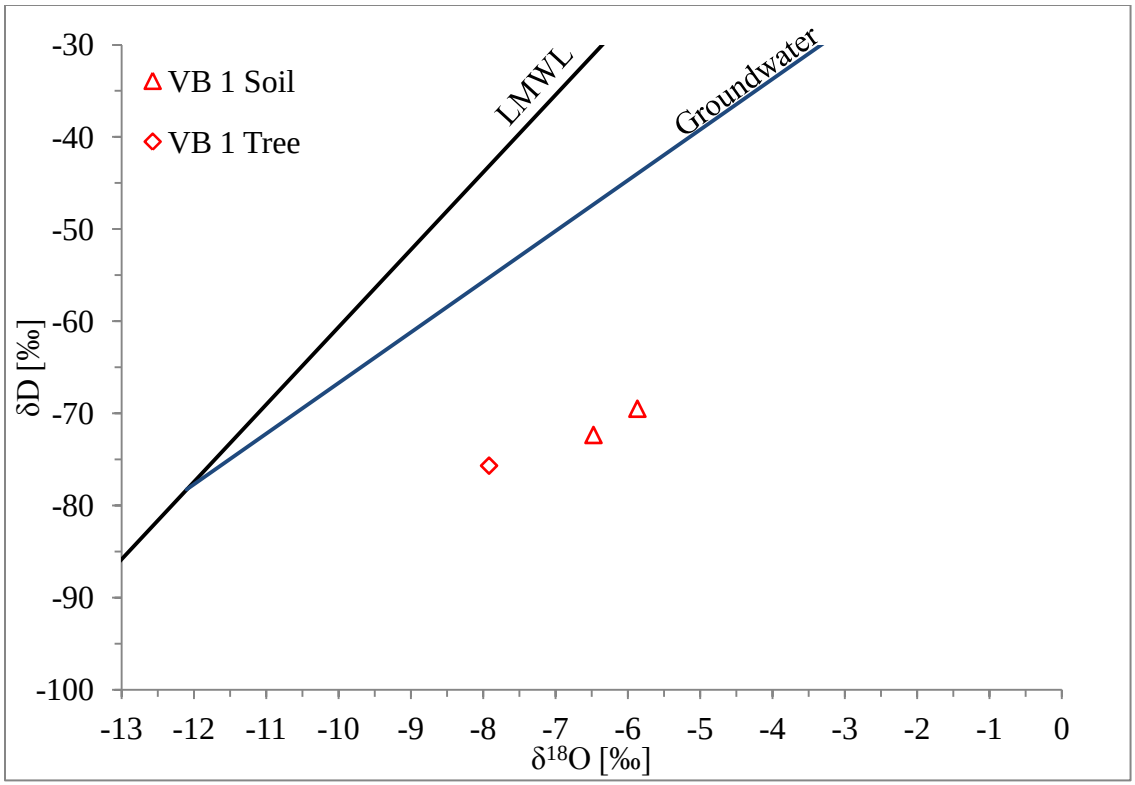

Figure 68: Tree water and bulk-soil-water isotope data plotted in $\delta^{18}O$ vs. δD space. The symbol sizes are approximately equal to the error associated with analysis. The VB 1 tree sample was taken from a tree near the VB 1 soil pit. The local meteoric water line (LMWL) and groundwater line are shown for reference.

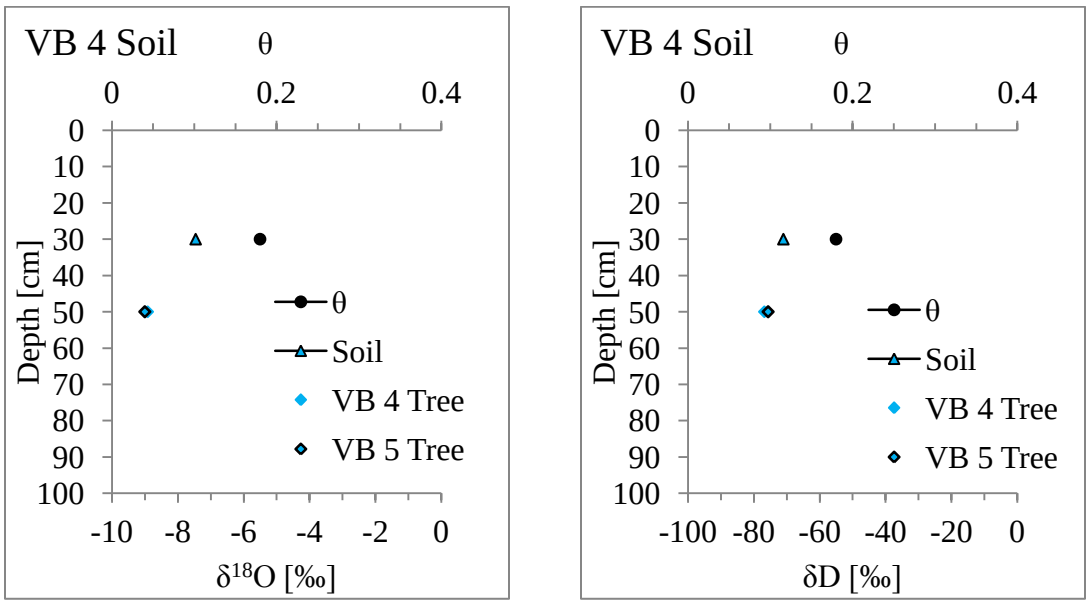

Figure 69: Gravimetric moisture content and stable-isotope values vs. depth for soil samples taken on a control plot located in the valley bottom in March 2011.

Corresponding tree-water isotope values are also shown. The plot from which these samples were taken has a tree density of 2964 trees/hectare.

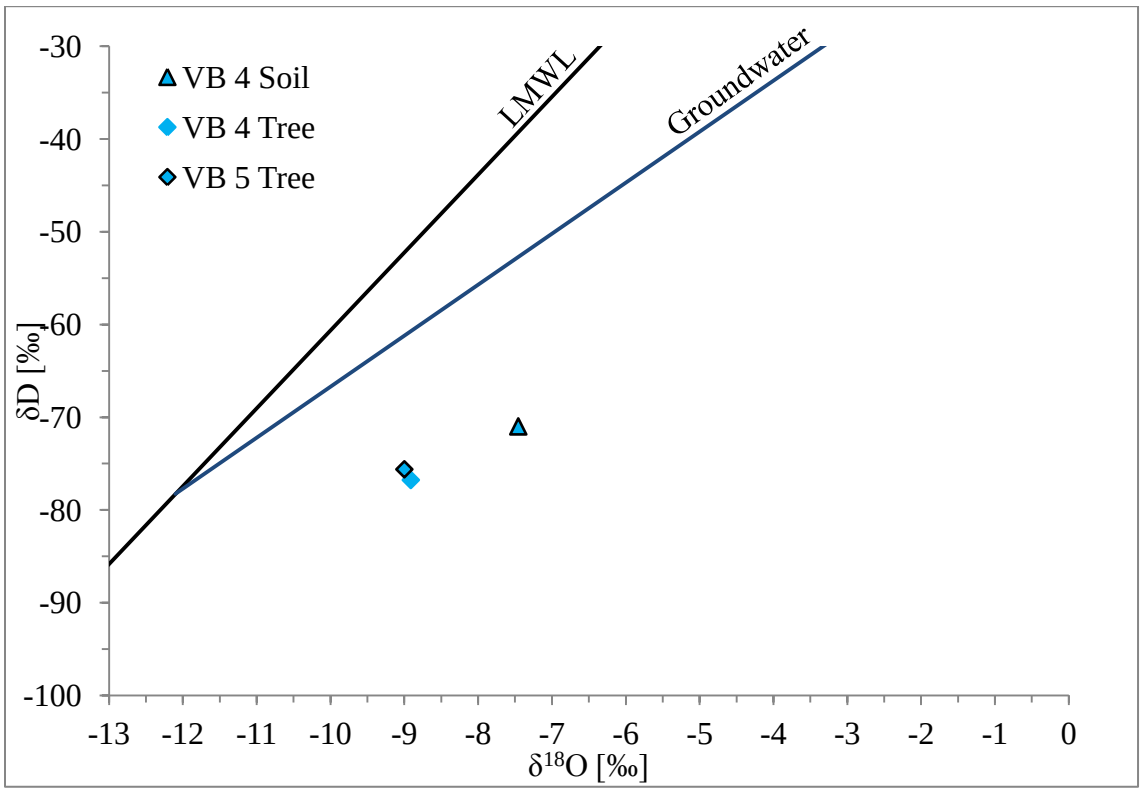

Figure 70: Tree and bulk-soil-water isotope data plotted in $\delta^{18}O$ vs. δD space. The symbol sizes are approximately equal to the error associated with analysis. The tree samples were taken from trees near the VB 4 soil pit. The local meteoric water line (LMWL) and groundwater line are shown for reference.

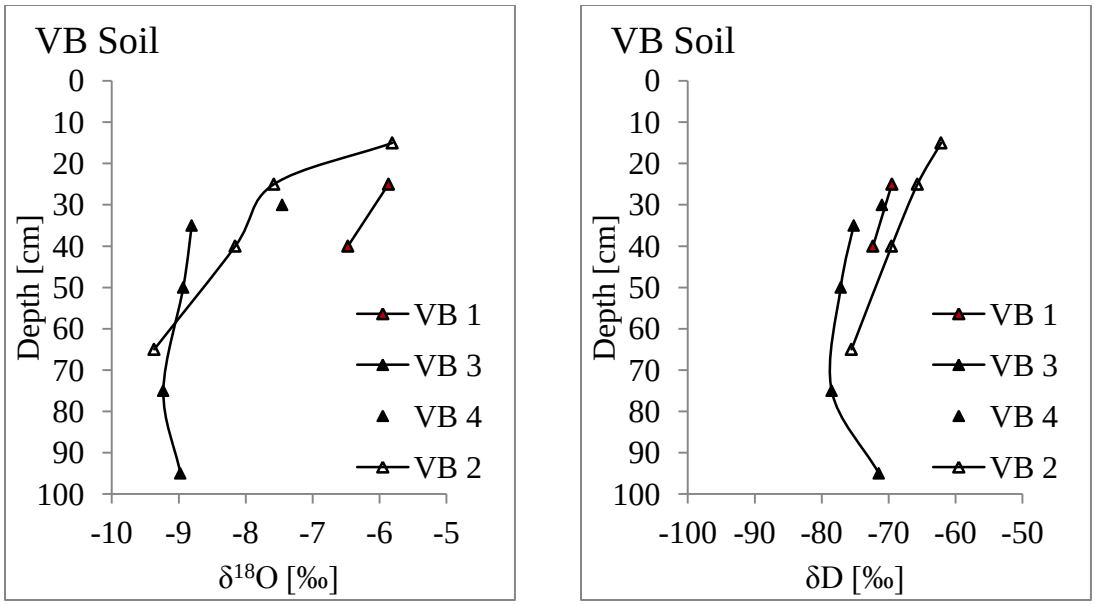

Figure 71: Stable-isotope values for soil samples taken from valley-bottom soil profiles in March 2011. Note that the x axis is different from other plots. The open symbols represent profiles taken from the thinned plot while the closed symbols represent profiles that lie on a control plot.

September 2011

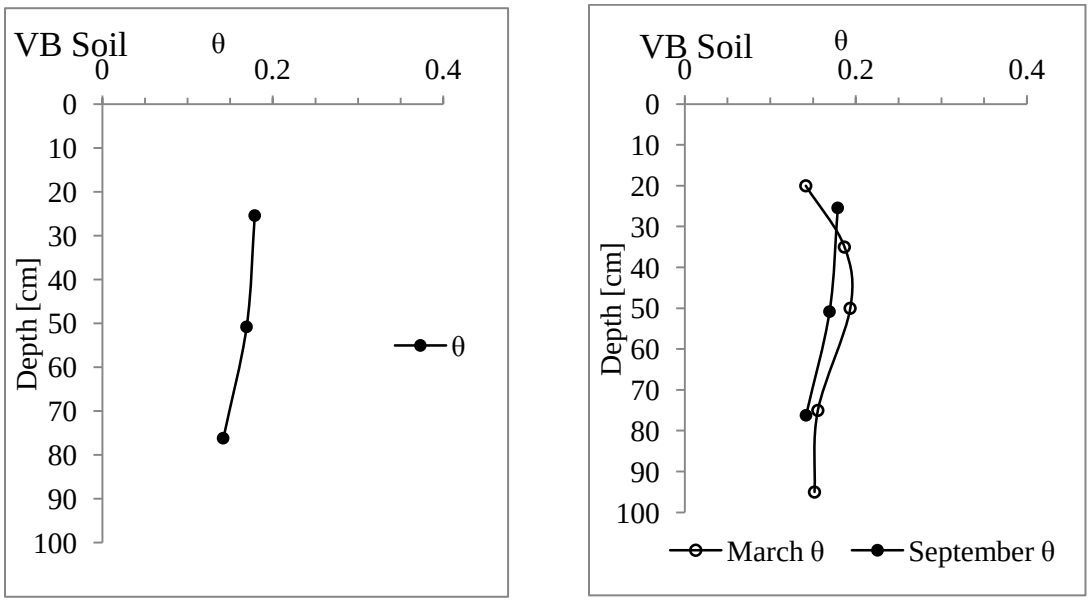

Figure 72: Gravimetric soil moisture content by depth for valley-bottom soils sampledin September 2011. The second figure compares a profile sampled at the same location in

March. The lack of change near the surface likely has to do with the shallow depth of the most shallow sample as well as the recent monsoonal precipitation inputs.

November 2011

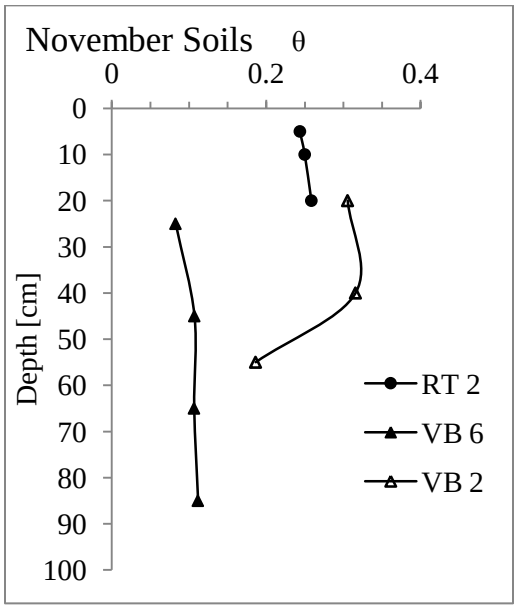

Figure 73: Gravimetric water content for soils sampled in November 2011. Closed symbols represent control plots while open symbols represent thinned plots. The increased moisture content at the VB 2 location is likely correlated with increased effective precipitation on a thinned plot.

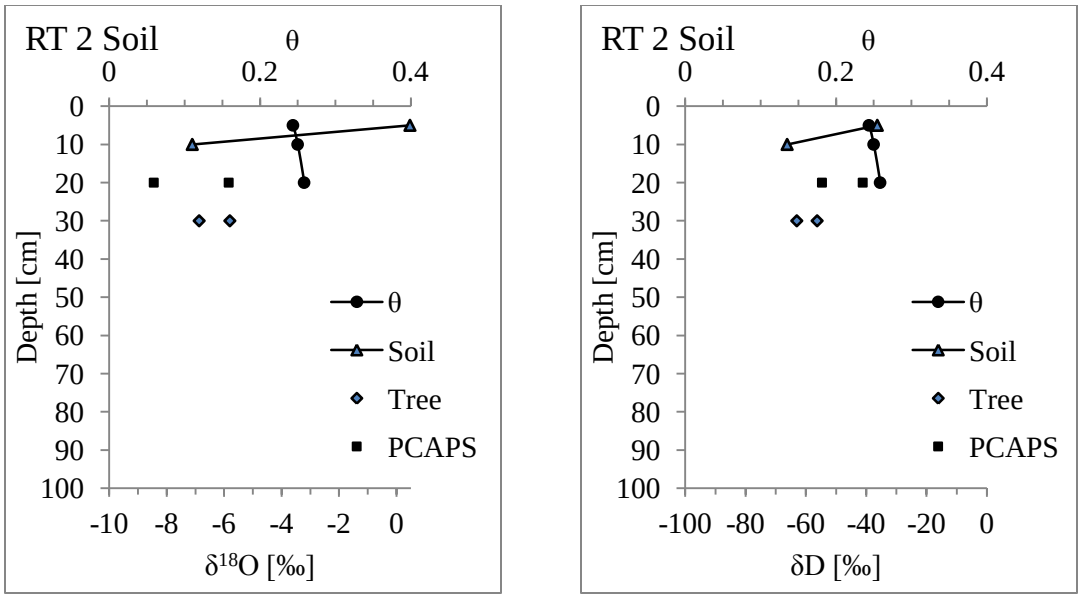

Figure 74: Gravimetric moisture content and stable-isotope values vs. depth for bulk-soil water collected from a ridge-top soil profile in November 2011. Tree water and mobile-soil-water isotope values are also shown. This profile lies on a control plot.

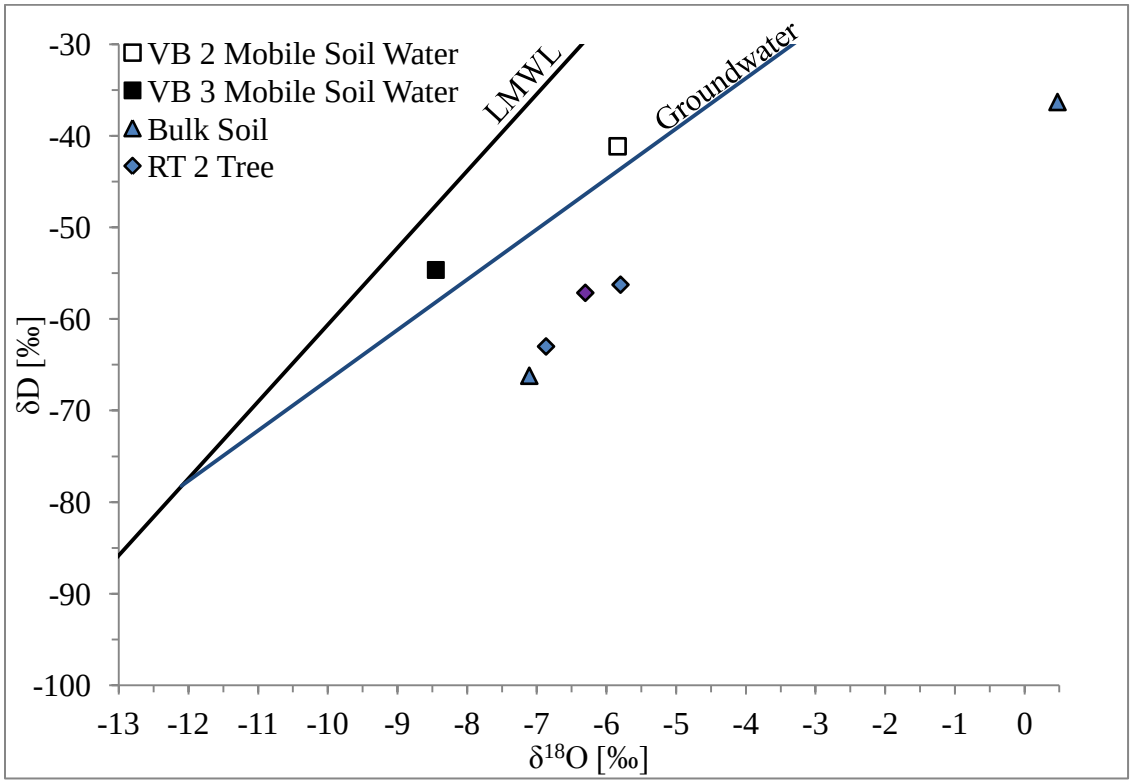

Figure 75: Tree water, bulk-soil-water and mobile-soil-water isotope data plotted in $\delta^{18}O$ vs. δD space. These samples were collected in November 2011, after the monsoon

season. This plot focuses on the ridge-top location though the mobile-soil waters were collected in the valley bottom. The symbol sizes are approximately equal to the error associated with analysis. The tree samples were taken from trees near the corresponding soil pits. Open symbols represent samples taken on the valley-bottom thinned plot while closed symbols represent samples taken on control plots. The local meteoric water line (LMWL) and groundwater line are shown for reference.

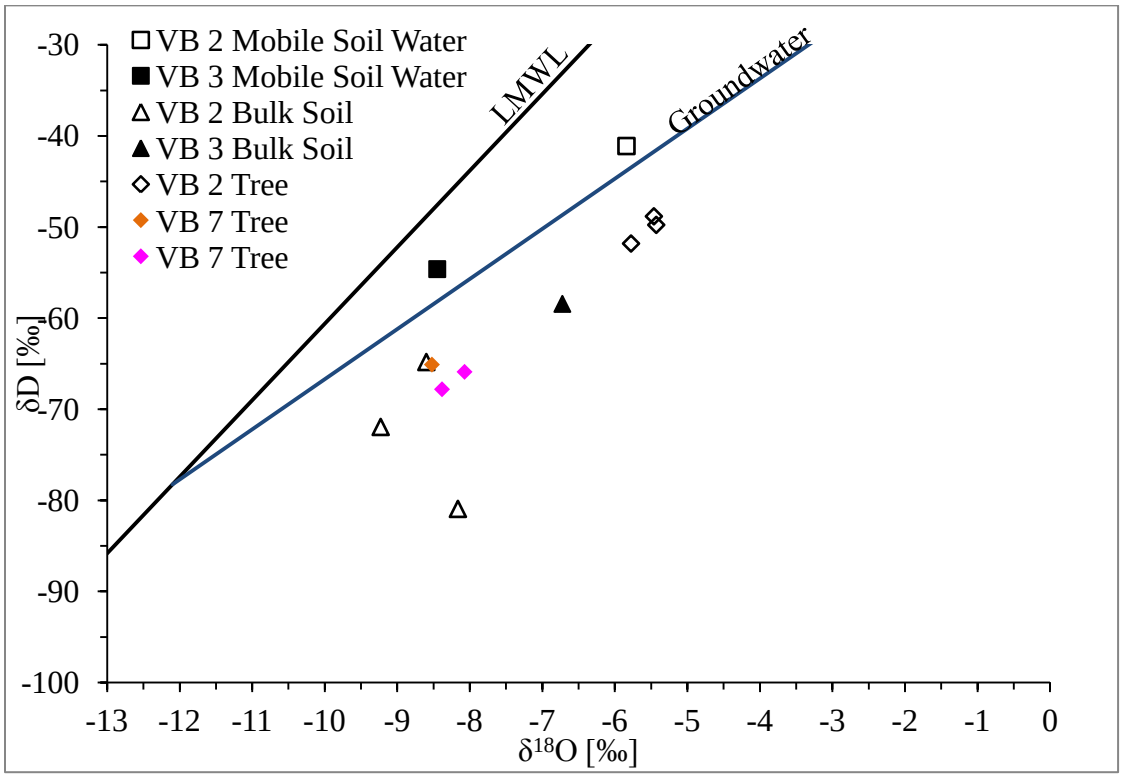

Figure 76: Tree water, bulk-soil-water and mobile-soil-water isotope data plotted in $\delta^{18}O$ vs. δD space. These samples were collected in November 2011, after the monsoon season. This plot focuses on the valley-bottom locations with soil samples from the VB 2 location and trees from a few locations near there. The symbol sizes are approximately equal to the error associated with analysis. The tree samples were taken from trees near the corresponding soil sample pit. Open symbols represent samples taken on the valley-bottom thinned plot while closed symbols represent samples taken on control plots. The local meteoric water line (LMWL) and groundwater line are shown for reference.

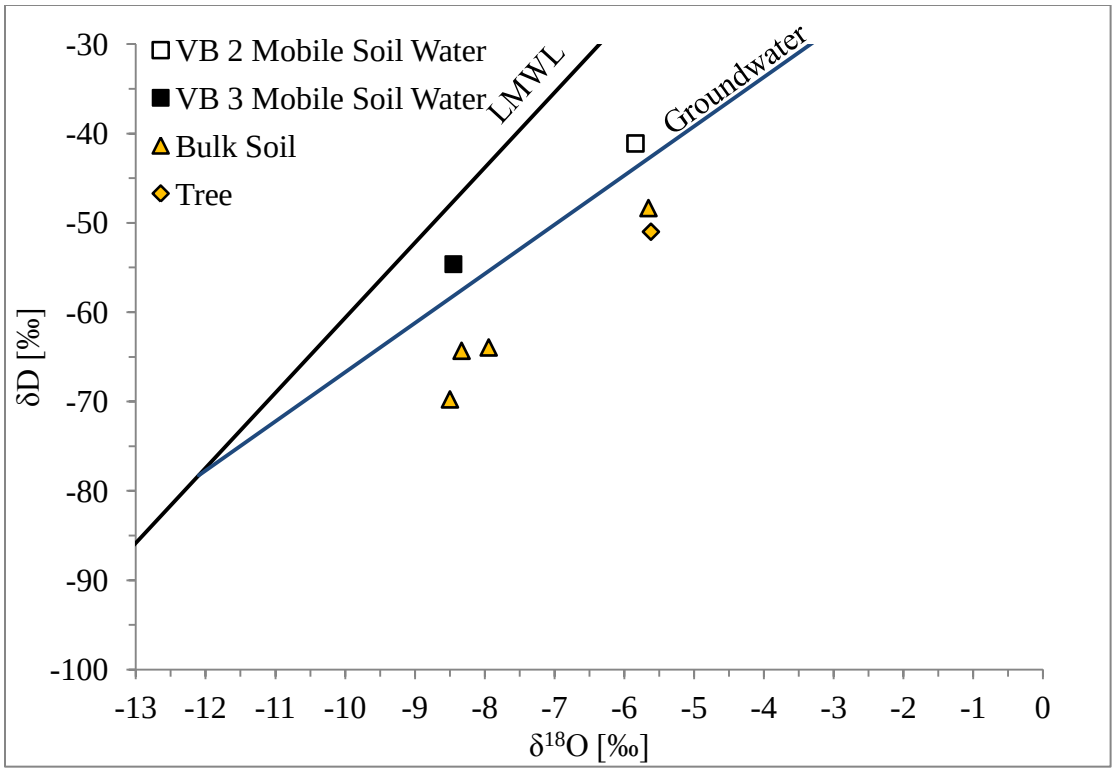

Figure 77: Tree water, bulk-soil-water and mobile-soil-water isotope data plotted in $\delta^{18}O$ vs. δD space. These samples were collected in November 2011, after the monsoon season. This plot focuses on the outlet drainage at the bottom of the watershed. The symbol sizes are approximately equal to the error associated with analysis. The tree samples were taken from trees near the corresponding soil pit. Open symbols represent samples taken on the valley-bottom thinned plot while closed symbols represent samples taken on control plots. The local meteoric water line (LMWL) and groundwater line are shown for reference.

February 2012

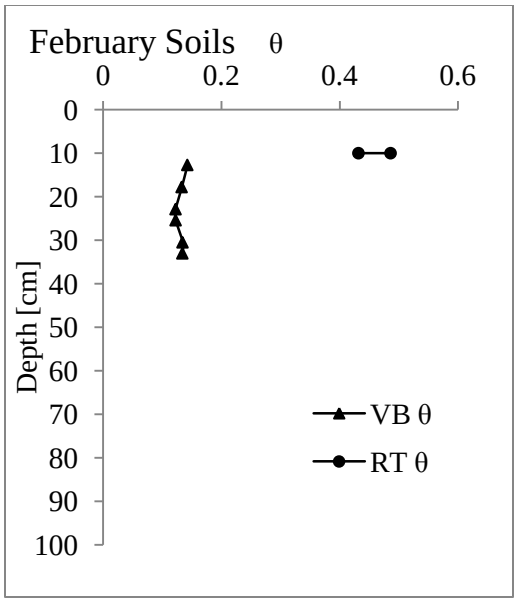

Figure 78: Gravimetric water content of soils sampled in February 2012. Note that the gravimetric moisture content scale is different than other plots in order to encompass the ridge top values. The increased moisture content of ridge-top samples is likely due to a later snow melt and possible increased water retention in organic litter present in the soil sample.

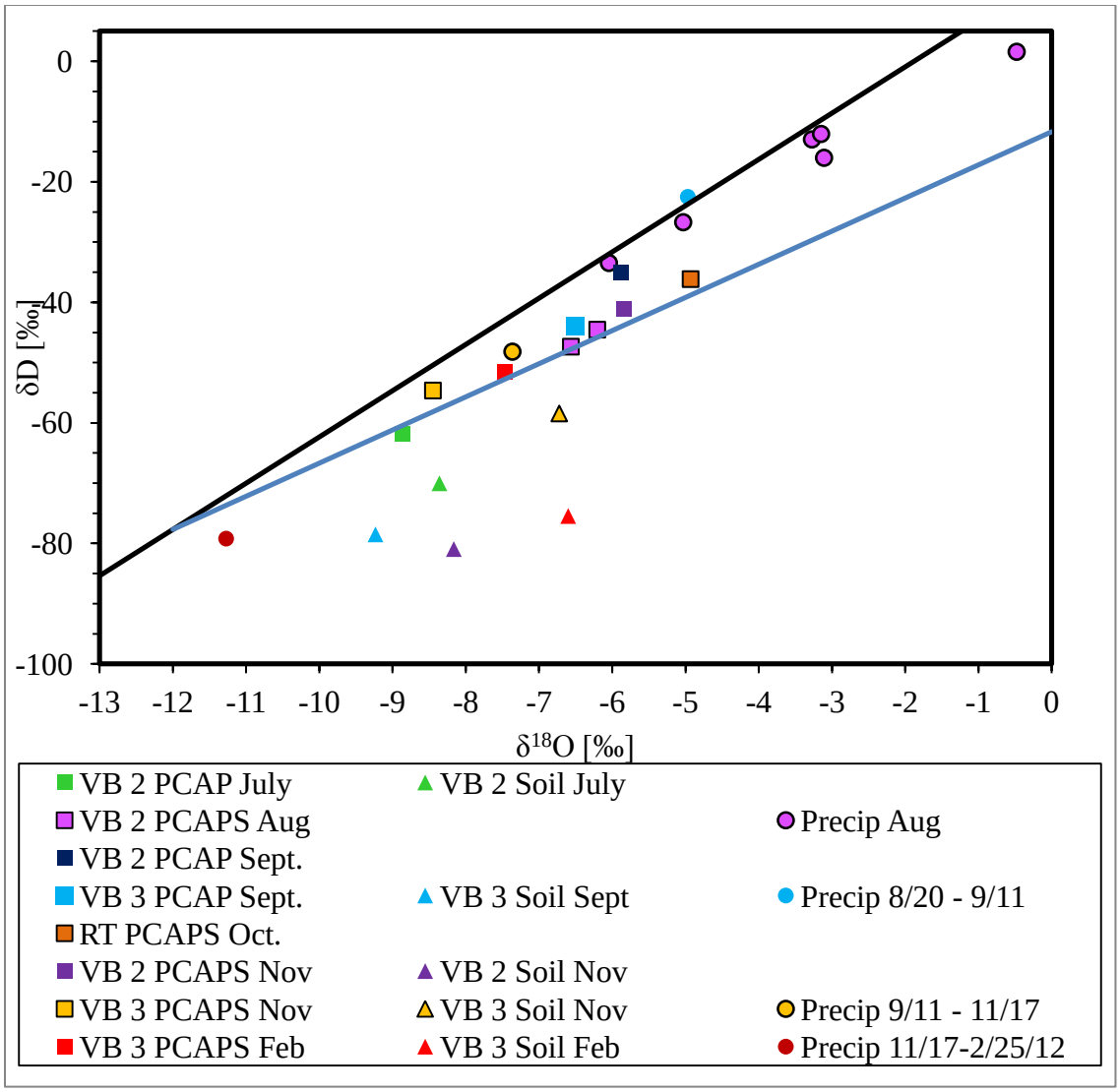

Figure 79: Passive-wick soil-water, bulk-soil-water sampled at the time of wick sampler collection and precipitation isotope data plotted in $\delta^{18}O$ vs. δD space. The symbol sizes are approximately equal to the error associated with analysis. The local meteoric water line (LMWL) and groundwater evaporation trend line are shown for reference.

Appendix III- Site Descriptions

Figure 80: RT 1 tree. The RT 2 soil pit and PCAPS installation is seen in the foreground.

Figure 81: RT 2 tree with the marking tape. The RT 2 soil pit and PCAPS installation can be seen in the foreground.

Figure 82: RT 2 soil pit. RT 1 tree is seen to the far right.

Figure 83: RT 3 soil pit. RT 3 is the dark tree with branches on the right. RT 5 is the tree leaning over the stump.

Figure 84: RT 3 soil pit. RT 3 is seen to the far right. RT 4 is on the right side of the group of small trees on the left. RT 5 is the tree leaning over the red bag.

Figure 85: Ridge top thinned plot PCAPS installation is near the red bag.

Figure 86: VB 1 tree is the smaller looking one in the center of the photo

Figure 87: VB 1 tree is the tree in the mid-ground area on the left. The VB 1 soil pit and PCAPS installation is down slope next to the red bag.

Figure 88: VB 3 tree and soil pit in foreground. This area is just below a break in the slope near the valley bottom.

Figure 89: VB 2 tree with covered VB 2 soil pit and PCAPS location covered in the foreground. This tree is on the down slope side of a thinned plot near the valley bottom.

BIBLIOGRAPHY

Adar, E. M., I. Gev, J. Lipp, D. Yakir, J. Gat, and Y. Cohen (1995), Utilization of oxygen-18 and deuterium in stem flow for the identification of transpiration sources: soil water versus groundwater in sand dune terrain, in *Application of tracers in arid zone hydrology, IAHS Publication*, vol. 232, edited by E. M. Adar and C. Leibundgut, p. 329-338, IAHS Press, Wallingford, U.K.

Augusti, A., T. R. Betson, and J. Schleucher (2006), Hydrogen exchange during cellulose synthesis distinguishes climatic and biochemical isotope fractionations in tree rings., *The New Phytologist*, *172*(3), 490-499, doi:10.1111/j.1469-8137.2006.01843.x.

Barnes, C. J., and G. B. Allison (1988), Tracing of water movement in the unsaturated zone using stable isotopes of hydrogen and oxygen, *Journal of Hydrology*, *100*, 143-176.

Bengtsson, L., R. K. Saxena, and Z. Dressie (1987), Soil water movement estimated from isotope tracers, *Hydrological Science Journal*, *32*(4), 497-520.

Boll, J., T. S. Steenhuis, and J. S. Selker (1992), Fiberglass wicks for sampling of water and solutes in the vadose zone, *Soil Science Society of America Journal*, *56*(3), 701-707.

Brooks, J. R., H. R. Barnard, R. Coulombe, and J. J. McDonnell (2009), Ecohydrologic separation of water between trees and streams in a Mediterranean climate, *Nature Geoscience*, *3*(2), 100-104, doi:10.1038/ngeo722.

Brunel, J. P., G. R. Walker, J. C. Dighton, and B. Monteny (1997), Use of stable isotopes of water to determine the origin of water used by the vegetation and to partition evapotranspiration. A case study from HAPEX-Sahel, *Journal of hydrology*, *188-89*(1-4), 466-481.

Brunel, J. P., G. R. Walker, C. D. Walker, J. C. Dighton, and A. Kennett-Smith (1991), Using stable isotopes of water to trace plant water uptake, in *International Symposium on the Use of Stable Isotopes in Plant Nutrition, Soil Fertility and Environmental Studies*, p. 543–551, IAEA-FAO, Vienna, Austria.

Campbell, A. R., F. M. Phillips, and R. J. Vanlandingham (1996), Stable isotope study of soil water, WIPP site New Mexico: Estimation of recharge to Rustler aquifers, *Radioactive Waste Management and Environmental Restoration*, *20*(2), 153-165.

Craig, H. (1961), Isotopic variations in meteoric waters, *Science*, *133*(3465), 1702.

Dansgaard, W. (1964), Stable isotopes in precipitation, *Tellus*, *16*(4), 436-468.

Dawson, T. E., and J. R. Ehleringer (1991), Streamside trees that do not use stream water, *Nature*, *350*(6316), 335-337.

Dietrich, W. E., R. Reiss, M. L. Hsu, and D. R. Montgomery (1995), A process-based model for colluvial soil depth and shallow landsliding using digital elevation data, *Hydrological Processes*, *9*(3-4), 383-400.

Earman, S., A. R. Campbell, F. M. Phillips, and B. D. Newman (2006), Isotopic exchange between snow and atmospheric water vapor: Estimation of the snowmelt component of groundwater recharge in the southwestern United States, *Journal of Geophysical Research*, *111*, 18 pp., doi:10.1029/2005JD006470.

Ehleringer, J. R., and T. E. Dawson (1992), Water uptake by plants: perspectives from stable isotope composition, *Plant Cell and Environment*, *15*(9), 1073-1082, doi:10.1111/j.1365-3040.1992.tb01657.x.

Elsenbeer, H., D. Lorieri, and M. Bonell (1995), Mixing model approaches to estimate storm flow sources in an overland flow-dominated tropical rain forest catchment, *Water Resources Research*, *31*(9), 2267-2278.

Farquhar, G. D., and K. S. Gan (2003), On the progressive enrichment of the oxygen isotopic composition of water along a leaf., *Plant, Cell & Environment*, *26*(6), 801-819.

Foxx, T. S., and G. D. Tierney (1987), Rooting patterns in the pinyon-juniper woodland, in *Pinyon-Juniper Symposium, Reno, Nevada*, edited by R. L. Everett, p. 581, U.S. Dept. of Agriculture, Forest Service, Intermountain Forest and Range Experiment Station, Ogden, UT.

Frechette, J. (2008), *Three L Canyon soil geomorphic units*, Unpublished consultant report to New Mexico Bureau of Geology and Mineral Resources, 10 p.

Frisbee, M. D., F. M. Phillips, A. R. Campbell, J. M. H. Hendrickx, and E. M. Engle (2010), Modified passive capillary samplers for collecting samples of snowmelt infiltration for stable isotope analysis in remote, seasonally inaccessible watersheds 2: field evaluation, *Hydrological Processes*, *24*(7), 834-849.

Frisbee, M. D., F. M. Phillips, A. R. Campbell, and J. M. H. Hendrickx (2008), Using passive capillary samplers to collect soil-meltwater endmembers for stable isotope analysis, in *Scientific Investigations Report– 5049, The Third Interagency Conference on Research in the Watersheds*, edited by R. M. T. Webb and D. J. Semmens, pp. 163-170, USGS, Estes Park, CO.

Gat, J. R., and C. Bowser (1991), The heavy isotope enrichment of water in coupled evaporative systems, in *Stable Isotope Geochemistry: A Tribute to Samuel Epstein; The Geochemical Society, Special Publication*, vol. 3, edited by H. P. Tayor, J. R. O'Neill, and I. R. Kaplan, pp. 159-168, The Geochemical Society, St. Louis, MO.

Gee, G. W., B. D. Newman, S. R. Green, R. Meissner, H. Rupp, Z. F. Zhang, J. M. Keller, W. J. Waugh, M. van der Velde, and J. Salazar (2009), Passive wick fluxmeters: Design considerations and field applications, *Water Resources Research*, *45*(4), 18 pp, doi:10.1029/2008WR007088.

Goldsmith, G. R., L. E. Muñoz-Villers, F. Holwerda, J. J. McDonnell, H. Asbjornsen, and T. E. Dawson (2011), Stable isotopes reveal linkages among ecohydrological processes in a seasonally dry tropical montane cloud forest, *Ecohydrology Preprint*, doi:10.1002/eco.268.

Gonfiantini, R., M.-A. Roche, J.-C. Olivry, J.-C. Fontes, and G. M. Zuppi (2001), The altitude effect on the isotopic composition of tropical rains, *Chemical Geology*, *181*(1-4), 147-167, doi:10.1016/S0009-2541(01)00279-0.

Granier, A. (1974), Une nouvelle méthode pour la mesure du flux de sève brute dans le tronc des arbres, *Annales des Sciences Forestieres*, *42*(2), 193-200.

Kelley, V. (1971), *Geology of the Pecos country, southeastern New Mexico*, New Mexico Bureau of Mines and Mineral Resources, Memoir 24, 78 p.

Knutson, J. H., and J. S. Selker (1994), Unsaturated hydraulic conductivities of fiberglass wicks and designing capillary wick pore-water samplers, *Soil Science Society of America Journal*, *58*(3), 721-729.

Landon, M. K., G. N. Delin, S. C. Komor, and C. P. Regan (1999), Comparison of the stable-isotopic composition of soil water collected from suction lysimeters, wick samplers, and cores in a sandy unsaturated zone, *Journal of Hydrology*, *224*(1), 45-54.

Lee, K.-S., D. B. Wenner, and I. Lee (1999), Using ^{2}H and ^{18}O isotopic data for estimating the relative contributions of rainy and dry season precipitation to groundwater: example from Cheju Island, Korea, *Journal of Hydrology*, *222*(1), 65-74, doi:10.1016/S0022-1694(99)00099-2.

Libby, L. M., and L. J. Pandolfi (1974), Temperature dependence of isotope ratios in tree rings., *Proceedings of the National Academy of Sciences of the United States of America*, *71*(6), 2482-2486.

Mathieu, R., and T. Bariac (1996), An isotopic study of water movements in clayey soils under a semiarid climate, *Water Resources Research*, *32*(4), 779-789.

McCarroll, D., and N. J. Loader (2004), Stable isotopes in tree rings, *Quaternary Science Reviews*, *23*(7-8), 771-801, doi:10.1016/j.quascirev.2003.06.017.

McMinn, R. G. (1963), Characteristics of Douglas-fir root systems, *Canadian Journal of Botany*, *41*(1), 105-122.

Merlivat, L. (1978), Molecular diffusivities of $H_2{}^{16}O$, $HD^{16}O$, and $H_2{}^{18}O$ in gases, *Journal of Chemical Physics*, *69*(6), 2864-2871.

Morse, J. T. (2010), The Hydrogeology of the Sacramento Mountains Using Environmental Tracers: Master's Thesis, New Mexico Institute of Mining and Technology, Socorro, NM.

Newman, B. D., A. R. Campbell, and P. Wilcox (1998), Lateral subsurface flow pathways in a semiarid ponderosa pine hillslope, *Water Resources*, *34*(12), 3485-3496.

Newton, B. T., G. C. Rawling, S. S. Timmons, L. Land, P. S. Johnson, T. Kludt, and J. M. Timmons (2012), *Sacramento Mountains Hydrogeology Study*, New Mexico Bureau of Geology and Mineral Resources, Open File Report, Socorro, NM. [online] Available from: http://geoinfo.nmt.edu/publications/openfile/details.cfml?Volume=543

Newton, T., S. Timmons, G. Rawling, F. Partey, T. Kludt, L. Land, M. Timmons, and P. Walsh (2009), *Sacramento Mountains Hydrogeology Study*.

Návar, J. de J., D. R. Barnes, and D. J. Turton (1995), Old and new water in subsurface flow from a forest soil block, *Journal of Environmental Quality*, *24*(1), 139-146.

Pray, L. C. (1961), *Geology of the Sacramento Mountains Escarpment, Otero County, New Mexico*, New Mexico Bureau of Geology and Mineral Resources, Bulletin 35, 144 pp.

Rozanski, K., L. Araguas-Araguas, and R. Gonfiantini (1993), Isotopic patterns in modern global precipitation, in *Climate Change in Continental Isotope Records, Geophysical Monograph Series*, vol. 78, edited by P. K. Swart, K. C. Lohmann, J. McKenzie, and S. Savin, pp. 1-36, American Geophysical Union, Washington, DC.

Rusanen, K., L. Finér, M. Antikainen, K. Korkka-niemi, B. Backman, and R. Britschgi (2004), The effect of forest cutting on the quality of groundwater in large aquifers in Finland, *Boreal Environment Research*, *9*, 253-261.

Simonin, K., T. E. Kolb, M. Montes-Helu, and G. W. Koch (2007), The influence of thinning on components of stand water balance in a ponderosa pine forest stand during and after extreme drought, *Agricultural and Forest Meteorology*, *143*(3), 266-276, doi:10.1016/j.agrformet.2007.01.003.

Tang, K., and X. Feng (2001), The effect of soil hydrology on the oxygen and hydrogen isotopic compositions of plants' source water, *Earth and Planetary Science Letters*, *185*(3), 355–367.

Tian, L., T. Yao, W. Sun, M. Stievenard, and J. Jouzel (2001), Relationship between δD and $\delta^{18}O$ in precipitation on north and south of the Tibetan Plateau and moisture recycling, *Science in China, D: Earth Sciences*, *44*(9), 789-796.

Unkovich, M. J., J. Pate, A. M. McNeill, and D. Gibbs (2001), *Stable isotope techniques in the study of biological processes and functioning of ecosystems*, edited by M. Unkovich, J. Pate, A. McNeil, and D. J. Gibbs, p 289, Kluwer Academic Publishers, Norwell, MA.

Vendramini, P. F., and L. D. S. L. Sternberg (2007), A faster plant stem-water extraction method, *Rapid Communications in Mass Spectrometry*, *21*(2), 164-168.

Wenner, D. B., P. D. Ketcham, and J. F. Dowd (1991), Stable isotopic composition of waters in a small Piedmont watershed, in *Stable Isotope Geochemistry: a Tribute to Samuel Epstein*, vol. 3, edited by H. P. Tayor, J. R. O'Neill, and I. R. Kaplan, pp. 195-203, The Geochemical Society, St. Louis, MO.

West, A. G., G. R. Goldsmith, P. D. Brooks, and T. E. Dawson (2010), Discrepancies between isotope ratio infrared spectroscopy and isotope ratio mass spectrometry for the stable isotope analysis of plant and soil waters, *Rapid Communications in Mass Spectrometry*, *24*(14), 1948-1954, doi:10.1002/rcm.4597.

West, A. G., S. J. Patrickson, and J. R. Ehleringer (2006), Water extraction times for plant and soil materials used in stable isotope analysis, *Rapid Communications in Mass Spectrometry*, *20*(8), 1317-1321.

White, J. W. C., E. R. Cook, J. R. Lawrence, and S. B. Wallace (1985), The ratios of sap in trees: Implications for water sources and tree ring ratios, *Geochimica et Cosmochimica Acta*, *49*(1), 237-246.

Wilcox, B. P., B. D. Newman, D. Brandes, D. W. Davenport, and K. Reid (1997), Runoff from a semiarid ponderosa pine hillslope in New Mexico, *Water Resources Research*, *33*(10), 2301-2314.

Winograd, I. J., A. C. Riggs, and T. B. Coplen (1998), The relative contributions of summer and cool-season precipitation to groundwater recharge, Spring Mountains, Nevada, USA, *Hydrogeology Journal*, *6*(1), 77-93, doi:10.1007/s100400050135.

Yakir, D. (1992), Variations in the natural abundance of oxygen-18 and deuterium in plant carbohydrates, *Environmental Sciences*, *15*, 1005-1020.

Yakir, D., and M. J. Deniro (1990), Oxygen and hydrogen isotope fractionation during cellulose metabolism in Lemna gibba L., *Plant Physiology*, *93*(1), 325-32.

Zimmermann, U., D. Ehhalt, and K. O. Münnich (1967), Soil water movement and evapotranspiration: Changes in the isotopic composition of the water, in *Proceedings of the symposium on isotopes in hydrology*, edited by M. Knippner, p. 567-584, IAEA, Vienna.